


1. Report No. FHWA/TX-90+1190-1	2. Government Accession No.	3.  L004050
4. Title and Subtitle TRUCK TIRE PAVEMENT CONTACT PRESSURE DISTRIBUTION CHARACTERISTICS FOR SUPER SINGLE 18-22.5 AND SMOOTH 11R24.5 TIRES	5. Report Date July 1989	6. Performing Organization Code
	8. Performing Organization Report No. Research Report 1190-1	
7. Author(s) Rex William Hansen, Carl Bertrand, K. M. Marshek, and W. R. Hudson	10. Work Unit No.	11. Contract or Grant No. Research Study 3-8-88/9-1190
9. Performing Organization Name and Address Center for Transportation Research The University of Texas at Austin Austin, Texas 78712-1075	13. Type of Report and Period Covered Interim	14. Sponsoring Agency Code
	12. Sponsoring Agency Name and Address Texas State Department of Highways and Public Transportation; Transportation Planning Division P. O. Box 5051 Austin, Texas 78763-5051	
15. Supplementary Notes Study conducted in cooperation with the U. S. Department of Transportation, Federal Highway Administration Research Study Title: "Tire Contact Pressure Distributions"		
16. Abstract Within the last 50 years truck sizes, allowable wheel loads, and tire inflation pressures have increased. In order to establish pavements capable of sustaining the increased loading, the actual loading mechanisms and their magnitudes had to be identified. To identify the magnitudes, static testing was performed at The University of Texas at Austin on a specially manufactured Armstrong 11R24.5 LR-G smooth tread tire and also on a commercially available Goodyear 18-22.5 LR-H wide-base, newly-recapped super single tire. Contact pressure distributions were obtained for the 11R24.5 radial tires at inflation 90 and 105 and loaded to 5,000, 6,000, and 7,000 pounds. The 18-22.5 recap bias tire was inflated to 85 and 100 psi and tested at wheel loads of 8,000, 10,000, and 12,000 pounds. The pressure data acquisition system used to obtain the tire contact pressures consisted of three main components: a load frame (powered by a manual hydraulic system) for mounting and loading the test tires, Fuji pressure sensitive film to record pressure distributions, and a film analysis package using the Adage 3006 Graphics system to process the pressure distribution data. The contact pressure data were presented as numerical pressure distribution maps and also illustrated as two-dimensional spectral graphics and three-dimensional surface plots. The experiments indicated that for the 11R24.5 tire and the 18-22.5 tire, increased wheel loads at constant inflation pressures generally resulted in more uniform contact pressures throughout the contact area. The same increased wheel loads were also accommodated by a lengthening of the contact area. On the other hand, increased inflation pressures at constant wheel loads resulted in a reduction of contact area and increased contact pressures in the contact patch's central region. Low inflation pressures tended to cause the wheel load to be distributed more heavily to the contact patch's central area for the radial tire and more heavily to the sidewall contact area for the bias tire.		
17. Key Words truck sizes, allowable wheel loads, tire inflation pressures, contact pressure distributions, contact area, magnitudes, static testing	18. Distribution Statement No restrictions. This document is available to the public through the National Technical Information Service, Springfield, Virginia 22161.	
19. Security Classif. (of this report) Unclassified	20. Security Classif. (of this page) Unclassified	21. No. of Pages 88
		22. Price

**TRUCK TIRE PAVEMENT CONTACT PRESSURE DISTRIBUTION
CHARACTERISTICS FOR SUPER SINGLE 18-22.5
AND SMOOTH 11R24.5 TIRES**

by

Rex William Hansen
Carl Bertrand
K. M. Marshek
W. R. Hudson

Research Report Number 1190-1

Research Project 3-8-88/9-1190

Tire Contact Pressure Distributions

conducted for

**Texas State Department of Highways
and Public Transportation**

in cooperation with the

**U.S. Department of Transportation
Federal Highway Administration**

by the

CENTER FOR TRANSPORTATION RESEARCH

Bureau of Engineering Research
THE UNIVERSITY OF TEXAS AT AUSTIN

July 1989

The contents of this report reflect the views of the authors, who are responsible for the facts and the accuracy of the data presented herein. The contents do not necessarily reflect the official views or policies of the Federal Highway Administration. This report does not constitute a standard, specification, or regulation.

PREFACE

This is the first of two reports which describe work done on Project 1190, "Tire Contact Pressure Distributions." The study was conducted at the Center for Transportation Research (CTR), The University of Texas at Austin, as part of a cooperative research program sponsored by the Texas State Department of Highways and Public Transportation and the Federal Highway Administration.

Many people contributed their help toward the completion of this report. Thanks are expressed to Dr. Tom Tielking for his guidance, to Mr. Larry Walker of Walker

Tire Company for his extraordinary support, to Mrs. Peggy Johnson, and to all the CTR personnel, especially Lyn Gabbert, Loretta McFadden, Art Frakes, and Rob Harrison.

We acknowledge their contributions and greatly appreciate their efforts to make this a successful project.

Rex William Hansen
Carl Bertrand
Kurt M. Marshek
W. Ronald Hudson

LIST OF REPORTS

Report No. 1190-1, "Truck Tire-Pavement Contact Pressure Distribution Characteristics for Super Single 18-22.5 and Smooth 11R24.5 Tires," by Rex William Hansen, Carl Bertrand, Kurt M. Marshek, and W. Ronald Hudson,

presents experimental data on the effect of tire inflation pressure and static wheel load on contact pressure distribution for the bias Goodyear 18-22.5 and the smooth radial Armstrong 11R24.5 tires. July 1989.

ABSTRACT

Within the last 50 years truck sizes, allowable wheel loads, and tire inflation pressures have increased. In order to establish pavements capable of sustaining the increased loading, the actual loading mechanisms and their magnitudes had to be identified. To identify the magnitudes, static testing was performed at The University of Texas at Austin on a specially manufactured Armstrong 11R24.5 LR-G smooth tread tire and also on a commercially available Goodyear 18-22.5 LR-H wide-base, newly-recapped super single tire. Contact pressure distributions were obtained for the 11R24.5 radial tires at inflation 90 and 105 and loaded to 5,000, 6,000, and 7,000 pounds. The 18-22.5 recap bias tire was inflated to 85 and 100 psi and tested at wheel loads of 8,000, 10,000, and 12,000 pounds. The pressure data acquisition system used to obtain the tire contact pressures consisted of three main components: a load frame (powered by a manual hydraulic system) for mounting and loading the test tires, Fuji pressure sensitive

film to record pressure distributions, and a film analysis package using the Adage 3006 Graphics system to process the pressure distribution data. The contact pressure data were presented as numerical pressure distribution maps and also illustrated as two-dimensional spectral graphics and three-dimensional surface plots. The experiments indicated that for the 11R24.5 tire and the 18-22.5 tire, increased wheel loads at constant inflation pressures generally resulted in more uniform contact pressures throughout the contact area. The same increased wheel loads were also accommodated by a lengthening of the contact area. On the other hand, increased inflation pressures at constant wheel loads resulted in a reduction of contact area and increased contact pressures in the contact patch's central region. Low inflation pressures tended to cause the wheel load to be distributed more heavily to the contact patch's central area for the radial tire and more heavily to the sidewall contact area for the bias tire.

SUMMARY

The rate of deterioration of highway pavements over the last 50 years appears to have been accelerating. During this time, legal truck sizes, weights, wheel loads and tire inflation pressures have also increased. This report is one of several studies seeking to establish tire-pavement contact pressure distributions, in order to serve the pavement designers in their estimations of pavement deterioration and to assist legislators in defining tire policies.

This report presents: (1) an extensive review of the literature related to this project and (2) the results of an experiment involving two truck tires statically loaded on a steel plate. The smooth radial Armstrong 11R24.5 LR-G and the bias Goodyear 18-22.5 LR-H super single tires were tested and studied for this report. The smooth radial Armstrong 11R24.5 was especially manufactured for research testing and was made available for this project. The bias Goodyear 18-22.5 super single was chosen for its popularity on Texas highways.

The testing consisted of making prints of a tire in contact with a solid steel plate at different axial loads and tire inflation pressures. These prints were produced by using Fuji prescale film. Fuji prescale film allowed the entire

pressure distribution to be captured under a color-intensity principle. By analyzing the Fuji prints, tire contact pressure distributions were defined. Tire side movements were measured for the smooth radial Armstrong 11R24.5 tire, to allow designers to relate their theoretical values with our experimental results.

The main contributions of this project can be summarized as follows:

(1) At low wheel loads, the load is supported by the central and edge portions of the smooth radial 11R24.5.

(2) As the wheel load was increased on the smooth radial 11R24.5 tire (while kept at constant inflation pressure), the contact pressures became more uniform.

(3) At constant wheel load, as the tire inflation pressure increased, the contact pressures in the tread's central region increased more than did the pressures in the sidewalls.

(4) Increased wheel load on the radial tire, at constant tire inflation pressure, was accompanied by a lengthening in the contact patch.

(5) For bias tires the shape of the contact area is more circular with an oval tendency, while for radial tires the shape is rectangular.

IMPLEMENTATION STATEMENT

The work undertaken in this project provides tire contact areas and tire contact pressure distributions for the tested truck tires at several inflation pressures and wheel loads. These values are available for use in evaluating the effects of truck tire inflation pressure and axle load on the structural

capacity of pavements. Such information could lead to changes in methods employed in current highway pavement design, and could also assist legislators in defining truck tire policies.

TABLE OF CONTENTS

PREFACE	iii
LIST OF REPORTS	iii
ABSTRACT	iii
SUMMARY.....	iv
IMPLEMENTATION STATEMENT.....	iv
 CHAPTER 1. INTRODUCTION	
Background.....	1
Objective.....	1
Scope and Organization of the Study	1
Research and Approach.....	1
 CHAPTER 2. RELATED STUDIES	
Surveys of Tire Types and Inflation Pressures.....	2
Future Trends in Tire Types and Inflation Pressures	3
Inflation Pressure Effects on Operator Costs	4
Results of Over-Inflation.....	4
Results of Under-Inflation.....	4
Results of Proper Inflation.....	4
General Tire Contact Pressure Characteristics.....	5
Membrane Theory and Historical Background.....	5
Tire-Pavement Contact Stresses	5
Stress Components and Orientation.....	5
Longitudinal Shear Pressure.....	5
Lateral Shear Pressure	6
Factors Affecting Contact Pressure Distributions	6
Inflation Pressure and Wheel Load.....	6
Speed and Pavement Friction	9
Steering.....	10
Tire Contact Pressure and Its Effect on Flexible Pavement Life.....	10
Wheel Load and Inflation Pressure Effects.....	10
Studies Discussing Wheel Loads and Inflation Pressures.....	10
Studies Discussing Fatigue.....	11
Studies Discussing Rutting	12
Surface Modulus, Base Modulus, and Thickness Effects	16
Possible Pavement Life Saving Solutions.....	16
Conclusions	17
 CHAPTER 3. EQUIPMENT, PARAMETERS, AND PROCEDURES	
Experimental Apparatus.....	18
Truck Tires and Rims.....	18
Load Frame and Platform.....	18
Manual Hydraulic Power Supply	18

Hewlett-Packard Data Acquisition System.....	18
Load Cell Calibration.....	19
Fuji Prescale Film and Teflon Shim Stock.....	19
Film Analytical Tools.....	20
Adage Analysis System.....	20
Experimental Parameters.....	20
Tires.....	20
Loads.....	21
Inflation Pressures.....	21
Experimental and Adage Analytical Procedures.....	21
 CHAPTER 4. EXPERIMENTAL RESULTS	
Radial Armstrong 11R24.5 Load Range-G Smooth Tread Tire.....	22
Bias Goodyear 18-22.5 Wide-Base Super Single Tire.....	37
Experimental Results.....	37
Discussion of Results.....	38
Characteristics of the Smooth Tread 11R24.5 Tire.....	38
Characteristics of the Wide-Base 18-22.5 Tire.....	38
Experimental Error.....	38
Fuji Prescale Film.....	53
Load Apparatus.....	53
 CHAPTER 5. CONCLUSIONS AND RECOMMENDATIONS	
Summary of Research.....	54
Conclusions.....	54
Recommendations.....	54
REFERENCES.....	56
APPENDIX A. TIRE MARKETING SURVEY.....	59
APPENDIX B. LOAD FRAME SCHEMATIC AND PARTS LIST.....	65
APPENDIX C. LOAD-CELL CALIBRATION.....	66
APPENDIX D. EXPERIMENTAL PROCEDURES FOR PRODUCING PRESSURE PRINTS.....	67
APPENDIX E. SMOOTH 11R24.5 LR-G MOVEMENT DATA.....	68
APPENDIX F. SMOOTH 11R24.5 LR-G TIRE PRESSURE HISTOGRAMS.....	70
APPENDIX G. WIDE-BASE 18-22.5 LR-H TIRE PRESSURE HISTOGRAMS.....	73
APPENDIX H. ADAGE PRINT ANALYSIS PROCEDURE.....	76
APPENDIX I. NUMERICAL PRESSURE MAP PROCEDURE.....	81

CHAPTER 1. INTRODUCTION

BACKGROUND

Within the last 10 years truck sizes, allowable loads, and tire inflation pressures have greatly increased. Tire manufacturers have been compelled to produce tires capable of operating at higher inflation pressures for various reasons.

- (1) Increased fuel costs have led tire manufacturers to attempt to decrease tire rolling resistance to increase fuel economy (Ref 1). One example is the production and marketing of wide-base super singles.
- (2) Higher inflation pressures are normally associated with increased axle loads (Ref 2).
- (3) High tire deflection due to low pressure leads to heat build-up and premature tire failure; high pressure tires will run cooler and, therefore, have a longer life (Ref 3).
- (4) Higher inflation pressure decreases the probability of hydroplaning and may influence skid resistance (Refs 2 and 3).
- (5) For a given load, a smaller tire may be used with a higher inflation pressure, decreasing the tire weight and thus allowing a greater pay-load to be carried (Ref 2).
- (6) Use of wide-base super single truck tires instead of dual rear tires decreases the tire weight, allowing a larger pay-load to be carried.

Item 6 is of special interest in this study because of the increased popularity of the wide-base super singles. Although weight savings appear to be the most important factor in the super single's popularity, other advantages also exist. The tire/wheel cost is reduced because it is less expensive to buy one super single tire and wheel than two dual tires and wheels. In addition, the vehicle handling ability is increased with super singles. It is also easier to maintain the single tire since it is not necessary to access an inside dual tire (Ref 4).

The increased popularity of super single tires has caused concern to pavement design engineers. In fact, the state of Utah has restricted their use through legislation. It appears the super single tire contact area is smaller than the contact area for a set of duals, and, therefore, higher pavement stresses are produced if pay-loads are not reduced. The super singles also have manufacturer-recommended inflation pressures as high as 120 psi, which may increase the contact pressure between the tire and the road surface, resulting in increased stress and strain within a pavement and decreasing pavement service life.

Although, historically, highway designers have attempted to counteract the effects of increased loading through improved pavement designs, pavement deterioration continues to increase. The actual pavement loading mechanisms and their magnitudes must be identified in

order to establish asphalt material properties capable of sustaining the increased loading conditions.

Current pavement design analyses assume a uniform pressure distribution nearly equal to the tire inflation pressure loaded over a circular tire-pavement contact area. Research has shown the actual tire-pavement contact area tends to have a non-circular pressure distribution and higher contact pressures, depending on the user and vehicle operating characteristics, tire manufacturer, tire type, wheel load, and tire inflation pressure.

OBJECTIVE

The objective of this study is to provide pavement design engineers with a better understanding of the actual contact pressures of tires currently running on U. S. highways. The results from this study will provide other research teams with data to confirm existing tire-pavement model pressures and to continue further research on pavement life management. The objective will be realized by studying and discussing results from related studies and by measuring tire contact pressure data for a smooth, radial, 11R24.5 load-range-G (LR-G) tire and a wide-base, bias, 18-22.5 load-range-H tire (LR-H).

SCOPE AND ORGANIZATION OF THE STUDY

Chapter 2 contains a brief summary of studies and results from similar experiments and from theoretical modeling. Descriptions of the tire types, test parameters, testing medium, and the testing apparatus used in the experiment are presented in Chapter 3. The pressure distribution data and results are discussed in Chapter 4. In Chapter 5 a summary, conclusions, and recommendations for the direction of future research are presented. Detailed descriptions of a tire marketing survey, load frame schematic, load cell calibration, experimental procedures, analytical procedures, smooth 11R24.5 radial tire movement data, and tire pressure histograms are contained in Appendices A through I.

RESEARCH AND APPROACH

To identify the pressure magnitudes, static testing was performed at The University of Texas at Austin on a smooth tread Armstrong 11R24.5, LR-G, and a wide-base Goodyear 18-22.5, LR-H, super single tire, at various inflation pressures and axle loads. Fuji prescale film was used to record the tire contact pressures. The images were then digitized using an Adage 3006 graphics system supported by a VAX work station in order to measure the tire contact pressures and display the data.

CHAPTER 2. RELATED STUDIES

It is essential, prior to experimentation, to study the existing state of knowledge relating to the proposed study. In order to identify tire-pavement contact pressures, the types of loading mechanisms must first be defined. To do so, a literature study of technical publications was carried out and the related information reviewed. These publications were also searched for suitable testing parameters, such as tire type, axle load, and tire inflation pressures, as well as existing tire technology, types of testing apparatus, analytical modeling methods, and the effects of increased tire inflation pressures. The summary and findings of the literature search are presented below, followed by conclusions.

SURVEYS OF TIRE TYPES AND INFLATION PRESSURES

In order to characterize the pavement loading mechanisms and their magnitudes, officials from various state Departments of Transportation conducted independent field surveys in Wisconsin (Ref 5), Texas (Ref 6), Montana (Ref 7), and Illinois (Ref 8). Additional surveys in New Mexico, Florida, and Washington have been mentioned in the literature, but their reports are currently unavailable (Refs 8, 3, and 9). The surveys were performed on trucks stopping at randomly selected, state-required weigh stations. The procedures, conditions, and items surveyed differed from state to state, but some measurements included tire size, tire type, manufacturer, axle load, inflation pressure, and tire temperature. Generally, the studies concluded that the tire inflation pressure varied according to tire type, size, and manufacturer.

The Wisconsin study tested 6,780 tires, and the most common brand observed was Michelin, followed by Goodyear and then Bridgestone. Wisconsin researchers discovered that the current recommended cold pressures exceeded those used in the AASHO tests (Ref 10), which were 70 to 80 psi, by 20 to 30 psi. When the surveyors allowed a 10 psi increase in tire inflation pressure to compensate for the heat caused by rolling resistance, they determined that 12 percent of the total survey population were still inflated by 10 psi above the manufacturer's recommended cold pressure. It was noted that, although this percentage may seem small, it can be significant when considering the effect in reducing pavement life. The report said the most common tire size observed was an 11-24.5 and the second was an 11-22.5.

In Texas 1,486 tires were measured and analyzed according to the type of truck on which the tires were mounted. The most prevalent truck type observed (70 percent) was a 3-S2, and it was used to carry most major types of commodities. Radials were the most common tire type, occurring twice as often as bias tires. The radial tires also had higher inflation pressures than the bias tires, but the researchers concluded that after adjusting for tire construction only a

small variation in inflation pressure existed. The maximum inflation pressure measured was 150 psi. The study also included an analysis considering five variables which may affect tire contact pressure, including tire construction, vehicle type, axle location, tire diameter, and tread depth. The Texas study concluded that axle location and tire diameter were insignificant and that tire construction was the most significant.

The Montana study reported 2,365 truck tires were measured during July and August, 1984. Their study showed that 81 percent of the tires observed were steel belted radials, with an average inflation pressure of 105 psi, and that 17 percent were bias ply, with an average inflation pressure of 84 psi. This study included measurements of ambient air temperature to determine its influence on the tire characteristics. It was reported that, as the ambient temperature rises, the tire temperature also rises, at approximately the same rate, but the tire inflation pressure is unaffected. They also reported that 11 percent of the truck tires had inflation pressures greater than 110 psi.

The Illinois data were never published but the results were made available through the Illinois Department of Transportation. The available data showed an average inflation pressure of 97 psi, with a high of 130 psi and a low of 52 psi. Their report did not include the number of tires observed nor the tire types.

To add to the field survey results available in the literature, tire manufacturers were polled to determine the most popular tire types currently running on U.S. highways. In September 1988 six leading tire manufacturers were contacted by telephone and then sent a survey letter from The University of Texas at Austin concerning popular truck tire marketing data. Five of the manufacturers responded: Michelin, Uniroyal Goodrich, Goodyear, Armstrong, and General Tire. Kelly Springfield did not respond, saying the requested information was proprietary. The Rubber Manufacturers' Association was also contacted but did not release any information, because the requested information was considered proprietary.

Most of the respondents answered that the majority of their truck tires marketed are radials; the exceptions were the Uniroyal Goodrich Company, which does not manufacture radial truck tires, and the Armstrong Tire Company, which said that only 40 percent of its total tire sales are radials. The responses indicated that the radial 11R24.5 load range-G (LR-G), radial 11R22.5 LR-G, bias 10.00-20 LR-F, and bias 11.00-22.5 LR-F are the most popular truck tires in use today. The most popular radial and bias wide-base super single tires are the 16.5R22.5 LR-J and 15-22.5 LR-H. The load range is a method tire manufacturers use to specify maximum recommended wheel loads. For example, the manufacturer's recommended maximum allowable wheel load for a single 11R24.5 LR-G tire is 6,430 pounds, and the

maximum allowable wheel load for a single 11R24.5 LR-H tire is 6,610 pounds. The survey letter, participants, and responses can be seen in Appendix A.

It appears from the literature that radial truck tires are becoming more predominant. Brown stated that use of bias tires is declining and that they are now replaced 80 to 100 percent by radials (Ref 3). Yeager also made similar comments when predicting future tire manufacturing trends (Ref 17). This also seems to agree with the operator/owner viewpoint, because, normally, radials can carry heavier loads and travel with less wear than bias tires (Ref 11).

The information from tire manufacturers and researchers is corroborated by truck operators, whose competitive environment forces them to carefully evaluate tire performance. Lee Butler, the tire supervisor for Central Freight Lines, Incorporated, related that, although radials have higher initial cost, bias tires cost more to operate because of their construction (Ref 4). The change to radials is also hastened by their increased safety margins, longer tread life, and lower rolling resistance, which results in increased fuel economy. The low profile radial, by design, has the same cross section whether loaded or unloaded, which results in better stress distribution, and improved travel wear, stability, cornering, and weight distribution. Because of the many advantages radial tires have over bias tires, Mr. Butler's company is converting almost completely to radials.

FUTURE TRENDS IN TIRE TYPES AND INFLATION PRESSURES

There is little available literature that predicts trends in tire design and manufacturing characteristics. However, what was obtained provided a data base from which some useful tire testing parameters could be selected. Most experts agree that the popularity of radials will continue to grow, especially in the case of all-season radials.

Yeager (Ref 17), while forecasting tire manufacturing trends, predicted that production of original equipment (OE) radial tires would continue at the 1983 rate through 2005. He also predicted that the amount of radial replacement tires would increase from 65 to 88 percent. The increase in radial production is apparently due to their increased wear life. Yeager states that, currently, the average set of radial automotive tires travels approximately 39,000 miles before being replaced, but some of the newer designs are capable of traveling 55,000 to 65,000 miles.

Because the all-season radial is fuel efficient and relatively quiet, and provides good traction on wet and snowy roads, it has become very popular. In 1990, 80 million all-season radials will be produced for both the OE and replacement markets. The all-season tire, with its performance capability and lower profile, is becoming more widely used. Yeager lists additional significant improvements for all-season tires, including new belt materials, improved handling, noise reduction, improved rolling resistance, and self-

sealing or run-flat capability with low pressure warning devices.

In order to reduce automobile costs, auto manufacturers are committed to eliminating the spare tire. They are experimenting with tires that are self-sealant or have run-flat capability. Yeager states that several major tire manufacturers currently have self-sealing tires and that a low pressure warning system is only a few years away.

Tire manufacturers are attempting to improve tire uniformity and further reduce rolling resistance by modifying design and production procedures and methods. Rolling resistance has also been reduced by increasing inflation pressures. This trend will continue to increase with the widespread use of low profile tires and variable comfort suspension systems. Roberts uses 125 psi inflation pressure in his theoretical study to establish material properties for thin asphalt concrete surfaces on granular bases (Ref 1). He justifies using this high pressure by stating that, although 125 psi may appear high, "representatives from tire manufacturers indicate within the next 5 years inflation pressures will continue to rise, to nearly 150 psi." He believes higher inflation pressures were brought about because increased fuel costs prompted the trucking industry to attempt to reduce rolling resistance and thereby increase fuel economy. Therefore, the tire manufacturers have responded by marketing both bias and radial tires that operate at higher inflation pressures.

Yeager believes the marriage of performance tires with all-season tires will dominate the tire market well into the 1990's. He expects that, by the year 2005, the performance and all-season tire will account for over 60 percent of the total OE and replacement market.

It appears likely that, within a decade, nearly a fourth of all auto tires will be made without human hands touching the material during the manufacturing process. Manufacturers are attempting to optimize tire uniformity by implementing computerized equipment. They are also performing various laboratory testing to determine wheel loads and slippage in order to reduce tread wear.

Another significant trend in truck tires is the replacement of dual tires with a wide-base super single. Pappagianakis and Haas (Ref 16) after interviewing tire manufacturers and trucking firms noted the increased popularity of wide-base super single tires. Bridgestone felt that within 10 years wide-base tires will be as common in North American trucking fleets as they are in Europe. The trucking firms of Labatt and Manitoulin Transport claim a superior performance for the wide-base tires as compared to conventional duals. The wide-based tires are mounted on non-driving axles and steering axles. Manitoulin also reported that wide-base tires have a longer service life. The drawbacks to wide-base tires appear to be the lower load limit commonly legislated for wide-base tires, vehicle down time, and inventory complexity (Ref 21). If load penalties for the wide-base tires are lifted, both fleet operators stated they

would use wide-base tires on all their non-driving axles. Both manufacturers and operators believe that, regardless of the current load penalties, the economical benefits obtained from using wide-base tires will cause their market to grow.

Zekoski, an engineer for the Goodyear Tire Manufacturing Company (Ref 21), believes radialization will continue to grow in applications that are traditionally bias-dominated, such as school buses, pick-up trucks, and delivery trucks, to increase fuel economy and driving factors. Zekoski also addressed the possible impact of European tires. He states that European tires generally are one load range higher than tires manufactured in the United States. Tires manufactured in the United States are built to the specifications of the Tire and Rim Association (T&RA). Recently, there has been a trend in Europe to manufacture tires having higher loads and inflation pressures to meet the increasing regional legal load limits. Zekoski believes that, as the global market place continues to mature, an increasing amount of these tires will enter the United States. The small, high-load tire, such as the 215/75R17.5, which has a suggested inflation pressure of 125 psi and a maximum load capability of 4,805 pounds, is a good example of tires which currently exceed T&RA allowable limits.

INFLATION PRESSURE EFFECTS ON OPERATOR COSTS

Vehicle and truck operators often believe that by reducing the rolling resistance of their tires they can achieve better fuel economy and thus lower operating costs. In order to reduce the rolling resistance, they increase the inflation pressure in their tires. Studies show that, although the majority of truck operators maintain tire inflation pressures within the manufacturer's recommended standards, some operators do not. Field data show that tire inflation pressures range between 40 and 150 psi, with the majority falling between 95 and 105 psi (Refs 3 and 6). As much as 12 percent of the tires surveyed in the Wisconsin study were over-inflated.

As was discussed previously, to better understand what inflation pressures are being used, it would be beneficial to know what causes an operator to vary his tire inflation pressure. Ultimately, it must be economics, but what proportion do tire expenditures represent of the total operator costs? Butler stated, "Tires are the number two cost in maintaining a fleet, second only to fuel" (Ref 4). In order to minimize the cost, proper tire maintenance is essential. Butler stated that improper inflation pressure accounts for more than 80 percent of required tire and truck service. He further discussed the results caused by tire over-inflation, under-inflation, and proper inflation, which are summarized below.

Results of Over-Inflation

A rolling tire that is over-inflated is more rigid and will not absorb road shocks properly, and, therefore, over-

inflation is detrimental to the vehicle suspension system. The tire becomes subject to impact breaks and is more likely to be cut, snagged, or punctured. Also, overstress is produced in the rim, possibly shortening rim life and increasing costs.

Costs are also increased because increasing the tire inflation pressure never improves tire performance or strength but, rather, it decreases the tire service life. An increase in air pressure above the manufacturer's rated specifications will not increase load carrying capacity, but will cause premature wear in the center or the crown of the tire, reducing tread mileage, and, thereby, increasing tire cost. Irregular tire carcass shoulder wear is also caused by over-inflation, which reduces the possibility for retreading.

Results of Under-Inflation

Under-inflation not only causes higher rolling resistance, thereby decreasing fuel economy, but increases stress in the shoulder areas of the tire. Thus, abnormal flexing occurs in the shoulders and sidewalls, which produces excessive heat. The heat breaks down rubber compounds or causes ply separation, resulting in lost tire strength. If heat build up continues the tire eventually blows out. An increase in heat also may shorten the tire's carcass life by decreasing its possibility of being retreaded.

The problems caused by under-inflation are increased when dual tires are used. If the two tires have different inflation pressures, the larger tire carries the majority of the load and possibly becomes overloaded. The smaller tire will scrub, causing irregular wear and resulting in shorter tread life.

Results of Proper Inflation

Properly inflated tires are more likely to distribute the load evenly, and, therefore, they have greater stability and lower rolling resistance. This combination results in increased fuel economy. The tires run cooler and have the proper casing deflection, thus increasing tire service life. The operator and cargo will be safer because the proper tread footprint is maintained. This proper footprint not only decreases the chance of hydroplaning but also allows proper braking and traction.

Butler (Ref 4) estimated that maintaining the proper inflation pressure can reduce tire costs by up to 20 percent. These cost savings are made through such things as improved retreadability, resulting in a lower tire cost per mile. A smoother ride also reduces costs because less damage to the vehicle suspension occurs if the proper load carrying capacity is maintained. From the operator's standpoint, it is very important to maintain the proper tire inflation pressure. Thus, it is reasonable to assume that most operators stay within the recommended load range and inflation pressure of their tires simply because of the cost saving incentives mentioned above.

GENERAL TIRE CONTACT PRESSURE CHARACTERISTICS

Currently very little data are available concerning truck tire contact pressures. Normally it is common in pavement design to assume the tire contact pressure distribution is circular and that the contact pressure is equal to the tire inflation pressure, as described by membrane theory. This section describes membrane theory and background and discusses more recent studies in tire contact pressure characteristics.

Membrane Theory and Historical Background

It is known that, if an inflated membrane lacking any bending stiffness (e.g., an infinitely thin wall) is in contact with a flat surface, the contact pressure at each point is equal to the membrane's inflation pressure. The ideal footprint would be circular, but in actuality a tire footprint is somewhat more rectangular. This line of reasoning indicates the primary component of the vertical contact pressure is the internal inflation pressure (Ref 12). Therefore, current tire data bases are comprised of inflation pressures, not tire/pavement contact pressures. These models are hardly accurate because carcass stiffnesses as well as the stiffness in the sidewalls prohibit equal pressure distribution in the contact area (Ref 18). To obtain a better knowledge of actual pavement loading it is helpful to understand the characteristics which influence the tire contact area. The actual contact area is a function of speed, inflation pressure, wheel load, wheel camber, steering, braking, vehicle suspension, and tire configuration, among others.

Knowledge of how a wheel load is transmitted to the road by a tire is essential to pavement design. The actual process a tire goes through when transferring an axle load to pavement is described by Tielking and Roberts (Ref 13). They state that a tire supports the axle load by establishing a contact area (footprint) between the tread and pavement surfaces. Changing the axle load or the tire inflation pressure altered the tire's footprint. As the load is adjusted changes in inflation pressure are slight, but when either the load or the inflation pressure is altered, the tire's contact area and shape are altered significantly.

Tire-Pavement Contact Stresses

In order to characterize the stress applied to the pavement by a tire, it is advisable to first define the stress components, their orientation, and causes. In this section the stresses are divided into components and some are subdivided into subcomponents.

Stress Components and Orientation. The tire-pavement contact force can be represented by two components, one perpendicular to the contact surface, called the normal component, and one tangential to the contact surface. This latter component may be further subdivided into two subcomponents, each lying in the contact plane.

One is parallel to the central plane of the tire and is called the longitudinal stress component; the other is perpendicular to the central plane of the tire and is called the lateral stress component (see Fig 2.1).

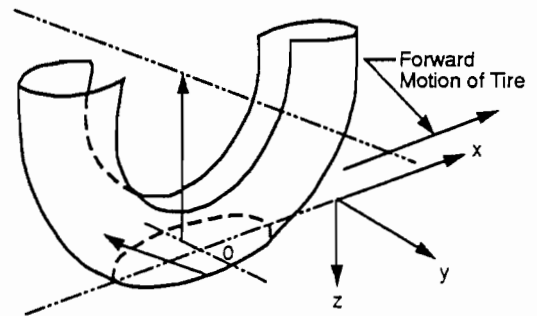


Fig 2.1. Force diagram representing the total reaction of the ground to the tire expressed as the combined effect of two forces, one normal and one tangential to the ground plane (Ref 12).

Longitudinal Shear Pressure. The two tangential sub-components, lying in the contact plane, are generally called the shear components. The shear components are created when an inflated tire is deflected against the pavement, causing the doubly curved surface of the tread to become a flat surface. When the tire is vertically deflected against a flat surface, the motion is restrained by friction between the tire and pavement, creating perpendicular horizontal shear components of contact pressure [see Fig 2.2(a)].

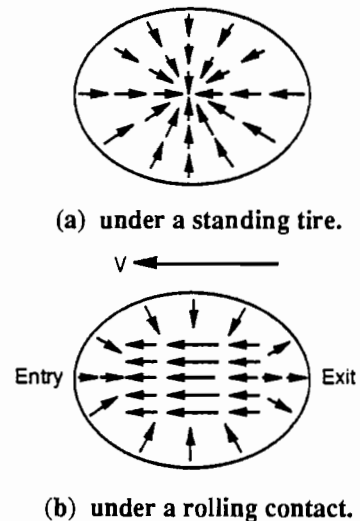


Fig 2.2. Direction of pavement shear forces (Ref 13).

When the tire rolls freely without camber, the shear pressure is redirected due to the superposition of an angular velocity on the tread surface. The longitudinal component of tire force on the pavement changes direction twice, as can

be seen in Fig 2.2(b). Bonse and Kuhn experimentally confirmed this in 1959 by rolling a tire over a circular force-measuring stud placed in a manhole cover (Ref 19).

Lateral Shear Pressure. The paths of two tread ribs can be seen in Fig 2.3. As the tread is flattened against the

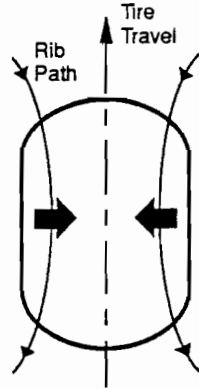


Fig 2.3. Rib path through the contact region of a rolling tire (modified from Ref 13).

pavement, the ribs are pulled toward the footprint center. Friction inhibits the ribs inward movement, creating a lateral shear pressure. Tielking and Roberts believe the magnitude of the lateral shear is dependent on tire construction, with the radial tires producing about 50 percent lower peak pressure values than bias tires. They also believe the lateral shear applies a much higher stress to the pavement than longitudinal shear pressure does. The experiments performed by Bonse and Kuhn, in which various vehicle tires were driven over a circular force measuring stud, seem to support this trend for automobile tires also (Ref 19).

Factors Affecting Contact Pressure Distributions

Although many factors, such as speed, steering, tire camber, braking, inflation pressure, pavement friction, and wheel load, affect the load components of the contact pressure distribution, published articles tend to be narrow in scope, discussing only one or two of the above stated variables. For this report the majority of the discussion is limited to inflation pressure, wheel load, speed, steering, and pavement friction.

Inflation Pressure and Wheel Load. Tielking and Roberts (Ref 13) state that the major influences on tire-pavement contact pressure are inflation pressure and axle load. In view of the small effects of speed and pavement friction on the normal pressure distribution for a free-rolling tire, it is believed that the normal contact pressures measured with nonrotating tires deflected against a frictionless surface are a realistic representation of the normal pressures under a real tire traveling at highway speeds. Therefore, significant effects of pavement deterioration accelerated by changes in inflation pressure and/or axle load can be studied using

contact pressures measured from a statically loaded tire. Zekoski contradicts this by stating the normal and horizontal components vary if they are examined in a static versus dynamic condition but does not explain his reasoning (Ref 21).

The earliest approach to quantifying the average contact pressure was to statically load a tire to a known value while simultaneously making an ink footprint. To calculate the contact pressure the known load was then divided by the footprint's area. Problems existed with this method, the greatest of which was the lack of a suitable method for determining contact pressure distributions and pressure quantities. Lippman and Oblizajek performed a variation of this experiment by producing a footprint and then multiplying the footprint area by the tire inflation pressure to obtain the load borne by the tire. When this value was compared to the actual load applied to the tire, a difference of 30 percent was not uncommon (Ref 15). The authors concluded that differences in the normal pressures from the inflation pressures are due to structural mechanisms, such as bending, local carcass and belt tensions, and buckling at the crown center. This proved that membrane theory was not appropriate for quantifying tire-pavement contact pressures.

In order to better quantify the foot-print pressures Lippman and Oblizajek used transducers to measure the actual contact pressures. The transducers were placed so as to measure the contact pressure at the center of each rib of a freely rolling tire moving at a velocity of 2 to 3 miles per hour. The measurement locations for three locations on a five-ribbed tire can be seen in Fig 2.4.

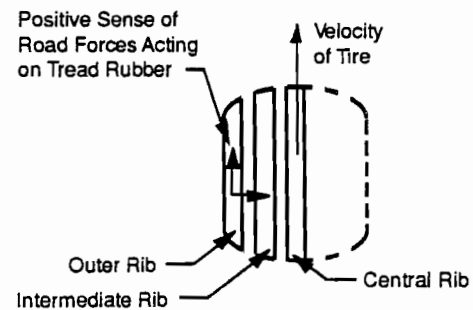


Fig 2.4. Identification of measurement locations for a five-ribbed tire (modified from Ref 15).

The trends in the pavement normal force distribution and both horizontal force distributions for each rib of a radial-ply tire loaded to 1,580 pounds and inflated to 26 psi can be seen in Figs 2.5, 2.6, and 2.7, respectively. In Fig 2.5 the normal contact pressure measured by transducers as the tire was rolled over at zero camber is shown. Note that the outer two ribs have slightly larger contact pressures and that the contact pressures are fairly constant throughout the contact area.

In Fig 2.6 the longitudinal shear force distribution for the same five-ribbed radial-ply tire is plotted. Note that the longitudinal stresses of the three internal ribs change direction twice, as previously discussed and also as shown in Fig 2.2(b). The result may sometimes be that the average traction over the length of the contact zone is zero, but for the entire tire's contact zone the resulting traction is generally equal to the rolling resistance of the tire.

The tractions on the right side of the median plane tend to oppose the forces on the left side, as shown in Fig 2.7, in which the lateral shear stresses are plotted. Lippman states that the lateral component tends to be negligible at the median plane of the tread, as required by symmetry. Lippman observed that the lateral traction in a free-rolling tire often rises continuously through the tire contact interface and then falls continuously during the exit half of the contact patch. The inflation pressure determines the length of the contact area, deflection of the tire, magnitude of the fore and aft forces, and magnitude of the contact pressure. Research performed by Seitz and Hussman, Bonse and Kuhn, and Ginn and Marlow exhibited similar trends for normal, lateral, and longitudinal stresses (Refs 18, 19, and 20, respectively).

The work performed by Lippman and Oblizajek measured the contact pressures for steel-belted radial-ply, glass-ply bias-belted, and 4-ply bias-belted tires. For a constant inflation pressure of 26 psi and loads of 1,580, 1,185 and 1,975 pounds, the maximum values of normal pressure usually occurred at the outer lateral edges of the footprint as shown in Fig 2.5. Normal contact pressure values lower than the inflation pressure sometimes occurred and were attributed to structural mechanisms, such as bending, local carcass and belt tensions, and buckling at the center crown. Contact pressures higher than inflation pressure can be attributed to tire design, which accounts for sidewall and tread stiffness, and to grooves and voids in the tread. These grooves and voids in the tread cause the pressure under the ribs to be higher than the inflation pressure because they must partially support the inflation over these grooves and voids. Although the maximum pressure seemed to always be at the outer ribs, the steel-belted radial tires tended to have a more uniform pressure distribution within the footprint than either the glass-ply and bias-ply tires did. In fact, the glass-ply and bias-ply tires had two and three times higher pressures, respectively, at the tires' outer ribs than at the inside ribs. The higher pressures

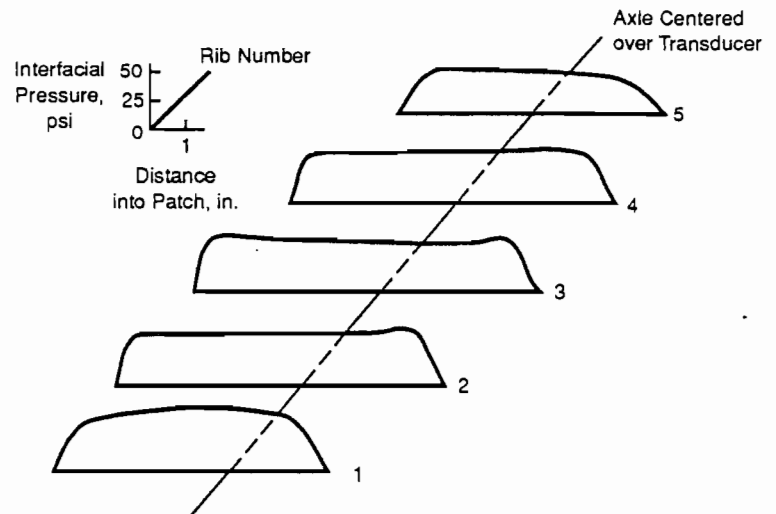


Fig 2.5. Pavement normal force distribution for radial-ply at 26 psi and axle load of 1,580 pounds (Ref 15).

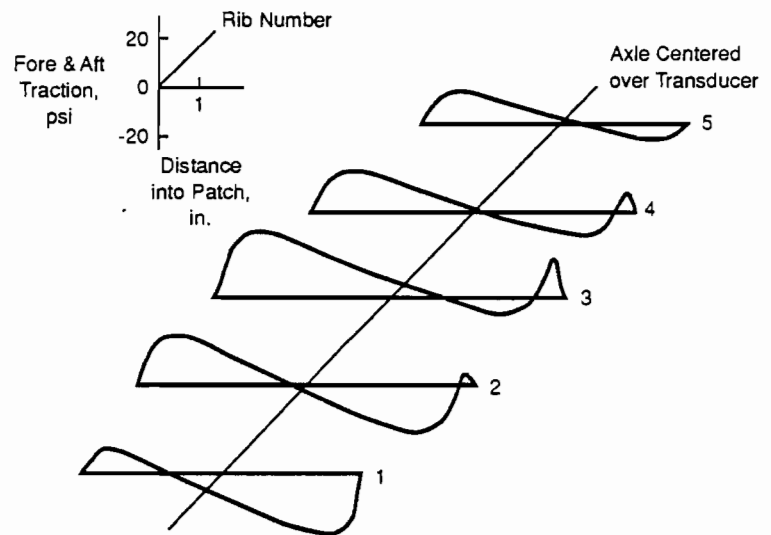


Fig 2.6. Pavement longitudinal shear force distribution for radial-ply at 26 psi and axle load of 1,580 pounds (Ref 15).

in the glass and bias-ply tires as opposed to radial tires can be attributed to stiffer side wall construction. The maximum normal pressure values ranged from 70 to 150 psi for bias-belted and radial-ply tires inflated to 24 psi and 55 to 60 psi, respectively. A common longitudinal component for freely rolling tires was 60 psi.

As the wheel load is increased, the normal contact pressure at the central ribs is redistributed slightly but the majority of the increased wheel load results in an increased contact area length. The outer ribs not only increased in

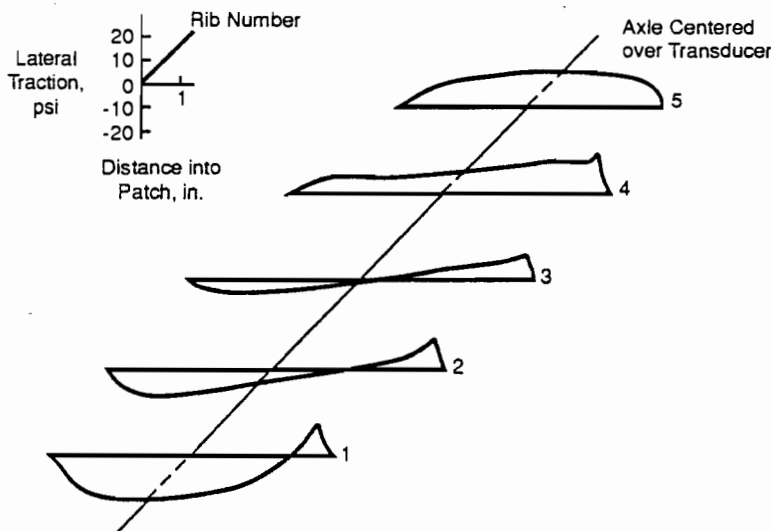


Fig 2.7. Pavement lateral shear distribution for radial-ply at 26 psi and axle load of 1,580 pounds (Ref 15).

contact length but also increased in average pressure values. Lippman and Oblizajek attributed this phenomenon to the growing bending stresses in the tire's sidewall and buttress regions combined with an increased sidewall overhang beyond the tread edge. The increased overhang results in an additional vertical component of air pressure acting on the inner surface of the sidewall beyond the tread edge. This subsequently causes the transmission of reaction forces to the two outer ribs and their two adjoining ribs.

While conducting research to determine the contact pressure characteristics of a freely rolling tire, Seitz and Hussman (Ref 18) also determined that tire inflation pressure has a large influence on a tire's contact pressure distribution. Within the operating range of a conventional automobile tire, higher inflation pressures led to more uniform contact pressures. In other words, as the inflation pressure increased, the centerline's contact pressure also increased while the shoulder's contact pressure remained relatively unchanged. The authors also noted that the contact pressure for bias tires was more sensitive to speed than it was for radial tires. As the speed was increased the contact pressure below the sidewalls decreased while the centerline contact pressure increased. They concluded that the horizontal stress is mostly affected by speed, not inflation pressure, whereas the normal stress is mostly affected by inflation pressure, not speed. Work conducted by Bonse and Kuhn (Ref 19) also concluded that tire inflation pressure has no effect on horizontal stress but does affect the normal stress.

Zekoski, performing experiments for Goodyear Tire and Rubber company (Ref 21), made similar conclusions concerning normal stresses. Using line haul operating conditions, which are characterized by long distance intercity

mileage, he assumed that cold inflation pressures were the same all around the vehicle and did not adjust them for load changes. As the wheel load was increased at a constant inflation pressure, the shoulder contact pressure increased relative to the unchanged centerline contact pressure. Figure 2.8 illustrates that bias-ply tires tend to be more sensitive to wheel loading than radial tires. Zekoski stated that, for an increase of one pound of load, the bias tire's shoulder pressure increased 0.03 psi versus a 0.02-psi increase for the radial tire. In contrast, when the inflation pressure was increased at a constant wheel load, the tire's shoulder contact pressure did not increase. The increased inflation pressure caused an increase in centerline contact pressure relative to the unchanged shoulder contact pressure. Figure 2.9 shows that radial-ply tires tend to be more sensitive to tire inflation pressure than bias-ply tires. For a one-psi increase in inflation pressure the radial tire's centerline pressure increased 1.5 psi, whereas the bias tire's inflation pressure increased one psi.

Zekoski concluded that the maximum contact pressure's sensitivity to wheel load and inflation pressure depends on the shape of the lateral cross-section of the normal contact pressure distribution. For example, if the centerline contact pressure is greater than the shoulder contact pressure, and inflation pressure is increased while maintaining a constant wheel load, the maximum contact pressure will increase. However, if the shoulder pressure was the greatest, increasing the inflation pressure would have little effect on the maximum contact pressure.

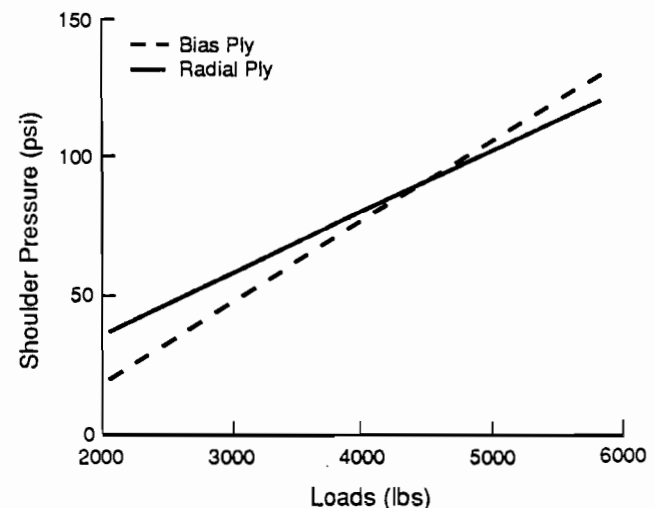


Fig 2.8. Shoulder pressure versus wheel load for bias-ply and radial-ply tires (modified from Ref 21).

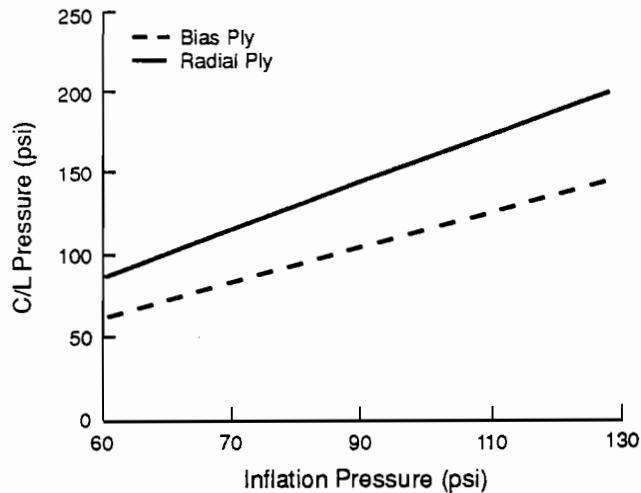


Fig 2.9. Centerline pressure versus tire inflation pressure for bias-ply and radial-ply tires (modified from Ref 21).

In order to quantify contact pressure magnitude, Zekoski compared contact pressures for bias-ply and radial-ply duals and wide-base super singles. The tires Zekoski tested are listed in Table 2.1.

In Fig 2.10 the maximum contact pressure values relative to operation inflation pressures are plotted. The single wide-base tires have larger contact pressures than either the bias or radial-ply duals, and the 385/65R22.5 wide-base singles have a contact pressure almost twice their inflation pressure. Zekoski reported the maximum contact pressure for the bias duals inflated to 100 psi was 105 psi, for the radial duals inflated to 105 psi was 130 psi, for the 385/65R22.5 wide-base single inflated to 130 psi was 190 psi, and for the 425/65R22.5 wide-base single inflated to 120 psi was 155 psi, all at the same wheel load. As can be seen in Fig 2.10, the wide-base singles had much higher contact pressures than the bias-ply or the radial-ply duals.

In order to show a correlation between inflation pressure and average contact pressure for use in design, Van Vuuren (Ref 2) plotted contact pressures versus tire inflation

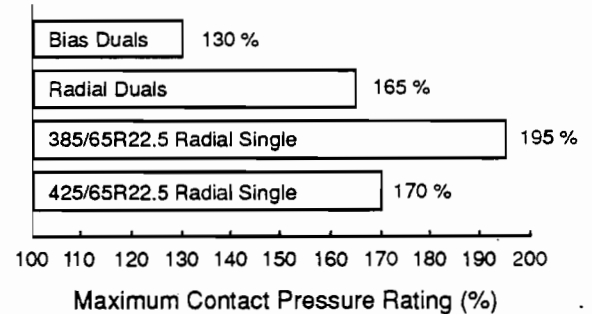


Fig 2.10. Maximum contact pressure relative to inflation pressure (modified from Ref 21).

pressures. An equation enabling the prediction of the average contact pressure from a given inflation pressure was obtained. From Fig 2.11 he concluded that, for a constant wheel load, the change in contact pressure is only about 30 percent of the change in the inflation pressure.

Speed and Pavement Friction. Although researchers Tielking and Roberts (Ref 13) primarily investigated the effect of inflation pressure and wheel load on contact pressure, they also conducted a small study of the effect of speed and pavement friction. Their results showed that both speed and pavement friction only slightly influence the contact area. If the speed or pavement friction is increased, the contact area is only slightly increased. Seitz and Hussman confirmed the speed phenomenon in their study (Ref 18).

To quantify the effect of speed, Bonse and Kuhn (Ref 19) drove various vehicles having various types of tires over a circular force measuring stud having a cross-sectional area of one square inch and a stress recorder box mounted inside a manhole cover. They found that vehicle speed had no significant effect on the normal stress but did have an effect on the horizontal shear stresses. With a tire inflation pressure of 28 psi the normal pressure measured at the tire centerline was 30 to 44 psi. At an inflation pressure of 70 psi the peak force at the centerline was 70 to 88 psi, and the maximum peak force was 15 to 24 psi greater at the edge than at the center. At constant speed the longitudinal stress for a car tire was 11 psi and for a truck tire was 22 psi. During acceleration or deceleration the longitudinal stress increased up to 40 psi. The lateral pressures were zero psi at the tire's center and 33 psi near the edge, and the direction of the lateral stress was always towards the footprint's center.

While conducting research to determine the contact pressure characteristics of a freely rolling tire, Seitz and Hussman (Ref 18) noted that the contact pressures for bias tires were more sensitive to speed than those for radial tires. As the speed was increased, the contact pressures below the sidewalls decreased

TABLE 2.1. TIRES TESTED BY ZEKOSKI IN ORDER TO QUANTIFY CONTACT PRESSURE MAGNITUDE (REF 21)

Axle Configuration	Ply Type	Tire Size	Recommended Cold Inflation Pressure (psi)
Duals	Bias	1000-20/22	85
		11-22.5/24.5	85
	Radial	11R22.5/24.5	105
		285/75R24.5	110
		295/75R22.5	110
Wide-Base Singles	Radial	385/65R22.5	120
		425/65R22.5	110

while the centerline contact pressure increased. They concluded that the horizontal stress is mostly affected by speed, not inflation pressure, whereas the normal stress is mostly affected by inflation pressure, not speed.

Steering. Lippman and Oblizajek (Ref 15) measured the contact pressures for steel-belted radial-ply, glass bias-belted, and 4-ply bias-belted tires at a constant inflation pressure of 26 psi and loads of 1,580, 1,185 and 1,975 pounds. Their data show that generally the maximum values of normal pressures usually occurred at the outer lateral edges of the footprint. When they altered the steering angle by one degree, only a slight redistribution of pressure and an increase in lateral pressure occurred. No difference in footprint area was documented for either the glass-ply or the bias-ply tires. In contrast, the one degree steering angle modification caused the steel-belted radial tire's footprint to shorten on one side and lengthen a similar amount on the other side. Lippman and Oblizajek attribute this phenomenon to the twisting distortion of the relatively rigid belt structure in the radial tire. Steering results in the broadening of the slip region at the end of the footprint area, releasing stresses, and therefore decreasing the load.

TIRE CONTACT PRESSURE AND ITS EFFECT ON FLEXIBLE PAVEMENT LIFE

A pavement must be able to provide the load bearing surface for which it is designed. This depends on the expected traffic loads, density of traffic, and desired service life. The pavement must maintain an adequate surface condition such that it is able to permit comfortable and safe driving within the design speed limit. The service life is dependent on the actual loading the pavement receives. Traditionally, pavement design engineers have been primarily concerned with only the wheel loading effects, but, recently, additional research efforts have investigated how environmental loading and pavement structure affect asphalt pavement life. The discussion below is limited to stresses in an asphalt pavement system caused by wheel and inflation pressure, base and surface modulus effects, and thickness.

Wheel Load and Inflation Pressure Effects

This section includes research summaries pertaining to the effects of wheel and inflation pressure on asphalt pavements as well as studies that discuss the influence wheel loads and inflation pressures may have on pavement fatigue and rutting.

Studies Discussing Wheel Loads and Inflation Pressures. Chen (Ref 27) used various computer pavement models to determine the difference between uniform and nonuniform contact pressure distributions on asphalt pavement systems. The uniform contact pressure was equated to the inflation pressure, according to traditional membrane

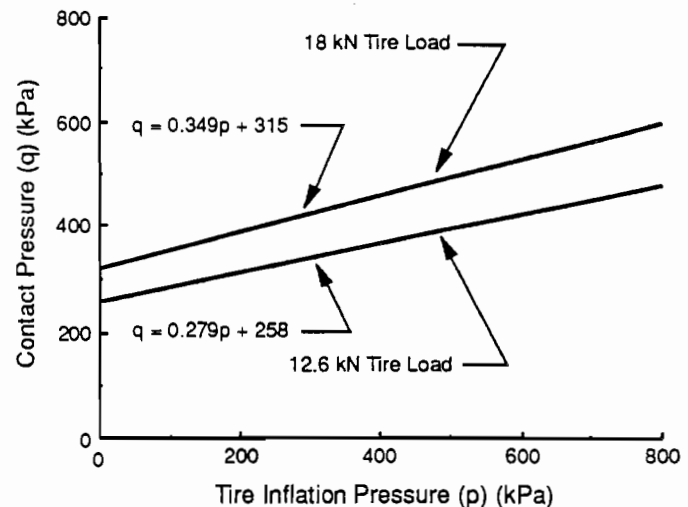


Fig 2.11. Relationship between tire inflation pressure and contact pressure for constant wheel load (Ref 2).

theory, but the nonuniform contact pressures were based on experimentally produced contact pressures. Chen used TEXTGAP-3D, a linearly elastic, finite element program, to predict the performance of Texas farm-to-market flexible pavements under various inflation pressures and wheel loading conditions. The computer model used inflation pressures of 75, 90, and 110 psi and wheel loads of 4,500 and 5,400 pounds. Chen assumed the nonuniform pressure distributions were symmetrical about the tire print's longitudinal and lateral axes, and, therefore, he needed to analyze only one-quarter of the tire-pavement interaction.

Chen found that an increase in inflation pressure from 75 psi to 110 psi results in an approximate increase of 102 microstrain (1 microstrain = 1×10^{-6} inch/inch) at the bottom of a 1.5-inch-thick pavement (Fig 2.12). The figure also shows that as the pavement thickness increases the effect of tire pavement contact pressure decreases.

Chen also compared the tensile strains at the bottom of the pavement surface calculated using the TEXTGAP-3D uniform pressure model with those of layer program ELSYMS5 using a circular uniform pressure model. The ELSYMS5 model tended to over predict the strains, except for the 1.5-inch-thick pavement (see Fig 2.12).

Figure 2.13 shows the effect of wheel load on critical tensile strain for both the experimental uniform pressure model and the theoretical uniform pressure model. For both models, as the load increased, the tensile strains at the bottom of the pavement surface also increased.

Figure 2.14 shows that an inflation pressure increase of 47 percent produced an insignificant increase in compressive strain at the top of the subgrade for both theoretical uniform pressure and experimental nonuniform pressure models. Chen reported that the uniform pavement model consistently produced larger subgrade compressive strains, except for thick surface pavements.

Figure 2.15 shows that the wheel load has a significant effect on the compressive strains at the top of the subgrade for both uniform pressure and nonuniform (experimental) pressure models. The figure shows that for a 20 percent increase in wheel load there is a corresponding 20 percent increase in subgrade compressive strain.

Tielking (Ref 13) reported that in pavement analysis an empirical approach is inappropriate when tire contact pressure effects are considered because the current pavement condition is the result of past traffic applications with varying and unknown inflation pressures. Tielking developed a model which could input various tire parameters, such as inflation pressure, tire deflection, and tire rigidity. He then computed tire-pavement contact pressures for a 10.00-20 F nylon cord truck tire. The calculations were performed using representative conditions currently found on Texas highways. The inflation pressures were 75 and 125 psi and the wheel load was 4,500 pounds. The calculated contact pressures are shown in Fig 2.16, from which it can be seen that an increase in inflation pressure caused a decrease in contact area and, subsequently, increased contact pressures.

Roberts and Rosson (Ref 6) used a modified version of the finite element program ILLIPAVE in order to determine the required material properties for the proper performance of an asphalt pavement. The modifications allowed a nonuniform contact pressure distribution to be input for a tire foot-print symmetrical about the footprint's centerline. The tire modeled was Tielking's 10.00-20 bias-ply truck tire loaded to 4,500 pounds and inflated to 75 psi and 125 psi, as shown in Fig 2.16. In Fig 2.17 the effect of the change in inflation pressure on the tire contact pressure can be seen.

Roberts and Rosson noted that as the inflation pressure increased, the tensile strain, for various surface thicknesses, decreased (see Fig 2.18). The data in Fig 2.18 were produced by modeling various thicknesses of an asphalt pavement having a modulus of 400 ksi over an 8-inch-thick base having three different stiffness moduli. For a thin surface on a low modulus base, the tensile strains were near or exceeding 1,000-microstrain, which Monismith (Ref 26) considers to be the upper limit for linear behavior of asphalt concrete mixes.

Roberts and Rosson also compared the strains calculated using the uniform contact pressure model (having a contact pressure equal to the inflation pressure) with the strains calculated by the nonuniform contact pressure. The horizontal arrows for both pressure types demonstrate that as inflation pressure increases the tensile strain also increases, but the nonuniform contact pressure results in much higher strains. For a surface thickness of 2 inches or less the tensile strains are almost 100 percent higher. For thick pavements the strains increase but the change in strain is much less (Fig 2.19).

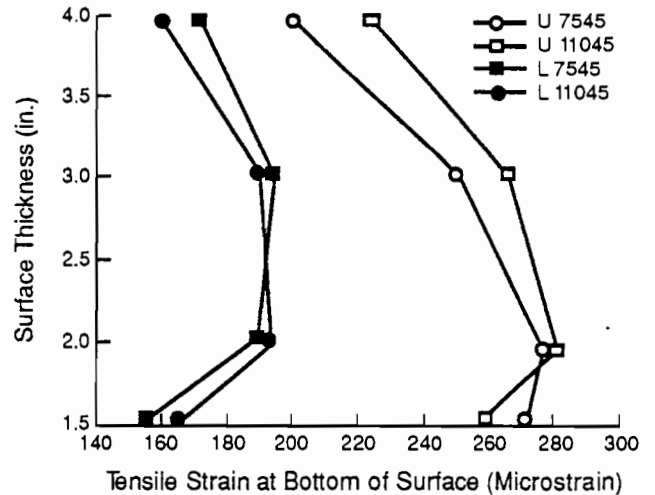


Fig 2.12. Effects of Pressure Distribution model on critical tensile strain at the bottom of the surface. [Note: U and L, respectively, represent the results obtained using TEXGAP-3D and ELYSYM5. The values 7545 and 11045 are for a wheel loaded at 4,500 pounds with inflation pressures of 75 and 110 psi, respectively (Modified from Ref 27).]

Studies Discussing Fatigue. Traditionally fatigue has been associated with high tensile strains in the bottom of the pavement surface layer. Chen used the tensile strains computed by TEXGAP-3D at the bottom of the asphalt layer to approximate the number of 18-kip axle load applications required to cause alligator cracking to appear. By substituting the tensile strains computed from TEXGAP-3D into

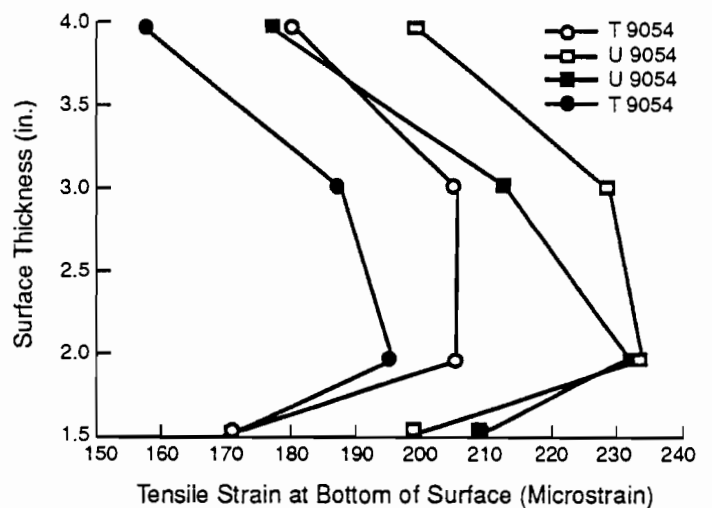


Fig 2.13. Effects of axle load on critical tensile strain at the bottom of the surface. [Note: T designates a treaded tire with nonuniform (experimental) pressure model, and U designates a uniform pressure model. The values 9045 and 9054 represent, respectively, a 90 psi tire inflation pressure with loads of 4,500 and 5,400 pounds (Ref 27).]

Eqs 2.1 and 2.2, the number of loads of constant stress were predicted:

$$\log N_f (10\%) = 15.947 - 3.291 \log e_i - 0.854 \log E^* \quad (2.1)$$

$$\log N_f (45\%) = 16.086 - 3.291 \log e_i - 0.854 \log E^* \quad (2.2)$$

N_f = the number of loads of constant stress necessary to cause fatigue cracking,

e_i = the initial tensile microstrain at the bottom of the surface, and

E^* = the complex modulus of the asphalt-concrete surface (ksi).

Figure 2.20 shows the effect increasing the inflation pressure has on fatigue damage life for various surface thicknesses for cracking that is less than 10 percent and greater than 45 percent of the wheel path area. As can be seen, an increase in inflation pressure (for a constant wheel load) results in a significant increase in surface tensile strain and therefore a significant decrease in pavement service life for both the 10 percent and 45 percent cracking models. For a 2-inch pavement a 47 percent increase in inflation pressure resulted in 33 percent reduction in pavement life. Figure 2.21 shows that for increased wheel load, at a constant inflation pressure, a reduction in pavement life for both fatigue cracking models occurred. For a 4-inch pavement, a 20 percent increase in wheel load resulted in a 36 percent reduction in pavement life.

Earlier pavement modeling was performed by Van Vuuren (Ref 2), using the Chevron computer program to analyze various linear elastic pavement structures under many combinations of wheel loads and inflation pressures. He attributed high contact pressure to four types of pavement failure: (1) fatigue of the surface layer, (2) fatigue of cement stabilized bases, (3) surface densification, and (4) consolidation of the subgrade.

Van Vuuren also attributed pavement fatigue to excessive horizontal tensile stresses and strains in the bottom of the surface layer. For a 1.97-inch (50-mm) pavement, his model showed that an increased wheel load caused a decrease in horizontal tensile stress at the bottom of the surface layer. This implies that higher wheel loads were less detrimental to an asphalt pavement than lower wheel loads, for tires kept at a constant contact pressure. However, it is very seldom that a reduction in wheel load is not also associated with a decreased contact pressure, as lighter vehicles are generally fitted with tires which operate at lower inflation pressures (58 psi). He computed that, for dense-graded premix and high stiff gap-graded premix surfaces, a contact pressure of 87 psi will require as many as 10^6 to 10^7 load repetitions to initiate cracking. Thus, contact pressures larger than 87 psi should be avoided.

Van Vuuren's results show that pavement failure caused by the failure of a cement-stabilized base could be primarily attributed to increased wheel loads. He said that an increase in wheel load would cause a far higher increase

in the cement-stabilized base's horizontal tensile strain than would an increase in contact pressure. Therefore, the cement-stabilized base is much more sensitive to changes in wheel load than increased contact pressures.

Failure caused by the surface densification of thick asphalt pavements was shown to occur at contact pressures of 41 psi and 84 psi. This was determined using the stable state of air voids content (a measure of compaction under a repeated load) for various mixes at various temperatures. Van Vuuren's results indicate that for the same mixture under similar environmental conditions, contact pressures of 41 and 84 psi caused an average permanent deformation of about 3 and 4 percent, respectively.

Finally, Van Vuuren stated that pavement failure induced by soil subgrade consolidation could not be attributed to an increase in contact pressure. An increase in contact pressure is mostly dissipated throughout the the asphalt layer and does not cause significant increases in the subgrade stresses and strains. In other words, soil subgrade consolidation is caused primarily by increased wheel load, not increased contact pressure.

Studies Discussing Rutting. Traditionally, rutting has been associated with high compressive strains at the top of the subgrade. It is generally distinguished in two separate types: (1) rutting caused by mechanical abrasion and (2) rutting due to irreversible deformations.

In order to measure horizontal pavement deformation, Eisenmann and Hilmer (Ref 25) repeatedly rolled both single and dual tires over a steel box containing an asphalt test specimen placed on top of a rubber plate. The rubber plate represented the soil subgrade. The specimens were cut perpendicular to the rolling direction and pavement displacements measured. The vertical deformation was reduced by lowering the wheel load and using duals rather than single tires. Horizontal deformation occurred at both the surface and the upper region of the asphalt base course, and, therefore, rutting is also a resultant of lateral displacement of the material in the pavement surface and base. These lateral shifts of the material were observed in the asphalt cross-section.

Eisenmann and Hilmer also stated that rutting caused by irreversible deformation may be prevented either by optimizing the pavement design and construction, such that the heavier loads and inflation pressures can be sustained, or by optimizing the loads and conditions, so that the asphalt design strength and integrity is not exceeded. Eisenmann and Hilmer felt that rutting is influenced by a change in wheel load as well as a change in the inflation pressure.

Eisenmann and Hilmer concluded that rutting can be influenced by a combination of both wheel load and tire inflation. Theoretical investigations based on the elastic multilayer theory using computations made by BISAR, an elastic layer computer model, showed that increases in the wheel load, at constant inflation pressure, resulted in increased deformation in the lower regions of the pavement.

Conversely, a change in inflation pressure at a constant load caused deformation at the pavement surface.

Chen (Ref 27) stated that rutting can be attributed to high compressive strains and permanent deformation in the subbase. Figure 2.22 shows the effect increasing the wheel load has on the subgrade rutting damage life for various surface thicknesses. The number of loads required to cause rutting was calculated by substituting in the strain computed by TEXGAP-3D into Eq 2.3 :

$$W_{18} = 6.15 \times 10^{17} (1/e_c)^{4.0} \tag{2.3}$$

where

- W_{18} = the number of weighted 18-kip axle loads before excessive permanent deformation, and
- e_c = the compressive microstrain at the top of the subgrade.

As the wheel load is increased the subgrade compressive strain also increases, resulting in a reduced pavement life. A wheel load increased 20 percent increased the subgrade compressive strain 19 percent, resulting in a 50 percent reduction in pavement life.

Chen also demonstrated that tire inflation pressure has an insignificant effect on subgrade rutting. Axle loads have a significant effect on subgrade compressive strain and therefore cause subgrade rutting.

Huhtala (Ref 22) experimented by rolling common truck radial tires over two different thicknesses of asphalt pavement. Both pavements had strain gages located throughout the asphalt and subgrade layers. By testing various radial tires at three different loads and inflation pressures, he was able to perceive that pavement strains were different for different tires and inflation pressures. He determined that:

- (1) Wide-base tires tended to be more aggressive, producing greater strains under the same load than dual tires, by a factor of 3.5 to 7.
- (2) The load was very seldom evenly distributed on both of the dual tires, as is assumed in design.
- (3) Stresses varied between various wide-base tires. The narrower wide-base tires produced greater strains under the same wheel loads.
- (4) Smaller dual tires produced larger strains at the same wheel loads than normal size conventional dual tires.
- (5) As tire inflation pressure was increased, the tires produced larger strains. An optimum inflation pressure does not seem to exist as far as the pavement is concerned, but an inflation pressure increase of 20 percent increased the tires' ability to produce 120 to 140 percent larger strains.
- (6) The contact pressure was highest in the tire centerline, for the limited amount of data obtained.

Huhtala also addressed the fact that common asphalt design practices are based on a circular, even contact pressure distribution, which does not account for two unevenly

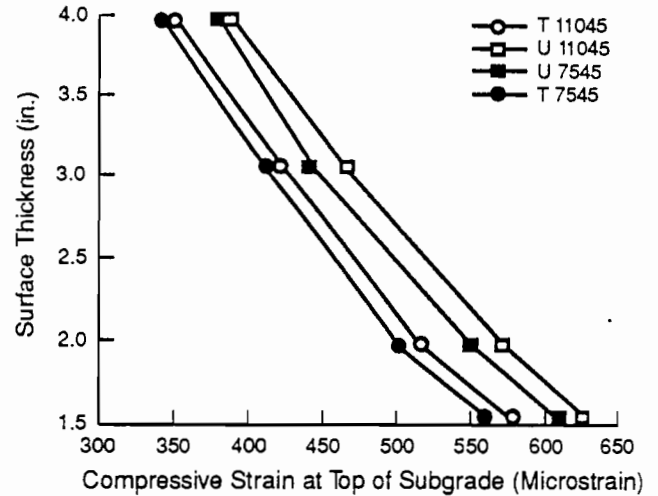


Fig 2.14. Effects of inflation pressure on compressive strain at the top of the subgrade layer. [Note: T designates a treaded tire with nonuniform (experimental) pressure model, and U designates a uniform pressure model. The values 7545 and 11045 represent, respectively, a tire loaded at 4,500 pounds with inflation pressures of 75 and 110 psi (Ref 27).]

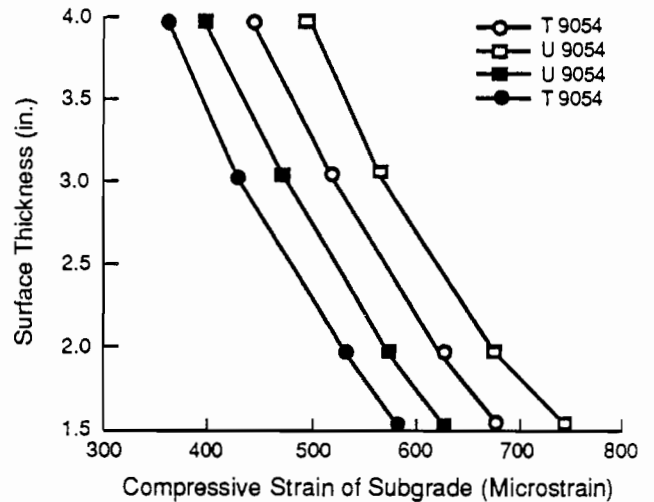


Fig 2.15. Effects of wheel load on compressive strain at the top of the subgrade surface. [Note: T designates a treaded tire with nonuniform (experimental) pressure model, and U designates a uniform pressure model. The values 9045 and 9054 represent, respectively, a 90 psi tire inflation pressure with loads of 4,500 and 5,400 pounds (Ref 27).]

loaded dual tires. In other words, it is assumed in pavement design that the wheel load is evenly divided between the two tires. His experiments exhibited that an uneven load is more likely the case. He attributed this uneven loading to the difference in tire structure, which varies from manufacturer to manufacturer, the difference in increased "hot" inflation

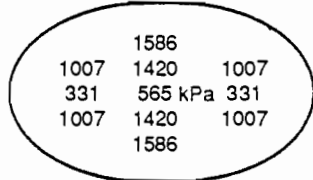
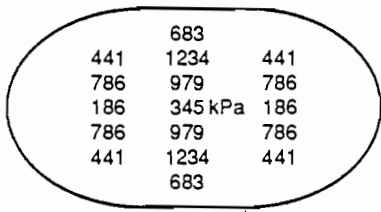


Fig 2.16. Contact pressures in footprint of 10.00-20 truck tire: wheel load held constant at 4,500 pounds.

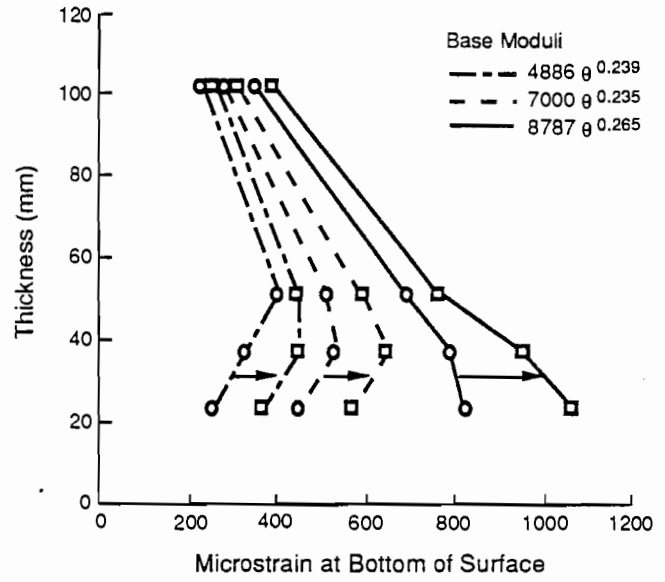


Fig 2.18. Effect of tire inflation pressure on horizontal tensile strain in surfaces of different thicknesses (modified from Ref 13).

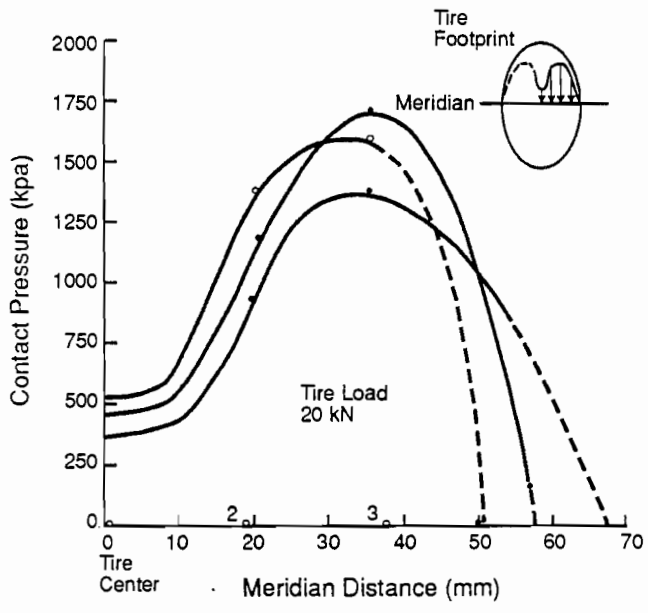


Fig 2.17. Effect of inflation pressure on contact pressure calculated for 10.00-20 bias truck tire with 4,500-pound load (modified from Ref 7).

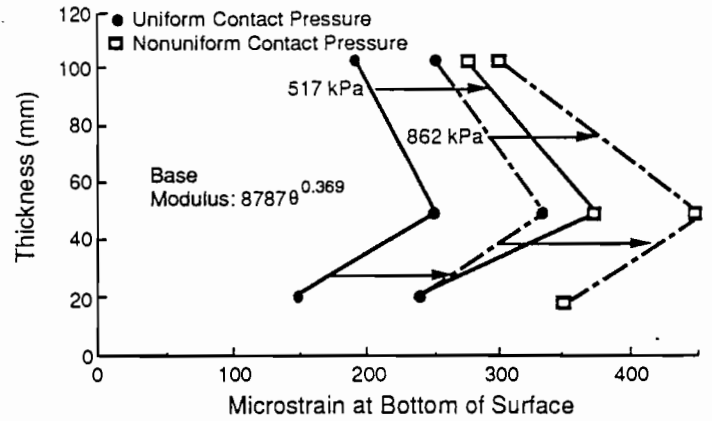


Fig 2.19. Comparison of strain calculated for uniform contact pressure with strain calculated for nonuniform contact pressures; surface modulus 400 ksi (modified from Ref 13).

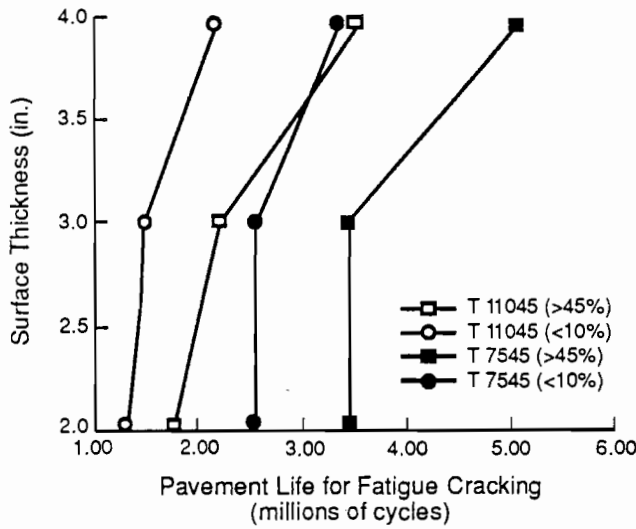


Fig 2.20. Effects of inflation pressure on pavement fatigue damage life. [Note: T designates a treaded tire. The values 7545 and 11045 represent a tire loaded at 4,500 pounds with inflation pressures of 75 and 110 psi, respectively (Ref 27).]

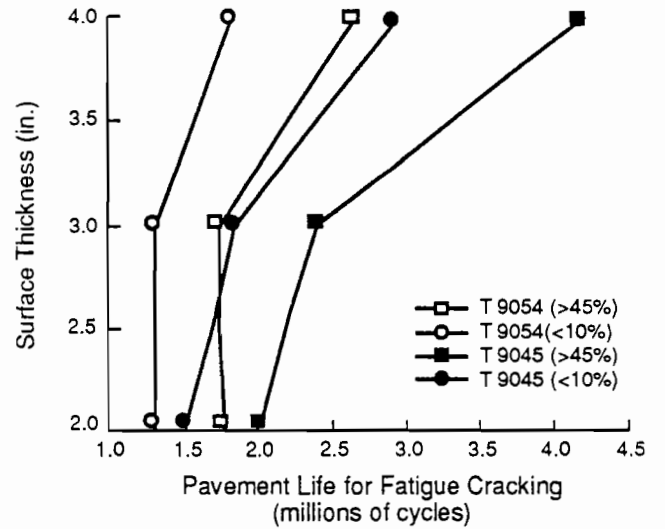


Fig 2.21. Effects of axle load on pavement fatigue damage life. [Note: T designates a treaded tire. The values 9045 and 9054 represent a 90 psi tire inflation pressure with loads of 4,500 and 5,400 pounds, respectively (Ref 27).]

pressure occurring during driving, and the direction in which the wheel load is applied to the pavement. To apply the same load, both tires must have the same wear, manufacturer and brand, age, and tire pressure, and both must also be either new or retreaded. He also stated that common design practices neglect the differences in loading caused by uneven roads and the vehicle's suspension.

Haas and Papagianakis, in an article addressing pavement rutting, stated that inflation pressures, regardless of tire type, are much higher than they were two decades ago. They explain that the increased popularity of radial-ply tires seems to be partially responsible for the increased inflation pressure. They felt that tire manufacturers design tires with higher inflation pressures in response to the trucking industry's request for lower rolling resistance. These pressures are on the order of 110 psi, as opposed to the 75 to 80-psi pressures used 20 years ago (Ref 24).

Haas and Papagianakis state that it is well known that pavement deformation takes place in all the pavement layers, not only in the subgrade, and, therefore, longitudinal cracking could originate at the surface rather than at the asphalt base. It was evident to them that stress contributing mechanisms pertaining to rutting required further study. For example, the compressive strains at the top of the subgrade which contribute to asphalt rutting have been shown to be affected by changes in inflation pressure. The higher the inflation pressure the higher the compressive stress and the higher the rutting potential.

Papagianakis and Haas (Ref 16) state that higher inflation pressure may cause pavement rutting by the shear displacement of the surface area. The higher pressure seems to cause the double ruts which have been recently appearing on many Ontario, Canada, highways. They state that experimental investigations and their analytical study indicate that the tire inflation pressure impact on pavement distress, in terms of shear deformation of the asphalt surface area, appears to be severe.

They also state (Ref 16) that early research efforts have shown that at comparable loads, axles on single tires cause higher pavement damage than axles on dual tires.

Surface Modulus, Base Modulus, and Thickness Effects

Roberts (Ref 6), performing analytical studies on flexible pavements using ILLIPAVE, a layer computer model, determined that when designing thin surfaces, less than 1.5 inches, it is best to use low (flexible) surface moduli. When designing thick surfaces, greater than 2 inches, it is best to use high (rigid) surface moduli. If a thin pavement is used with a high modulus or a thick pavement is used with a low modulus, excessive strains (greater than 300 microstrain) will occur. For a surface thickness of between 1.5 and 2 inches, the surface modulus must be greater than 300 ksi. If a surface modulus of less than 300 ksi is used, the pavement's service life will be reduced. Roberts states that

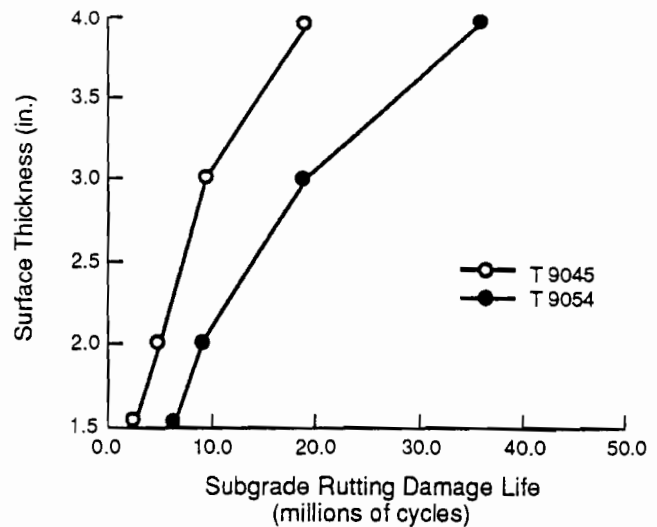


Fig 2.22. Effects of axle load on pavement subgrade rutting damage life. [Note: T designates a treaded tire, and the values 9045 and 9054 represent a 90 psi tire inflation pressure with loads of 4,500 and 5,400 pounds, respectively (Ref 27).]

all the pavements discussed above should be placed on a strong base having a high modulus of rigidity. Premature fatigue cracking can occur when the surface thicknesses are between one and three inches and are placed over flexible bases. The author summarizes that only through a combination of good surface and base materials can tensile strains be reduced to levels that will provide adequate fatigue resistance and service life.

POSSIBLE PAVEMENT LIFE SAVING SOLUTIONS

The literature clearly states that a major cause of pavement fatigue and rutting is increased wheel load and tire inflation pressure. Various researchers and highway officials have attempted to address this problem. Brown (Ref 3), at a symposium for high pressure truck tires, said that, through legislation and improved engineering, pavement life could possibly be maintained and extended.

The possible legal measures he mentioned were (1) placing legal limits on tire pressures, (2) placing controls on the manufacture of high pressure tires, (3) requiring approval of any new tire carcass design by FHWA, (4) requiring approval, both for safety and reduced road damage, for any new suspension system (considering tires as a component of the suspension system), and (5) using tire pressure as a factor in setting truck user taxes.

Nine states have already implemented conditional provisions for load as a function of tire inflation pressure. The regulation is generally expressed as two allowable loads per tire, one for an inflation pressure below 100 psi and another for inflation pressures above 100 psi (e.g., in Colorado,

allowable wheel loads are 9,000 and 8,000 pounds for inflation pressures less than 100 psi and over 100 psi, respectively).

Sharma (Ref 14) states that, generally, vehicle legislation requires lower axle load limits for axles mounted with wide-base tires, compared to conventional dual tires. He believes that in countries that have not passed this kind of legislation the higher pavement damage caused by wide-base tires is recognized and possible legislative changes are becoming crucial issues. Some countries have implemented special provisions regulating load limits per unit tire width. He mentions that these provisions were initially intended for tires mounted on steering axles but invariably are applied to other axle positions. In conclusion, Sharma stated that very few jurisdictions regulate tire inflation pressures, because of concern over accelerated pavement damage. He also mentioned that he had no indication of how the tire inflation pressure provisions were enforced where they existed.

The possible engineering improvements Brown (Ref 3) gave were (1) use of a better mix criteria, (2) use of more appropriate and better calibrated structural design models, (3) possible development of better binders and cements, and (4) emphasis on better quality control and better and more timely maintenance.

Other researchers, Papagianakis and Haas (Refs 16 and 24), while investigating rutting and the effects wide-base tires have on asphalt, discussed possible paths for future research in order to deter pavement rutting and fatigue. They felt that structural analysis should concentrate on the tire-pavement interface in order to identify the additional distress contributing mechanisms. The currently used finite element programs, BISAR and ILLIPAVE, account for tensile bending only at the bottom of the asphalt layer and for compression only at the top of the subgrade layer. As previously discussed, these stresses historically have been used as the critical fatigue and rutting distress parameters. Papagianakis and Haas state that permanent deformation occurs in all layers of the pavement system, not just in the subgrade. Therefore, the compressive strains at the top of the asphalt surface must be accounted for, because they have been shown to be dramatically affected by high inflation pressures.

CONCLUSIONS

From the literature review the following conclusions may be made.

- (1) Generally, for bias tires, as the inflation pressure increases, the pressure distribution at the center of the tire increases and approaches a pressure similar to that at the outside edges.
- (2) Steel-belted radial tires tend to have a more uniform footprint than glass-ply or bias-ply tires because radials have less stiff side walls.
- (3) It is in the operator's interest to maintain his tires at the manufacturer's recommended tire inflation pressures and wheel loads.
- (4) An increase in wide-base super single popularity is likely to decrease pavement service life.
- (5) Thin farm-to-market (FM) pavements should have a low modulus, and thick pavements should have a high modulus. Both thin and thick pavements should be placed on strong base material in order to provide an adequate service life.
- (6) Wheel loads have a significant effect on the compressive strain at the top of the subgrade, and therefore may cause rutting.
- (7) Increased inflation pressure does not significantly affect the compressive strain at the top of the subgrade.
- (8) Both wheel load and tire inflation pressure have a significant effect on the horizontal tensile strains at the bottom of the pavement layer. These increased tensile strains may cause cracking. Tire inflation pressure has a significant effect on the tensile strains at the bottom of thin pavement layers (less than 2 inches). Thus, high inflation pressures may cause premature fatigue failure. Both increased wheel load and increased inflation pressure may decrease pavement service life by over 30 percent.
- (9) Modeling asphalt strains using a tire having uniform contact pressures will generally yield greater strains than models using a tire having nonuniform contact pressures.
- (10) More legislation and improved engineering may be possible means to curtail pavement fatigue and rutting caused by high wheel loads and inflation pressures.

CHAPTER 3. EQUIPMENT, PARAMETERS, AND PROCEDURES

Increases in truck axle loads and in truck tire inflation pressures, particularly during the last decade, have generated increased interest in their possible effects on pavement life. As shown in the literature, many static and dynamic experiments have been conducted in an attempt to model and analyze the actual loading the pavement receives. Static testing and analysis was performed at The University of Texas at Austin. The equipment, parameters, and procedures have been changed from experiments previously performed at The University of Texas and therefore are discussed in detail below.

EXPERIMENTAL APPARATUS

To obtain the tire-pavement contact pressure distribution of various tires, a static method of loading the tires was used. The experimental apparatus consisted of truck tires and rims, a load frame and platform, a manual hydraulic power supply, a load cell and data acquisition system, two sheets of 5-mil (0.005-inch) Teflon, and the Fuji prescale film.

Truck Tires and Rims

The truck tires tested were a specially manufactured smooth tread Armstrong 11R24.5, load range-G tire, mounted on a Budd rim and a newly recapped, commercially available Goodyear wide-base super single 18-22.5, load range-H tire mounted on a 13.00 x 22.5 rim. The average tread depth of the bias super single was 0.5 inch as measured at a location 2 inches from the tire's exterior tread edges.

Load Frame and Platform

The load frame and platform were constructed at The University of Texas in 1984 for CTR Project 386 (Ref 23) and reassembled for this project. At the time of this report the load frame and platform were located at The University of Texas at Austin. The load frame, tire, and load platform configuration can be seen in Fig 3.1.

A new axle and hub assembly was constructed which enabled the wheel hub to be moved and secured such that the applied load was transferred through the tire and rim's approximate centroid. This enabled the production of a more uniform pressure print. The load platform used was a 2-inch polished steel platen placed on top of the concrete

surface. A detailed schematic of and parts list for the load frame are in Appendix B.

Manual Hydraulic Power Supply

Various systems for applying and controlling the load were considered and evaluated. Eventually a manual hydraulic power system was selected because of its user friendliness, availability, and economy. The system consisted of a hydraulic hand pump, a manifold, hydraulic hoses, and a 5,000-psi in-line pressure gage, as shown in Fig 3.1.

This system was very simple to use, convenient, and accessible. The hand pump was capable of delivering over 20,000 pounds of force. The in-line pressure gage was simply used to measure the in-line pressure which, when multiplied by the ram's bore area (7.069 square inches), served as a check on the load values calculated from the voltages displayed by the data acquisition system.

Hewlett-Packard Data Acquisition System

The actual loads applied to the tires were monitored using a Hewlett-Packard (HP) 3497A Data Acquisition system, an HP 150 computer, and a HP 44421 A 20-channel guarded input module. Communication was accomplished via a HP IB interface. The 20-kip load cell output voltage was monitored on the acquisition system's front panel. A calibration curve, previously derived as discussed below, enabled the user to monitor the output voltage and obtain the

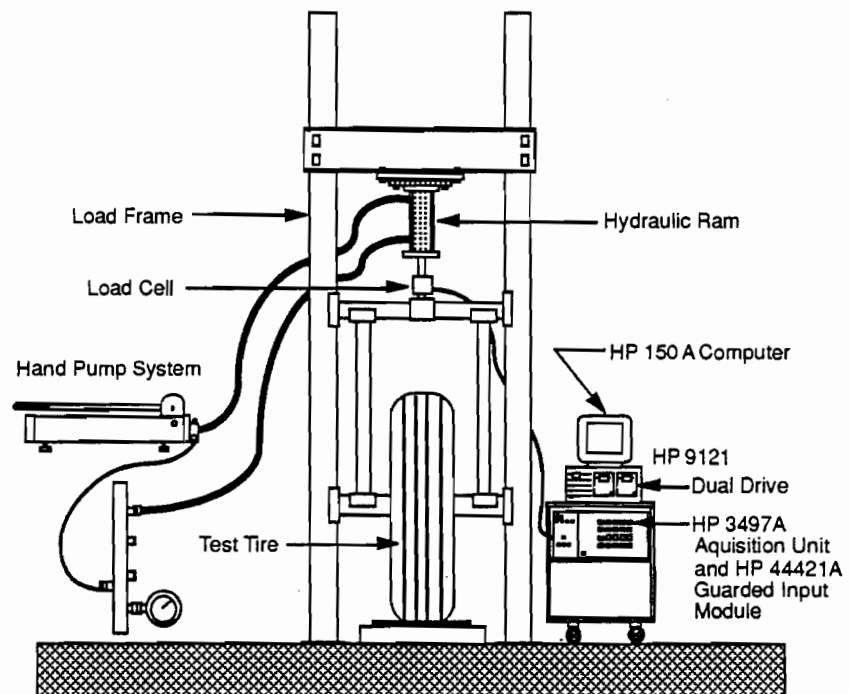


Fig 3.1. Load frame schematic using the OTC manual hydraulics.

voltage which corresponded to the desired maximum load. The acquisition program, written in GW BASIC, allowed horizontal and vertical deflection data to be obtained for each tire, as well as the applied load value.

To monitor and obtain a desired maximum load, the output voltage given by the data acquisition system was constantly monitored. The load was then held and released according to Fuji's recommendations, described in Appendix D.

Load Cell Calibration

To determine the applied load a Lebow 20-kip load cell was used. In order to assure the load cell's accuracy it was calibrated against a Conamp 20 Digital Calibration system. The Conamp system was calibrated and certified September 15, 1986, by the National Standards Testing Laboratory in accordance with ASTM Specifications E 74-81. The Conamp system includes both 10-kip and 100-kip load cells. To determine the applied load for this experiment, it was decided that the 10-kip load cell would provide the most accurate representation of the expected load range. The Conamp system displayed a direct digital readout of the loads on the calibration cell.

The calibrations of the Lebow load cell and of the HP acquisition system's output voltage readings were accomplished using the following procedure. Prior to tire installation the topmost cross member of the load frame was lowered to a position above the steel loading platen with enough room to allow insertion of the calibration cell. The calibration cell readout was zeroed using the zero adjustment knob. Then the CAL button was depressed and the specified calibration offset was dialed on the display. The calibration offset adjustment knob was then locked into position and the zero load value rechecked.

Pressure was applied to the system by pumping the hydraulic pressure pump. A record was kept of the HP load cell voltages, calibration cell load readouts, and the in-line pressure as monitored by a pressure gage. The ram was lowered until the calibration cell indicated a slight compressive load was being applied to the system. At various voltage increments the operator stopped applying pressure to the system and locked the pump to prevent the hydraulics from leaking back, which would have allowed the pressure to dissipate. While the pump was locked the parameters mentioned above were recorded. This process was continued through the entire 10-kip range of the calibration load cell.

The calibration curve and the resulting line equation were derived by plotting the HP voltages versus the calibration cell's load outputs. The resulting line did not go through the origin since there was an initial tensile load on the Lebow load cell. This tensile load was caused by the weight of the load cell and its connectors hanging from the end of the ram. The slope of the resulting line equation and the Y-intercept

were then used in the acquisition program to obtain the load on the tire specimen from the voltages read by the HP system. A diagram of the calibration curve and data used to produce the curve can be seen in Appendix C.

Fuji Prescale Film and Teflon Shim Stock

The Fuji prescale film was used to convert the contact pressure distributions to various intensities of red. The prescale film is comprised of "A" and "C" films. Both films have a low compressibility, polyester base. The A film has a thin coating of microcapsulated, color-forming material, and the C film has a thin coating of color developing material. The microcapsules on the A film are of various sizes, which allows them to break at different pressure levels. Large microcapsules break at relatively low pressures (e.g., 70 psi) while small capsules break at higher pressures (e.g., 285 psi).

To produce a color density image, the A and C film sheets are superimposed, with the coated surfaces face to face. As pressure is applied to the film, the microcapsules on the A film break, releasing the color forming material. This color-forming material then reacts with the color developing material on the C film. The result is permanent reds of varying intensities on the C film (see Fig 3.2).

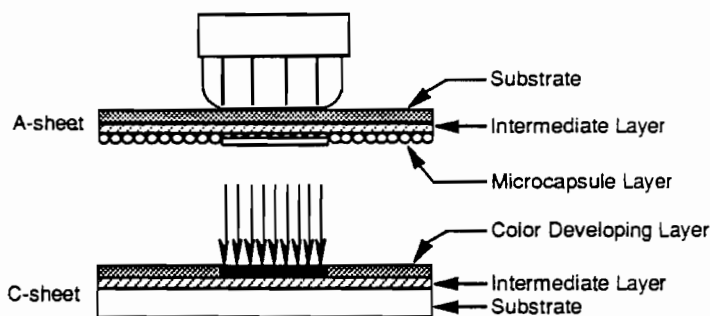


Fig 3.2. Working principle of the Fuji prescale film (modified from Ref 2).

A sheet of 5-mil (0.0005-inch) Teflon is placed above and below the Fuji film to prevent shearing from occurring between the Fuji Film's A and C sheets. As discussed in Chapter 2, a tire statically loaded on a pure frictionless surface probably closely resembles the same tire rolling on an asphalt surface at highway velocities. Previously, brass shim stock was used to prevent shearing, but to further reduce the amount of friction between the surfaces, a more frictionless shim stock was desirable. Therefore, the 10-mil sheets of Teflon were selected. Being an almost frictionless surface they would not only prevent shearing between the A and C film but also allow the tire surface to fully expand when loaded to allow production of a full tire footprint.

For the wide-base super single tire, two sets of film sheets had to be overlapped because the tire was wider than one sheet. Wider film is currently unavailable. The film

overlap, shim stock, and tire configuration can be seen in Fig 3.3.

FILM ANALYTICAL TOOLS

Many analytical tools were considered for interpreting the color densities on the Fuji film (Refs 23, 29, and 30). The Adage system was chosen as the prime analytical tool because of its user friendliness, digitizing speed, and availability. The primary reason for using the Adage system was because its results can be quickly confirmed as discussed by Chan (Ref 30), by either rerunning the analysis and then comparing the results, or by comparing the load calculated by the Adage with the actual applied load. The user may also adjust the calibration curve, permitting a better approximation of the contact pressures. At the time of this writing the Adage analysis system was located at The University of Texas at Austin.

Adage Analysis System

The Adage system was used to determine the tire contact pressure from color density prints. Pressure values and plots can be obtained much quicker using the Adage system than by using the CIPD densitometer used in CTR Project 386 (Ref 23). A short discussion of the Adage Analysis System's components and their purposes is given below. A more comprehensive explanation of the Adage system, including its uses and procedures, can be found in Chan (Ref 30) and in the Advanced Graphics Lab (AGL). The procedure for using the Adage analysis system is included in Appendix H.

The Adage analysis system consists of an Eikonix Scanner and an Adage 3006 Graphics System controlled by a tire image analysis program. The Eikonix Scanner is used to scan and digitize the color density image for processing by the Adage system. An image is scanned horizontally line-by-line and concurrently displayed line-by-line on the Adage monitor until the image is fully displayed.

A scanner program provided by the AGL controls the scanner. The scanner resolution can be selected from the defaulted 512 x 512 pixels (i.e., 512 lines by 512 picture elements per line) per image to a maximum of 1024 x 1024 pixels per image, from a control panel on the Adage's monitor. The 1024 x 1024 resolution was used for all image digitizing performed using the tire analysis program, as shown in Appendix H.

The Adage 3006 Graphics system is supported by a VAX work station, the VAXSTATION II (VSII), which is networked to the AGL's VAX 11/780. The University of Texas ETHERNET, a computer communication network, handles the communication protocol. The graphic monitor can display digitized images either directly as the image is

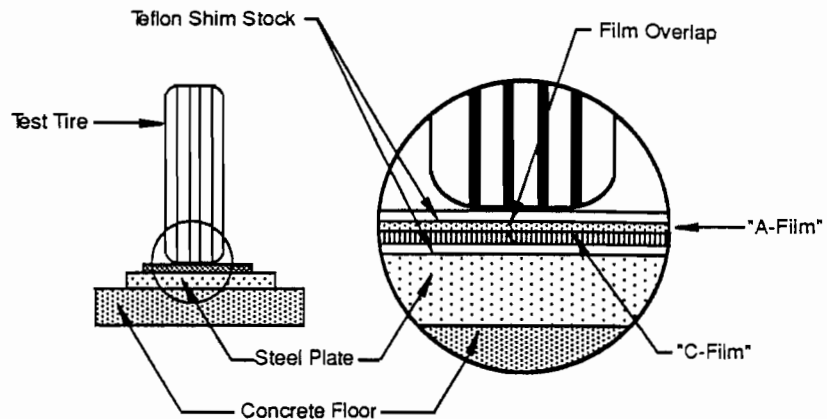


Fig 3.3. Teflon shim stock and film layout.

scanned or from an image previously stored on a disk file. Each byte of the digitized image represents a brightness level at that byte's location on the graphics screen. The tire print's pressure distribution is determined by using a calibration curve to transform the image array of pixel intensities into a corresponding pressure value array. The system is controlled by a tire image analysis program written by Wakeland (Ref 31) and modified by Chan (Ref 30).

After the image data are digitized the Adage system allows the user to display the results in several graphical presentations. The user may choose to display the calibration curve or display the data as a two-dimensional spectral plot, three-dimensional surface plot, or two-dimensional contour plot. The data are smoothed using a boxcar smoothing technique in order to add some continuity to the graphics.

The pressure values can also be downloaded from the Advanced Graphics Laboratory's VAX 11/780 to a Macintosh II and printed using a Macintosh laser printer.

EXPERIMENTAL PARAMETERS

As with any experiment, the test parameters must be chosen with care. Pressure prints were produced for various combinations of tires, loading, and inflation pressures. The actual parameter values and reasons for their selection are discussed below. The parameters can also be seen in Table 3.1.

Tires

After careful consideration two truck tires were selected for experimentation, an Armstrong 11R24.5 tire and a Goodyear super single 18-22.5 tire. The reasons for their selection are discussed below.

The Armstrong 11R24.5 LR-G smooth tread tire was specially manufactured for research testing and was on loan to this project. The smooth tire surface allowed the footprint area to be easily measured and the average pressure to be

TABLE 3.1. TIRE EXPERIMENTAL PARAMETERS

<u>Tire Type</u>	<u>Inflation Pressure (psi)</u>	<u>Load (lb)</u>
11R24.5 Load Range G	90	5,000
		6,000
		7,000
	105	5,000
		6,000
		7,000
18-22.5 Load Range H	85	9,000
		10,000
		12,000
	100	9,000
		10,000
		12,000

calculated in order to confirm the testing equipment's accuracy. The 11R24.5 is generally considered to be the truck tire most commonly found on U.S. highways today (Refs 1 and 5) and is commercially available.

The wide-base 18-22.5 truck tire was selected because of increased interest in the effects wide-base super single tires have on highway pavement service life. Super singles have become very common on European highways and are now becoming more popular on the North American Continent. A recapped bias-ply tire was selected because the wide-base 18-22.5 tires' increased popularity with Texas users made a recap readily available for testing.

Loads

The loads chosen for this experiment are based on 20,000-lb and 18,000-lb axle loads. The 11R24.5 tire was

treated as a single tire, commonly paired with another tire of the same make to form a pair of "duals." The super single 18-22.5 tire was treated as a single tire normally replacing a set of "duals," and, therefore, the allowable wheel load on the super single was almost twice as high as the load allowed on the 11R24.5 tire. The applied loads were 5,000, 6,000, and 7,000 pounds for the 11R24.5 LR-G tire and 9,000, 10,000, and 12,000 pounds for the 18-22.5 bias LR-H tire.

Inflation Pressures

As stated in Chapter 2, tire inflation pressures have been measured as high as 150 psi (Ref 1) but for safety purposes it was decided to go only slightly above the manufacturer's recommended maximum tire inflation pressure. The tire inflation pressures used were 95 and 110 psi for the 11R24.5 LR-G tire and 90 and 105 psi for the 18-22.5 bias LR-H tire. Both the applied wheel loads and tire inflation pressures can be seen in Table 3.1.

EXPERIMENTAL AND ADAGE ANALYTICAL PROCEDURES

Standard experimental and analytical procedures were implemented to minimize experimental error. This also aided in reproducing similar results. The experimental procedures using the Fuji prescale film to produce a contact pressure footprint can be seen in Appendix D. The analytical procedures for the Adage system and for using Macintosh II can be found in Appendix H and Appendix I, respectively. For a more detailed analysis of the Adage system and its uses consult Chapter 5, Section 3 of Chan (Ref 30), the Digital Equipment Corporation guide (Ref 32), and the Research Systems Incorporated guide (Ref 33).

CHAPTER 4. EXPERIMENTAL RESULTS

Using the Fuji prescale film and the Adage analysis system, contact pressure distributions from the new, smooth Armstrong, 11R24.5 LR-G radial tire and the recapped Goodyear wide-base, super single 18-22.5 LR-H bias tire were recorded and analyzed. The experimental parameters, resulting contact pressures, and discussion of results for each tire are presented here, followed by a discussion of experimental errors.

RADIAL ARMSTRONG 11R24.5 LOAD RANGE-G SMOOTH TREAD TIRE

A smooth 11R24.5 LR-G radial tire was chosen for experimentation in order to aid other research teams to verify data they produced using Tielking's finite element computer model, as discussed in Chapter 2 (Refs 6 and 13). The experimental wheel loads and inflation pressures are presented, followed by the resulting tire contact pressures. The measured deflections for the 11R24.5 tire can be seen in Appendix E. Frequency histograms for each numerical contact pressure print can be seen in Appendix F. The experimental wheel loads and inflation pressures used to test the smooth, Armstrong radial 11R24.5 LR-G tire are listed in Table 4.1.

The resultant contact pressure distributions for the new, smooth tread, Armstrong 11R24.5 LR-G radial tire can be seen in Figs 4.2 through 4.19. The contact pressure maps are sample (50 x 50) subarrays of smoothed pressure data extracted from the original pressure distribution data arrays. For each pressure map, a two-dimensional spectrum graphic representation and a three-dimensional surface plot representation which were produced on the Adage analysis system are included (see Appendix H for Adage display procedures). The orientation of these numerical pressure maps, (e.g., Fig 4.2) and spectrum graphics (e.g., Fig 4.3) are indicated in Fig 4.1. The gaps and rough edges displayed on the two-dimensional spectrum graphics and three-dimensional surface plots are contact areas where the contact pressure was lower than the Fuji prescale film was capable of recording.

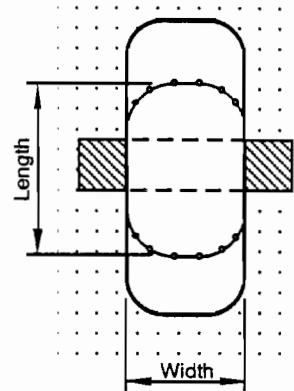


Fig 4.1. Numerical pressure map orientation.

The maximum pressure, mode, and contact area recorded from each tire print are tabulated in Table 4.2. Comparing the tabulated contact areas shows that, as the wheel load was increased at a constant inflation pressure, the tire contact area increased. The table also shows that, at a constant wheel load, as the inflation pressure increased, the contact area decreased.

Figures 4.2, 4.5, and 4.8 show the effect of an increase in wheel load on the contact area for the smooth surface radial tire, at a constant inflation pressure. As the load increased from 5,000 pounds to 7,000 pounds the contact pressures in all the contact regions increased. The contact pressures in the sidewall regions increased by the greatest amount, nearly approaching the central region pressures. These phenomenon are better illustrated in Fig 4.20. As the wheel load increased the contact pressures also tended to become more uniform throughout the contact area. The histograms in Appendix F verify this characteristic.

Figures 4.20 and 4.21 show the change in load distribution in the contact area by displaying the loads supported by five equal rectangular regions. These regions are oriented parallel to the tread rolling direction. Wheel loads of 5,000,

TABLE 4.1. RADIAL 11R24.5 TIRE EXPERIMENTAL PARAMETERS

Tire Type	Inflation Pressure (psi)	Load (lb)
11R24.5 Load Range G	90	5,000
		6,000
		7,000
	105	5,000
		6,000
		7,000

TABLE 4.2. RADIAL 11R24.5 TIRE EXPERIMENTAL RESULTS

Inflation Pressure (psi)	Wheel Load (lbs)	Maximum Contact Pressure (psi)	Maximum Location	Mode (psi)	Contact Area (in. ²)
90	5,000	136	Tread Center	78	68.2
	6,000	121	Tread Center	76	77.1
	7,000	139	Tread Center	74	88.4
105	5,000	110	Tread Center	76	66.0
	6,000	124	Tread Center	78	76.1
	7,000	133	Tread Center	84	82.5

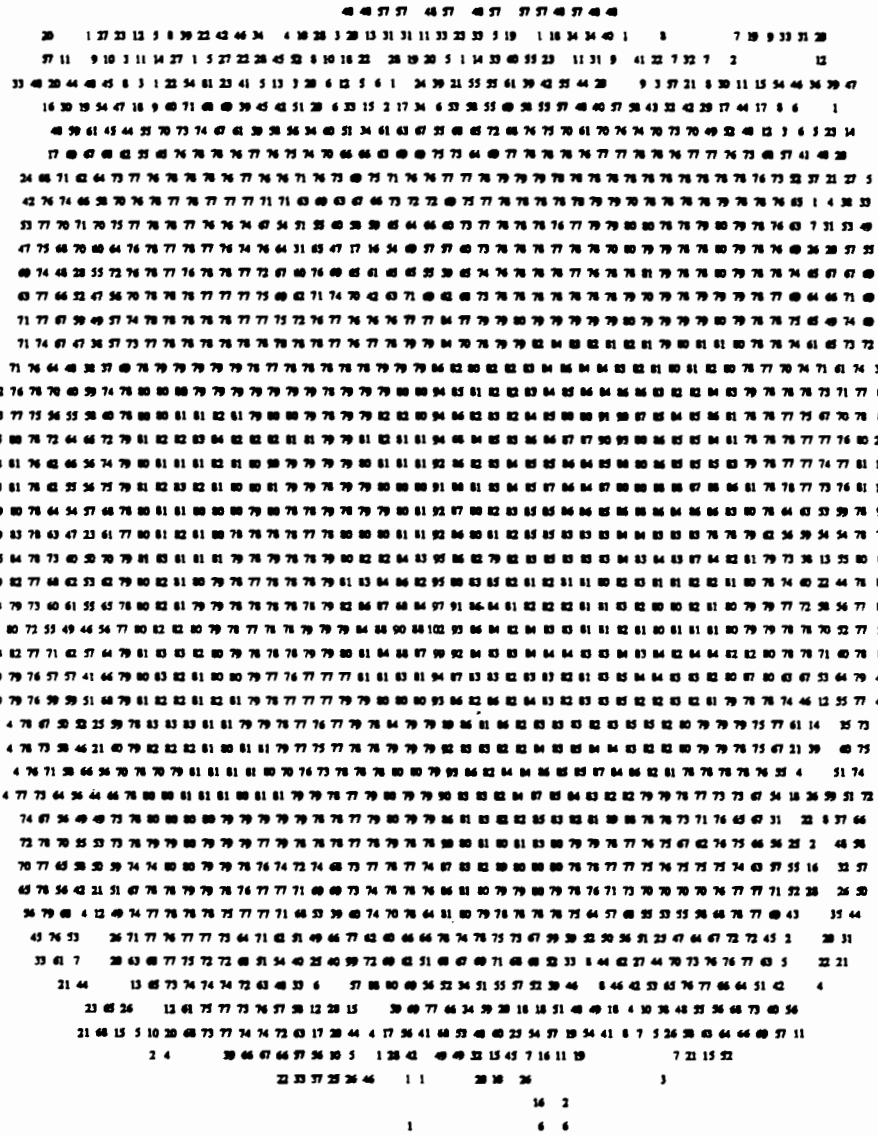


Fig 4.2. Pressure map for the smooth radial 11R24.5 load range-G tire inflated to 90 psi and loaded to 5,000 pounds. The pressure print is roughly 10.9 inches long and 7.5 inches wide.

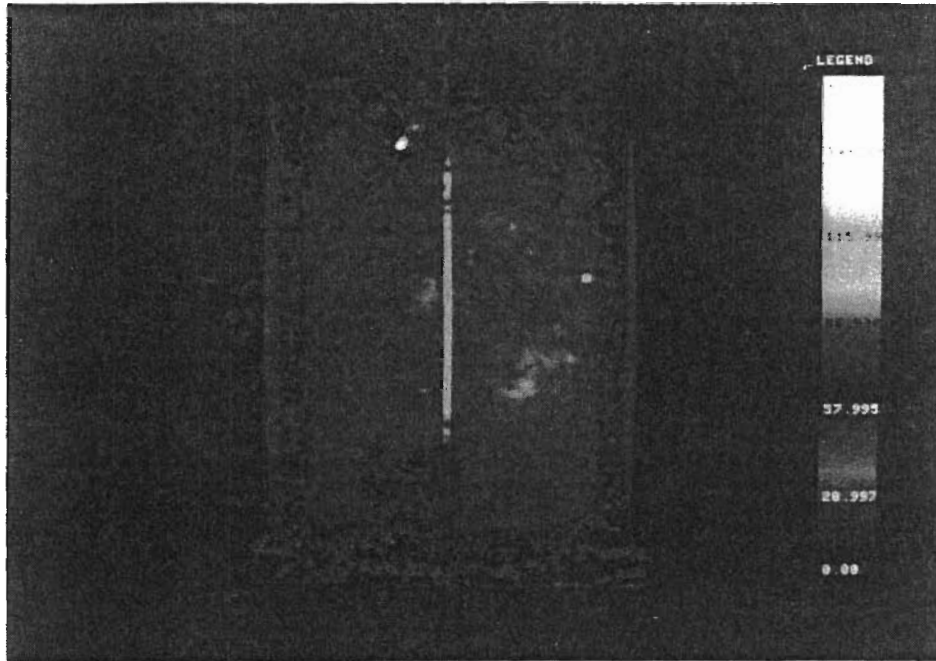


Fig 4.3. Two-dimensional spectrum graphic for the smooth radial-ply 11R24.5 load range-G tire inflated to 90 psi and loaded to 5,000 pounds.

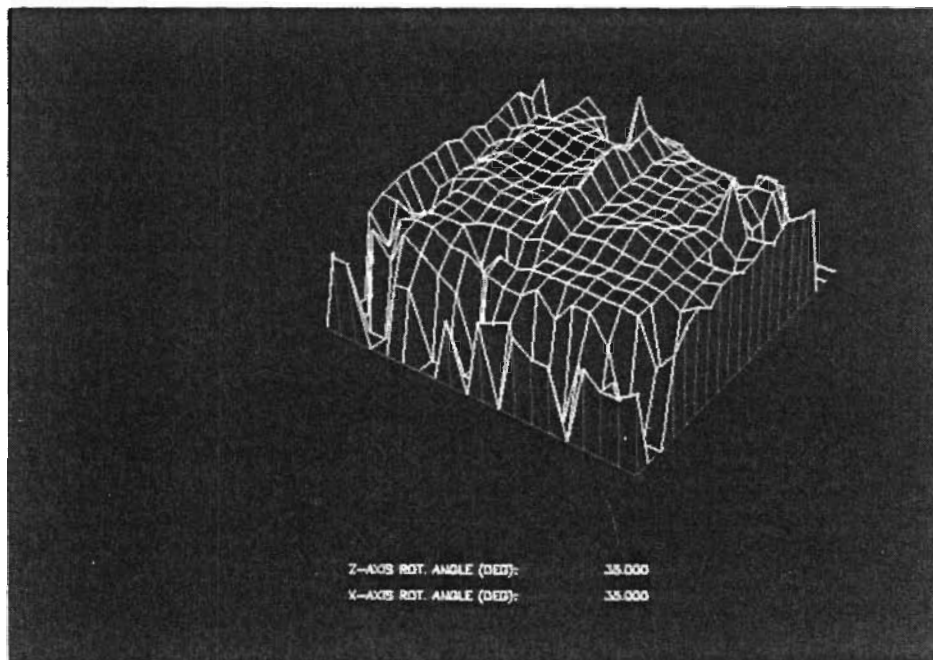


Fig 4.4. Three-dimensional surface plot for the smooth radial-ply 11R24.5 load range-G tire inflated to 90 psi and loaded to 5,000 pounds.

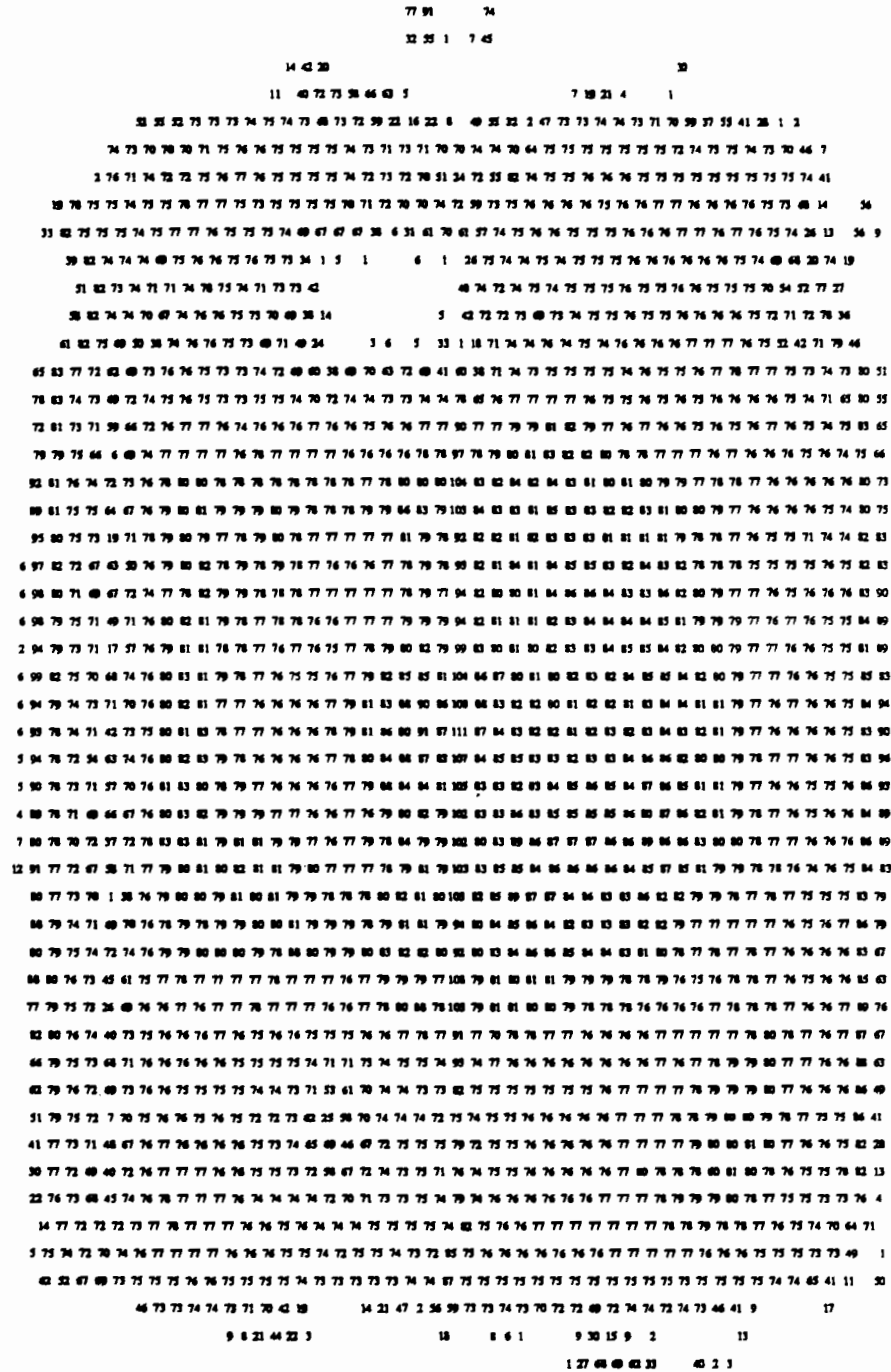


Fig 4.5. Pressure map for the smooth radial 11R24.5 load range-G tire inflated to 90 psi and loaded to 6,000 pounds. The pressure print is roughly 12 inches long and 7.6 inches wide.

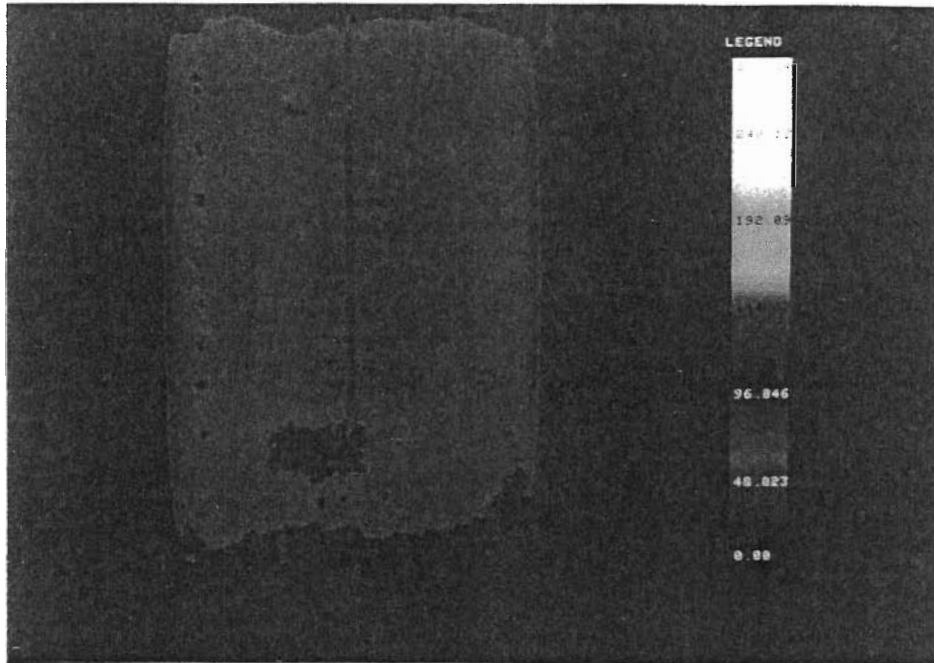


Fig 4.6. Two-dimensional spectrum graphic for the smooth radial-ply 11R24.5 load range-G tire inflated to 90 psi and loaded to 6,000 pounds.

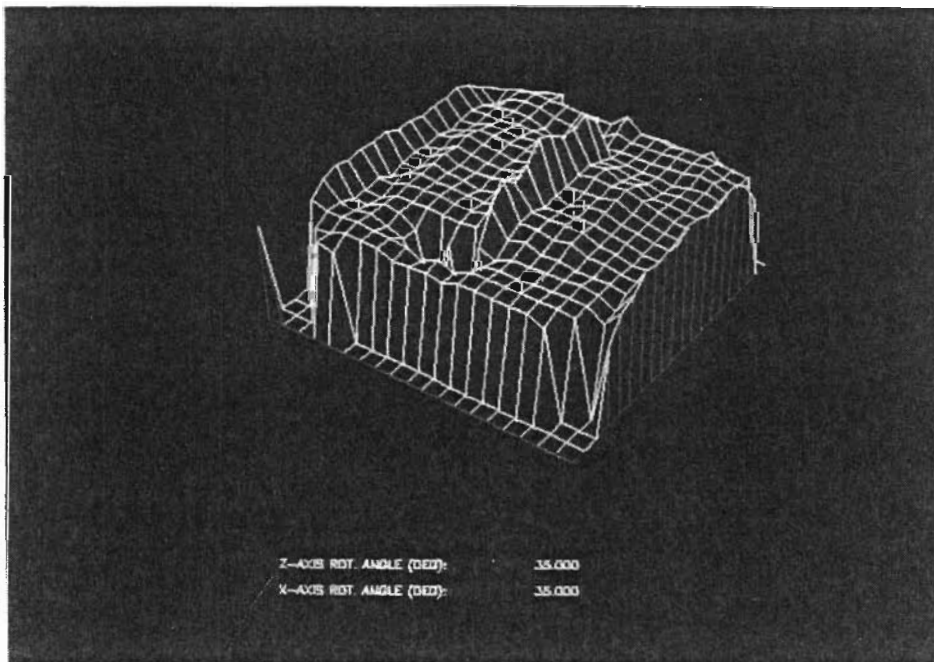


Fig 4.7. Three-dimensional surface plot for the smooth radial-ply 11R24.5 load range-G tire inflated to 90 psi and loaded to 6,000 pounds.

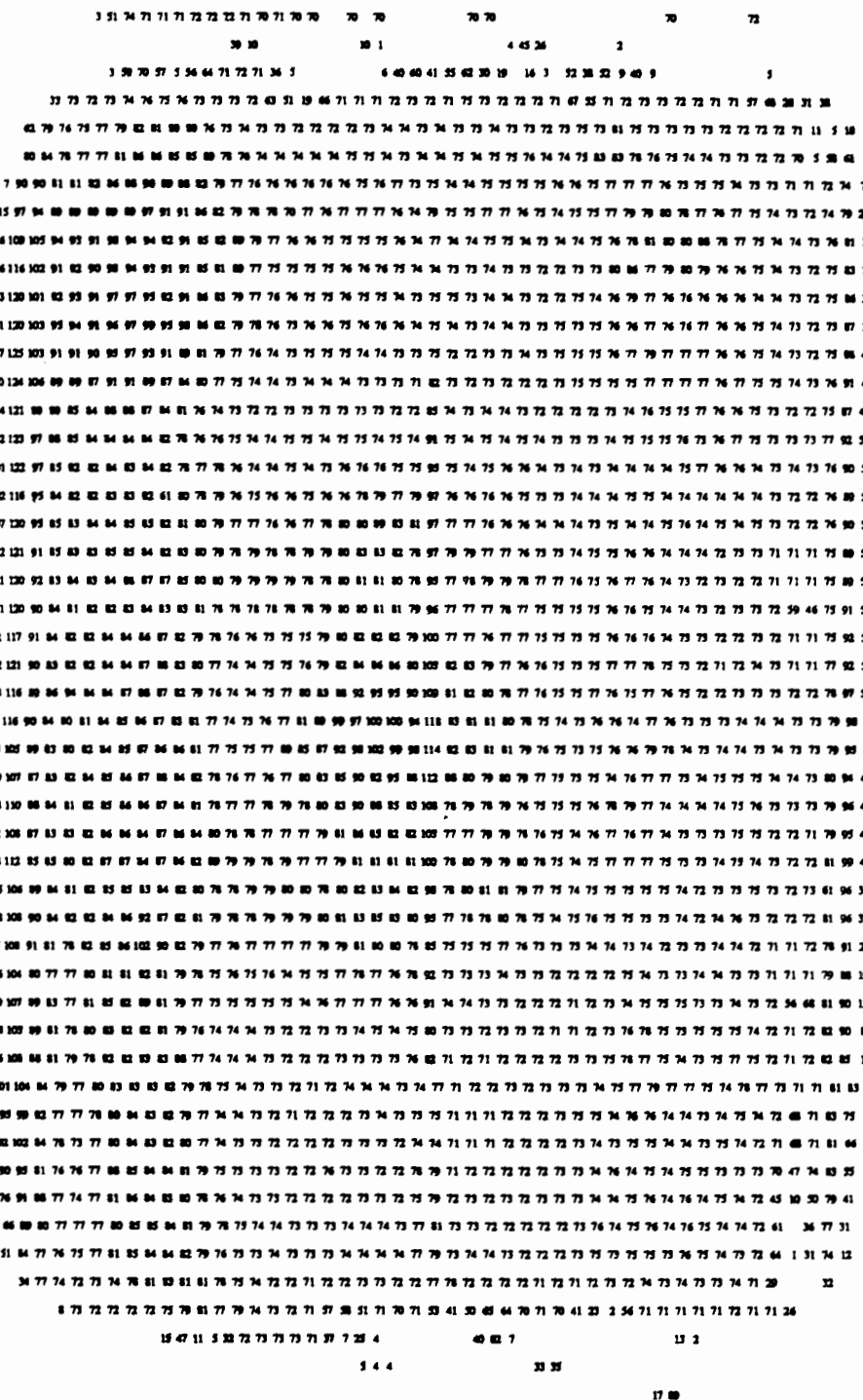


Fig 4.8. Pressure map for the smooth radial 11R24.5 load range-G tire inflated to 90 psi and loaded to 7,000 pounds. The pressure print is roughly 12.4 inches long and 7.6 inches wide.

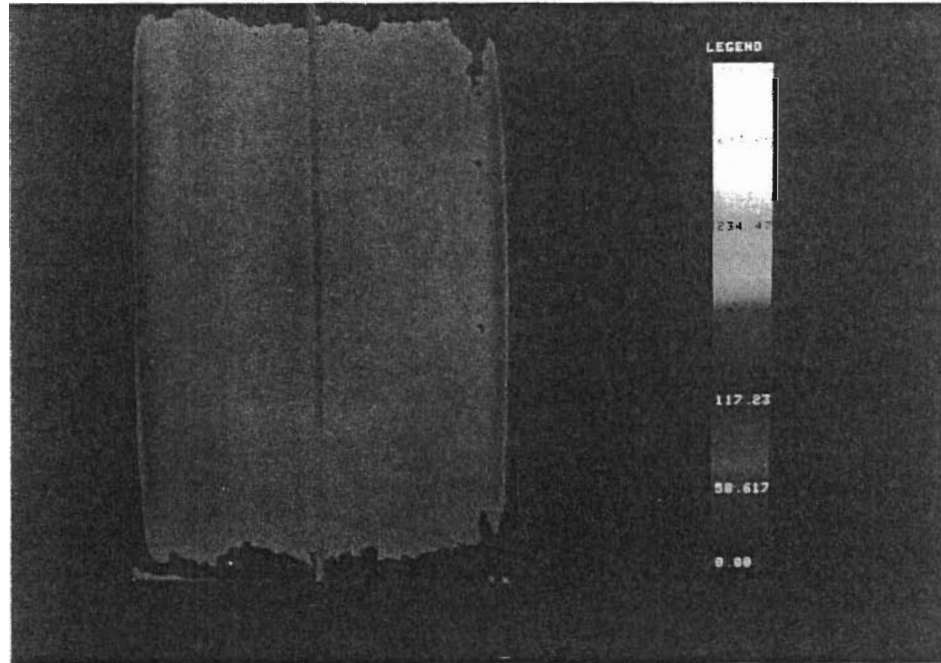


Fig 4.9. Two-dimensional spectrum graphic for the smooth radial-ply 11R24.5 load range-G tire inflated to 90 psi and loaded to 7,000 pounds.

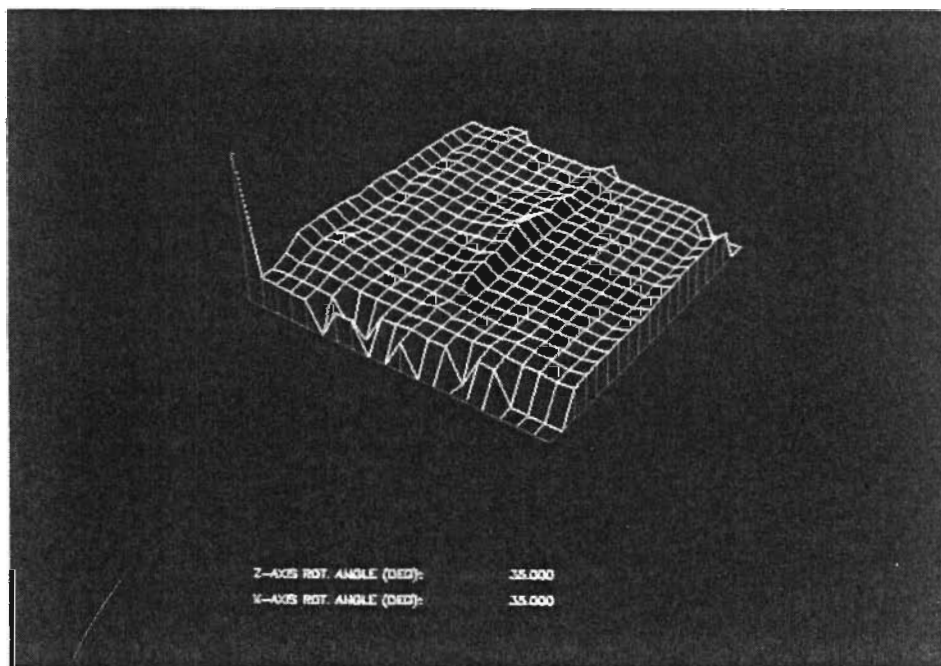


Fig 4.10. Three-dimensional surface plot for the smooth radial-ply 11R24.5 load range-G tire inflated to 90 psi and loaded to 7,000 pounds.

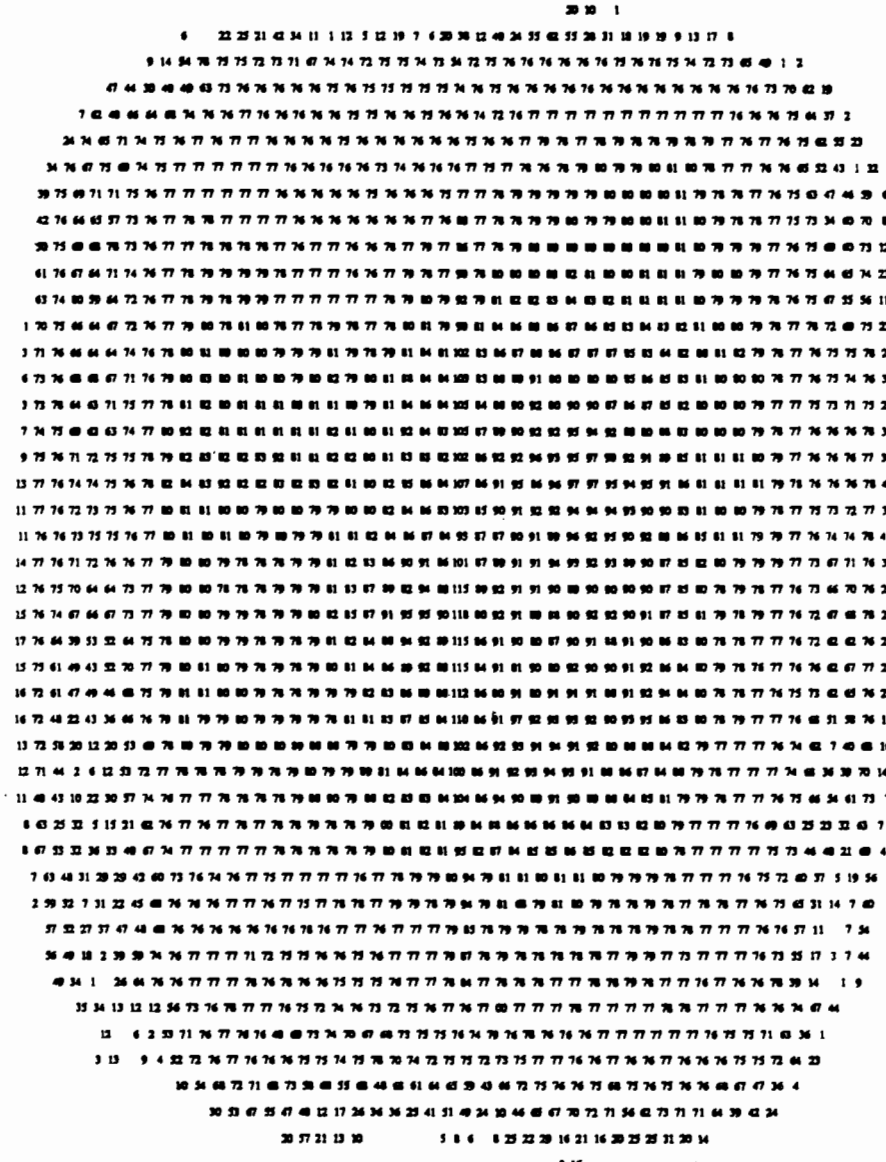


Fig 4.11. Pressure map for the smooth radial 11R24.5 load range-G tire inflated to 105 psi and loaded to 5,000 pounds. The pressure print is roughly 9.9 inches long and 7.5 inches wide.

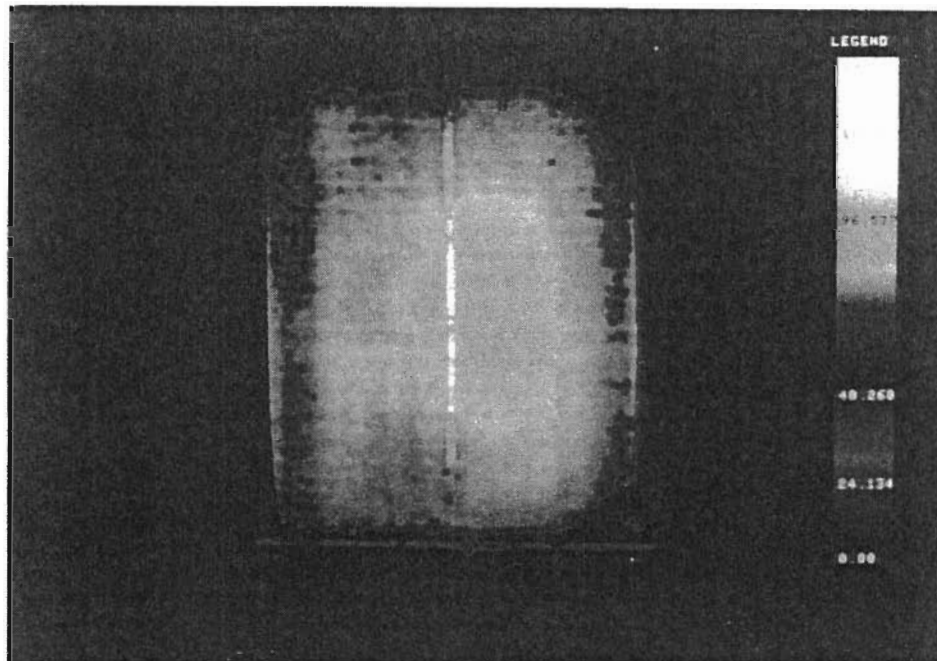


Fig 4.12. Two-dimensional spectrum graphic for the smooth radial-ply 11R24.5 load range-G tire inflated to 105 psi and loaded to 5,000 pounds.

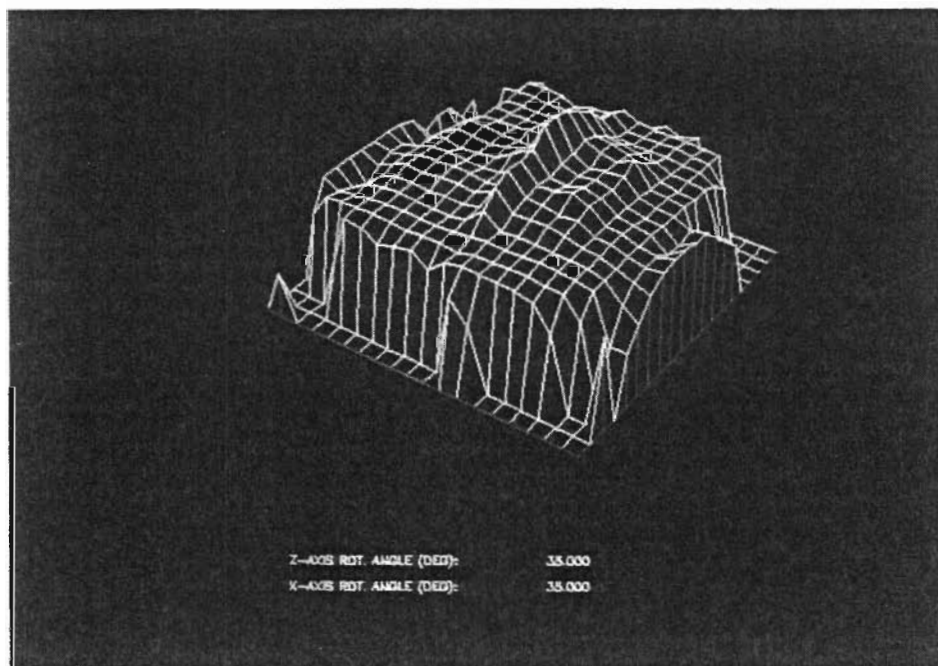


Fig 4.13. Three-dimensional surface plot for the smooth radial-ply 11R24.5 load range-G tire inflated to 105 psi and loaded to 5,000 pounds.

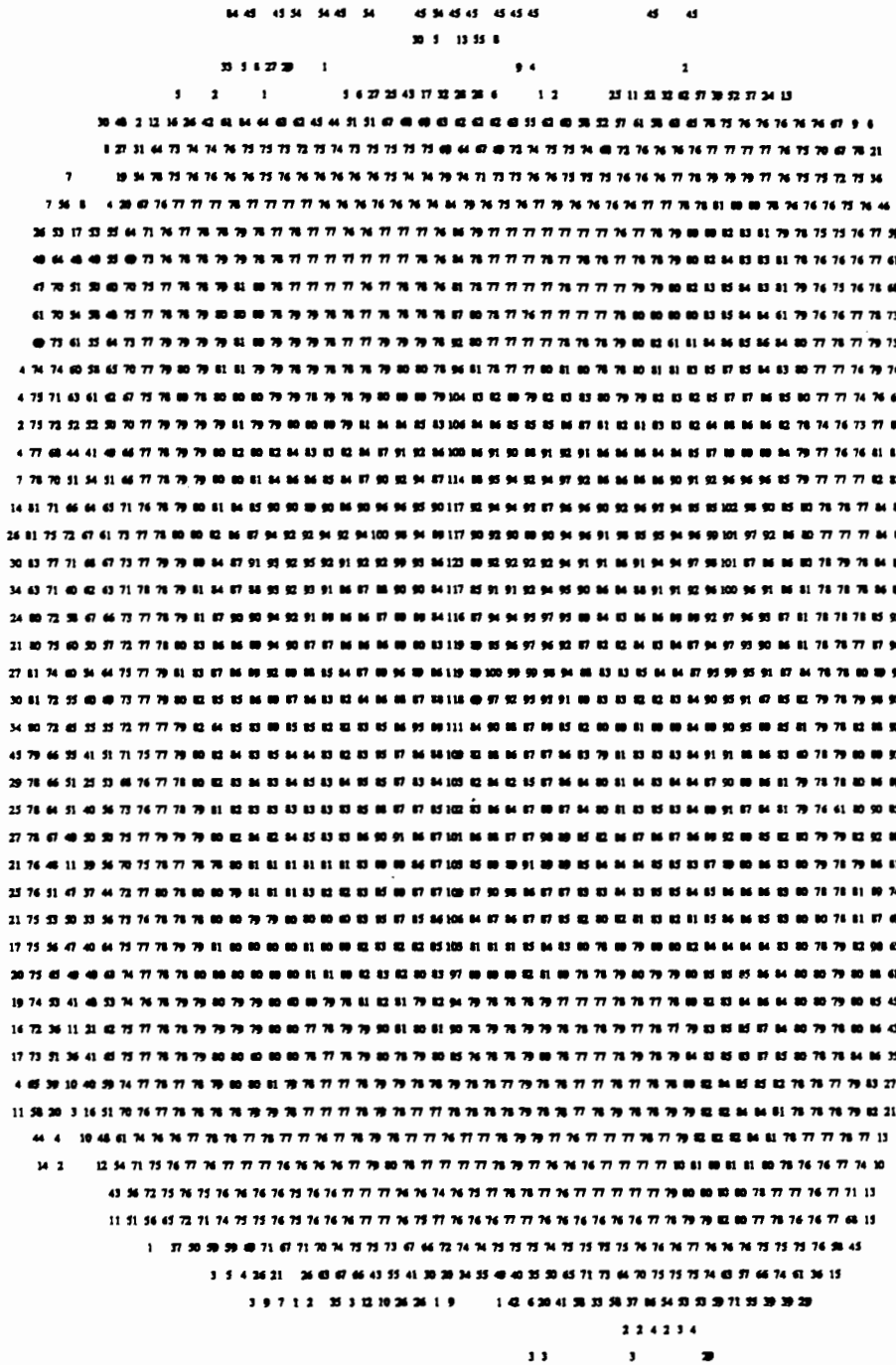


Fig 4.14. Pressure map for the smooth radial 11R24.5 load range-G tire inflated to 105 psi and loaded to 6,000 pounds. The pressure print is roughly 10.8 inches long and 7.6 inches wide.

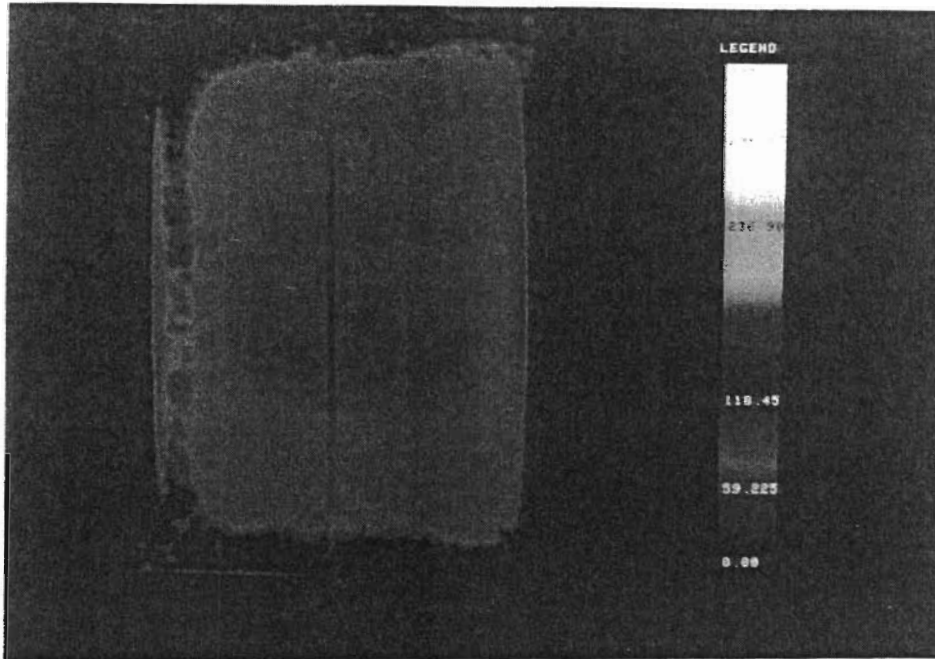


Fig 4.15. Two-dimensional spectrum graphic for the smooth radial-ply 11R24.5 load range-G tire inflated to 105 psi and loaded to 6,000 pounds.

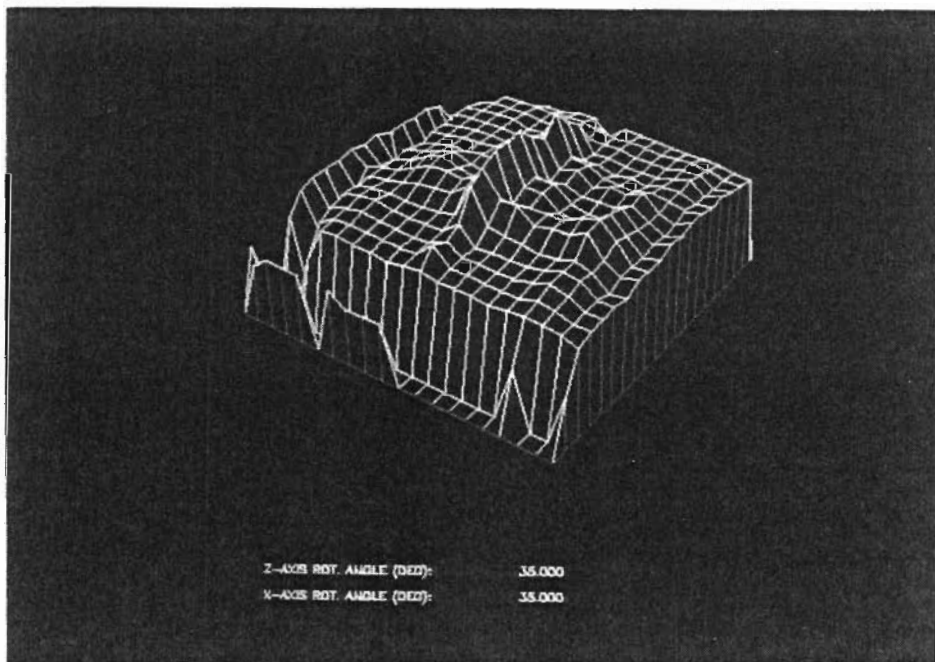


Fig 4.16. Three-dimensional surface plot for the smooth radial-ply 11R24.5 load range-G tire inflated to 105 psi and loaded to 6,000 pounds.

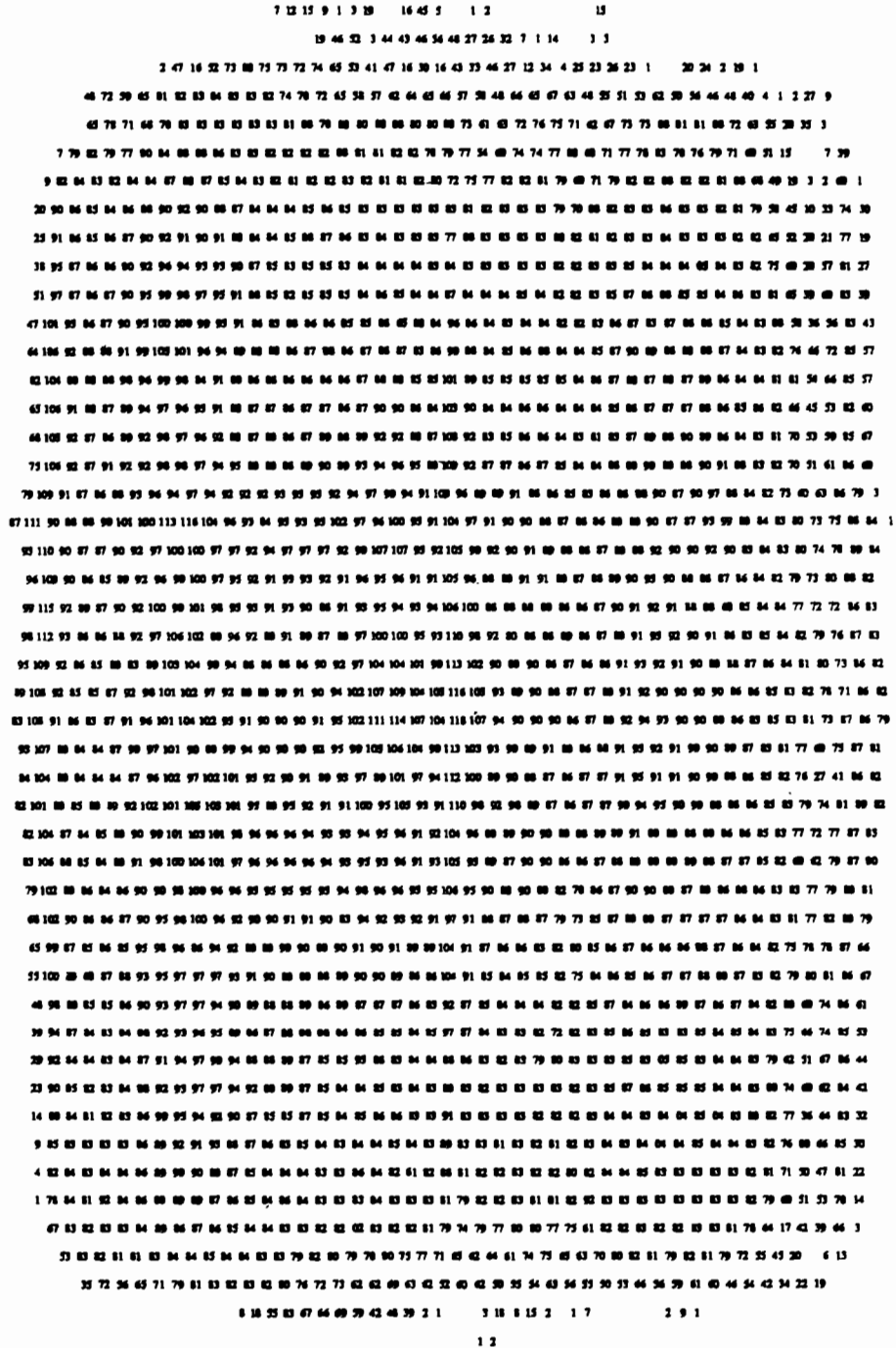


Fig 4.17. Pressure map for the smooth radial 11R24.5 load range-G tire inflated to 105 psi and loaded to 7,000 pounds. The pressure print is roughly 11.5 inches long and 7.6 inches wide.

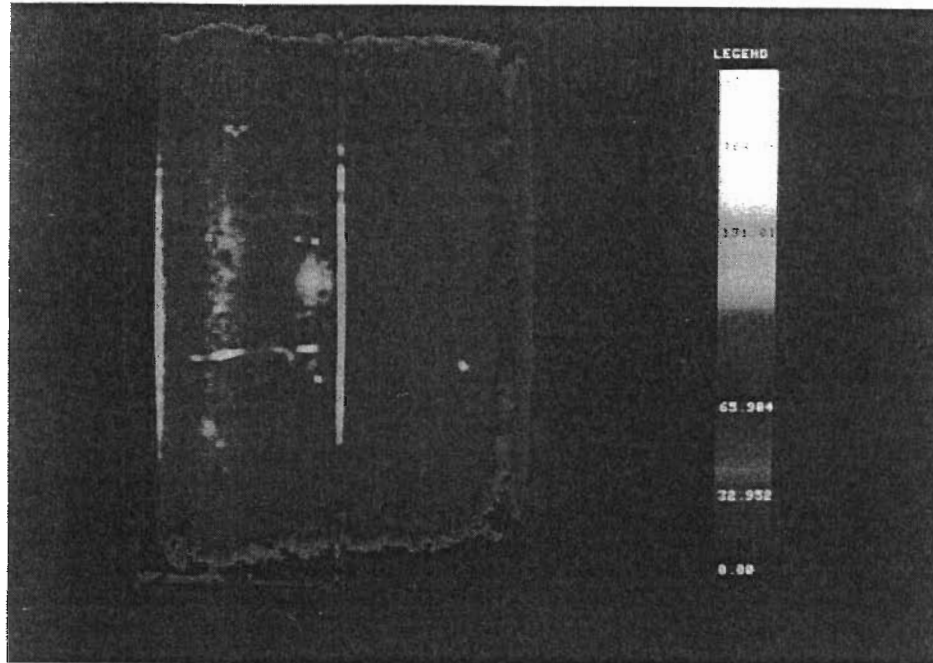


Fig 4.18. Two-dimensional spectrum graphic for the smooth radial-ply 11R24.5 load range-G tire inflated to 105 psi and loaded to 7,000 pounds.

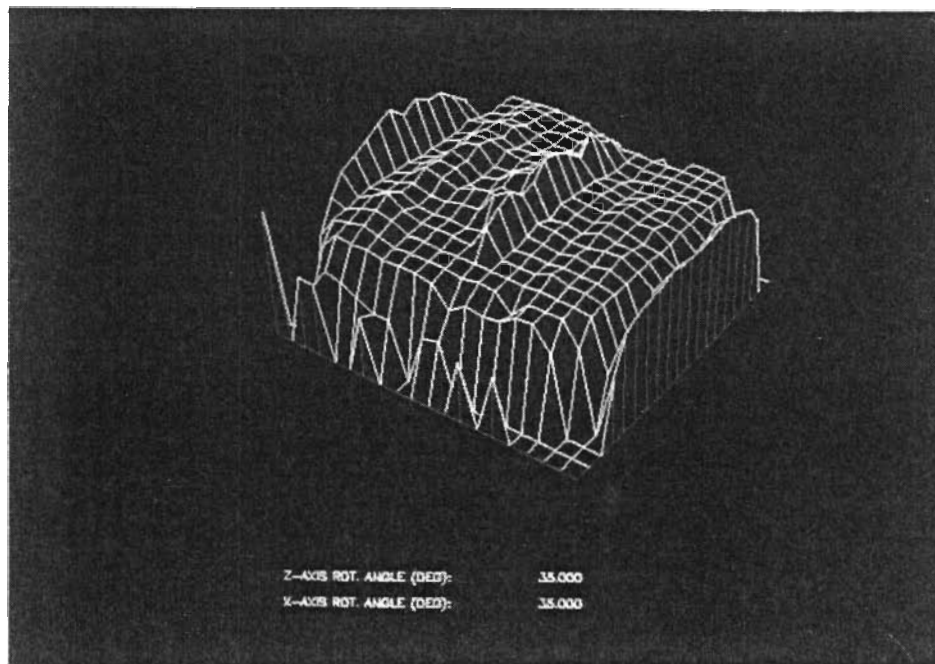


Fig 4.19. Three-dimensional surface plot for the smooth radial-ply 11R24.5 load range-G tire inflated to 105 psi and loaded to 7,000 pounds.

Fig 4.20. Histogram for the smooth radial 11R24.5 load range-G tire, showing the change in the load distribution across the tread width at an inflation pressure of 90 psi and wheel loads of 5,000, 6,000, and 7,000 pounds.

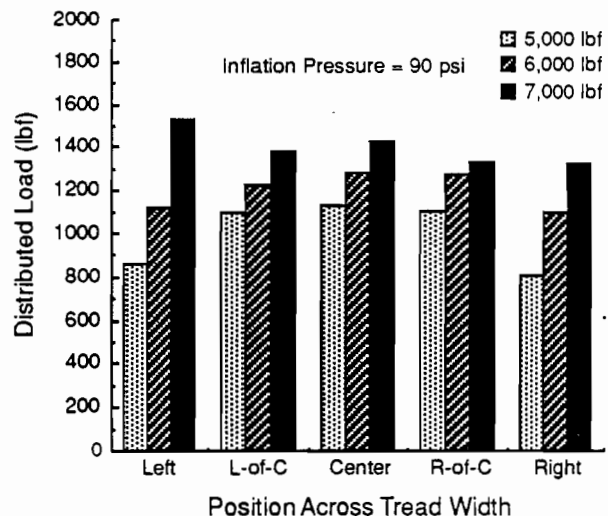


Fig 4.21. Histogram for the smooth radial 11R24.5 load range-G tire, showing the change in the load distribution across the tread width at an inflation pressure of 105 psi and wheel loads of 5,000, 6,000, and 7,000 pounds.

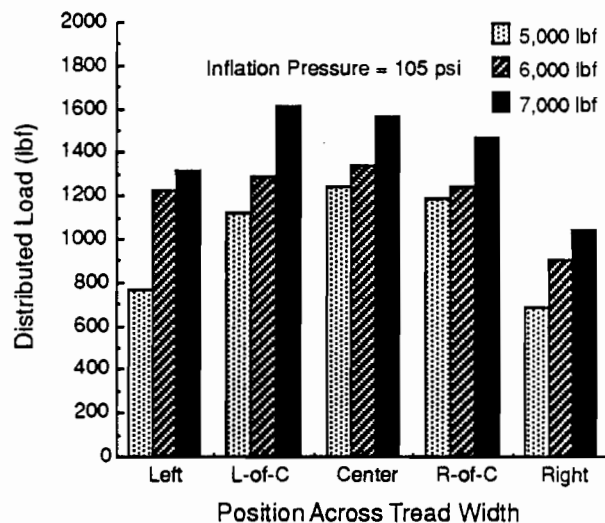
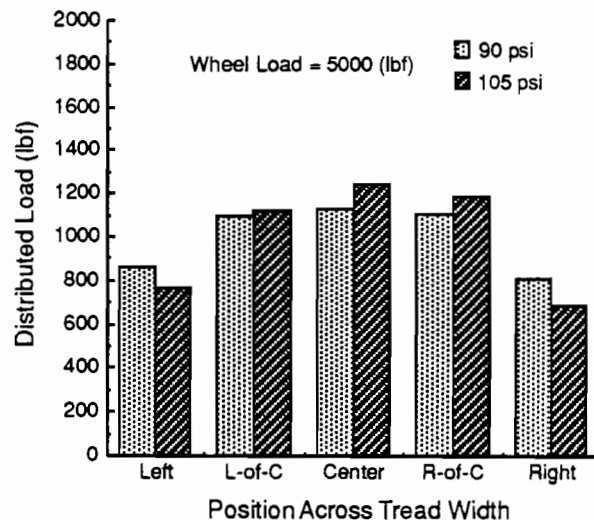


Fig 4.22. Histogram for the smooth radial 11R24.5 load range-G tire, showing the change in the load distribution across the tread width at 5,000 pound wheel load and inflation pressures of 90 and 105 psi.



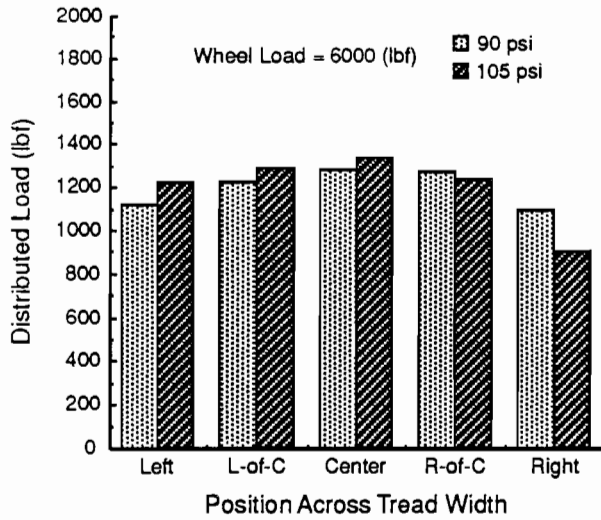


Fig 4.23. Histogram for the smooth radial 11R24.5 load range-G tire, showing the change in the load distribution across the tread width at 6,000 pound wheel load and inflation pressures of 90 and 105 psi.

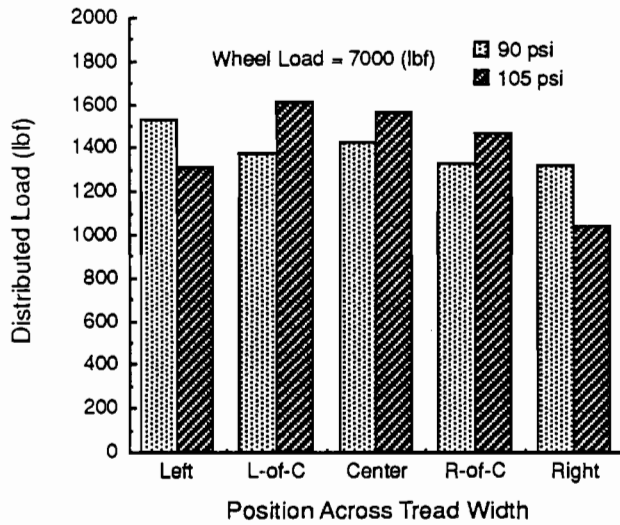


Fig 4.24. Histogram for the smooth radial 11R24.5 load range-G tire, showing the change in the load distribution across the tread width at 7,000 pound wheel load and inflation pressures of 90 and 105 psi.

TABLE 4.3. BIAS 18-22.5 TIRE EXPERIMENTAL PARAMETERS

Tire Type	Inflation Pressure (psi)	Load (lb)
18-22.5 Load Range H	85	9,000
		10,000
		12,000
	100	9,000
		10,000
		12,000

TABLE 4.4. BIAS 18-22.5 TIRE EXPERIMENTAL RESULTS

Inflation Pressure (psi)	Wheel Load (lbs)	Maximum Contact Pressure (psi)	Maximum Location	Mode (psi)	Contact Area (in. ²)
85	8,000	340	Tread Center	82	75.60
	10,000	391	Tread Center	91	99.90
	12,000	249	Tread Center	58	114.94
100	8,000	316	Tread Center	58	74.40
	10,000	342	Tread Center	66	87.70
	12,000	238	Tread Center	94	112.04

6,000, and 7,000 pounds are shown for each of the five regions. Figure 4.21 shows that, as the inflation pressure is increased for the same loading conditions, the five regions appeared to increase equally.

Comparing the contact spectrums shown in Fig 4.3 and Fig 4.12 reveals that, for a constant wheel load, an increase in inflation pressure causes the contact pressure located at the tire's central region to increase while the contact pressure at the side wall region decreases. Figures 4.22 and 4.24 clearly illustrate this pressure redistribution behavior for 5,000 and 7,000-pound wheel loads, respectively. However, because of eccentric loading and asymmetric tire construction, the response of this tire in Fig 4.23 appears distorted. Yet, the researchers still believed the data showed a valid trend, and, using this figure, verified it by comparing the sum of the right and left load distribution sections for the tire inflated to 90 psi with the sum of the right and left load distribution sections for the tire inflated to 105 psi. The sum for the tire inflated to 105 psi is less than the tire inflated to 90 psi, and, therefore, as the inflation pressure increased, the amount of wheel load carried by the side wall area decreased. At the same time, the amount of wheel load transferred to the central region of the contact patch increased.

BIAS GOODYEAR 18-22.5 WIDE-BASE SUPER SINGLE TIRE

A wide-base super single, 18-22.5 LR-H, bias-ply retread tire was chosen for experimentation because of its increased use on Texas highways. The experimental wheel loads and inflation pressures are presented, followed by the resulting tire contact pressures. Frequency histograms for each numerical contact pressure distribution print can be seen in Appendix G. The experimental wheel loads and inflation pressures used to test the recapped General wide-base 18-22.5 LR-H tire are listed in Table 4.3.

Experimental Results

The results of the contact pressure analysis are shown in Figs 4.25 through 4.42. The results for the 18-22.5 tire are presented, using numerical contact pressure maps, two-dimensional spectrum graphics, and three-dimensional surface plots, as were previously seen for the 11R24.5 smooth tread tire. The numerical contact pressure maps (e.g., Fig 4.25) and spectrum graphics (e.g., Fig 4.26) are oriented as shown in Fig 4.1. The gaps and rough edges displayed on the two-dimensional spectrum graphics and three-dimensional surface plots are areas where the contact pressure was lower than the Fuji prescale film was capable of recording.

The maximum pressure, mode, and contact area recorded from each tire print are tabulated in Table 4.4. Comparing the tabulated contact areas shows that, as the wheel load was increased, while keeping the inflation pressure constant, the tire contact area increased. The table also shows that, at a constant wheel load, as the inflation pressure increased, the contact area decreased.

Figures 4.25, 4.28, and 4.31 show the effect an increase in wheel load, at a constant inflation pressure, has on the contact area for the 18-22.5 tire. As the load was increased from 8,000 pounds to 10,000 pounds the contact pressures over the entire contact patch also increased, with the largest increase occurring in the central region. These phenomena are better illustrated in Fig 4.43. As the wheel loads increased the contact pressures tended to become more uniform throughout the contact patch. This trend is verified by the histograms in Appendix G.

Figures 4.43 and 4.44 show the changes in load distribution in the 18-22.5 tire contact area by displaying the portion of wheel load supported by five equal rectangular regions. These regions are oriented parallel to the tread rolling direction. Figure 4.43 shows that, as the load increased from 8,000 to 10,000 pounds and from 10,000 to 12,000 pounds, the contact pressures in all the regions increased. Figure 4.44 shows that as the load increased from 8,000 pounds to 10,000 pounds a similar trend occurred. For the increase from 10,000 to 12,000 pounds the trend discontinued. The pressure in the central region remained the same but the contact pressures in the sidewall regions increased.

Except for the contact pressures where the load was increased from 10,000 to 12,000 pounds in Fig 4.43, the results in both Figs 4.43 and 4.44 are in contradiction with the theory associated with bias-ply tires as discussed in Chapter 2. In Chapter 2, it was stated that the contact pressures for a bias-ply tire are normally highest at the sidewall regions for low inflation pressures but that as the inflation pressure increases it is accompanied by an increase in contact pressures at the contact area's central region. If the inflation pressure continues to increase at a constant wheel load the contact pressure in the center region will eventually surpass the pressures at the sidewall regions.

These strange contact characteristics can be attributed to the super single tire's construction. The tire is very rigid and its tread is convex so that at low wheel loads only the center portion of the tread is in contact with the pavement surface, which causes a circular contact print to be produced (Figs 4.26 and Fig 4.35). As the load is increased the contact area becomes wider and more oval shaped (Fig 4.29). When the applied load was increased from 10,000 pounds to 12,000 pounds, the full tread width established contact and the contact patch then lengthened to accommodate the additional load, as displayed in Fig 4.32. In Fig 4.32 it is also evident that the sidewall tread established contact with the pavement surface and thus the change in wheel load from 10,000 pounds to 12,000 pounds resulted in a large increase in contact pressure at both the tread's center and sidewall regions. These characteristics are better illustrated in Fig 4.43.

At a tire inflation pressure of 100 psi when the wheel load was increased from 8,000 to 10,000 pounds, the contact pressure increased only in the center region, which is in character for a bias tire inflated to high pressure. The high

inflation pressure also caused a smaller contact area to occur, preventing the sidewall tread from establishing contact with the pavement (compare Figs 4.35 and 4.38). However, as the load was increased to 12,000 pounds, the higher inflation pressure prevented lengthening of the contact area in order to transfer the additional wheel load, and, therefore, the additional load was transferred to the sidewall region. At the same time, the contact pressures in the central region remained relatively constant.

The comparison of Fig 4.26 and 4.35 revealed that, at a constant wheel load, an increase in inflation pressure from 85 to 100 psi caused the contact pressure in the center region to increase. This is logical because, if a decrease in contact area occurs because of an increase in inflation pressure, the contact pressures would be expected to increase.

Figures 4.45 and 4.46 show typical contact pressure trends for bias-ply tires. They show that an increase in inflation pressure, at a constant wheel load, is accompanied by an increase in contact pressure in the center region and a decrease in contact pressure at the sidewall region. However, the trends described by Fig 4.47 look the opposite of what is expected for a bias tire for an increase in inflation pressure at a constant wheel load. As the inflation pressure increases the distributed load in the center region should increase with an accompanying decrease in the sidewall region similar to that shown in Figs 4.45 and 4.46. It appears as if just the opposite has occurred. By looking at Fig 4.47 more closely, it can be seen that the largest differences between the 85 and 100-psi columns is less than one percent of the applied wheel load. This is about the accuracy of the load cell voltage readout of the load frame apparatus. Therefore, in order to determine the contact pressure characteristics for the change in inflation pressure for the 12,000-pound wheel load, it is necessary to look at the tabulated contact area in Table 4.4 and the pressure distribution maps (Figs 4.31 and 4.40). The contact patch produced from the tire inflated to 100-psi has a slightly smaller contact area than the patch produced at 85 psi, and, therefore, should have slightly larger contact pressures. Comparing Figs 4.31 and 4.40 shows that the contact pressures are almost the same. Thus, since the change in contact area is small and the data in Figs 4.31 and 4.40 appear the same, the increase in inflation pressure from 85 psi to 100 psi had a very small effect at the 12,000-pound loading.

DISCUSSION OF RESULTS

For both the smooth treaded 11R24.5 radial tire and the wide-base 18-22.5 bias tire at constant inflation pressures, an increase in wheel load was accompanied by an increase in contact area. Similarly, at constant wheel loads, both tires experienced a decrease in contact area as the tire inflation pressure was increased. This is where similarities between the two tires end. Both tires do have interesting characteristics unique to tires of the same construction type, and they are presented below.

Characteristics of the Smooth Tread 11R24.5 Tire

The 11R24.5 radial tended to be characterized by a fairly uniform contact pressure. The frequency histograms in Appendix F illustrate that most of the measured pressure values are within a small range of pressures. It appears that, as the wheel load increased, the contact pressure distribution becomes more uniform, especially in the range of 5,000 to 6,000 pounds at 95 psi.

For the same tire, as the wheel load increased, the contact pressures at the center portion of the tread were slightly redistributed, but the majority of the increased load was accommodated by an increased contact length. The outer ribs not only increased in contact length but also increased in average contact pressures. The largest contact pressures occurred in the center portion of the tread because the belt of a radial tire is more rigid than its sidewalls. The increased pressure in the sidewall regions can probably be attributed to growing bending stresses in the sidewall combined with an increase in sidewall overhang beyond the tread edge. Lippman and Oblizajek (Ref 15) stated that the increased overhang results in an additional vertical component of air pressure acting on the inner surface of the sidewall beyond the tread edge.

An increase in wheel load on a radial tire seems to cause the sidewall pressure to increase, and an increase in tire inflation pressure causes the center contact pressure to increase.

Characteristics of the Wide-Base 18-22.5 Tire

The pressure distribution data produced by loading the wide-base 18-22.5 bias tire show that the pressures were highest in the tread's center region. As the wheel load increased the pressures in the center of the tire increased until the load was large enough to establish contact of the full tread width. After this point the contact area lengthens to accommodate any additional wheel load.

The pressures were also high along the edges of the tread. This can be attributed to the tread grooves causing the tread ribs to support the inflation pressure over the tread grooves.

The pressures transmitted to the pavement by the super singles are much larger than the inflation pressure.

EXPERIMENTAL ERROR

As is customary in reporting experimental results, a section pertaining to the experimental error is included. In the methodology reported in this document, possible sources of error became apparent during trial runs, when ink prints were produced. The ink print experiments led to careful procedural practices which helped avoid experimental error during the Fuji film experimentation. The few errors which did occur during the actual tire testing, and which possibly affected the results, are discussed below.



Fig 4.25. Pressure map for the wide-base bias 18-22.5 load rang-H tire inflated to 85 psi and loaded to 8,000 pounds. The pressure print is roughly 11.5 inches long and 11.9 inches wide.

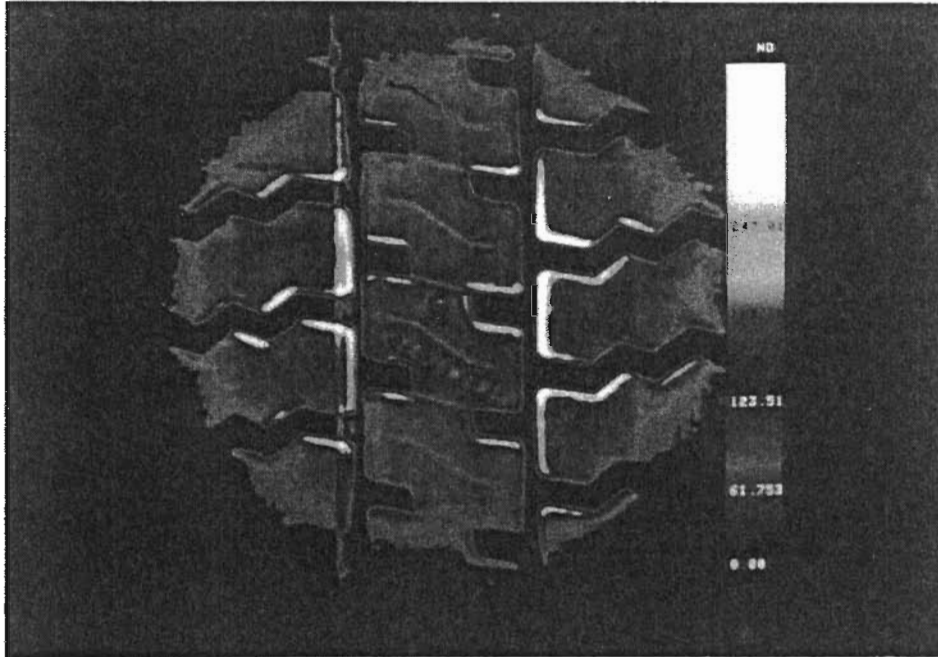


Fig 4.26. Two-dimensional spectrum graphic for the wide base bias 18-22.5 load range-H tire inflated to 85 psi and loaded to 8,000 pounds.

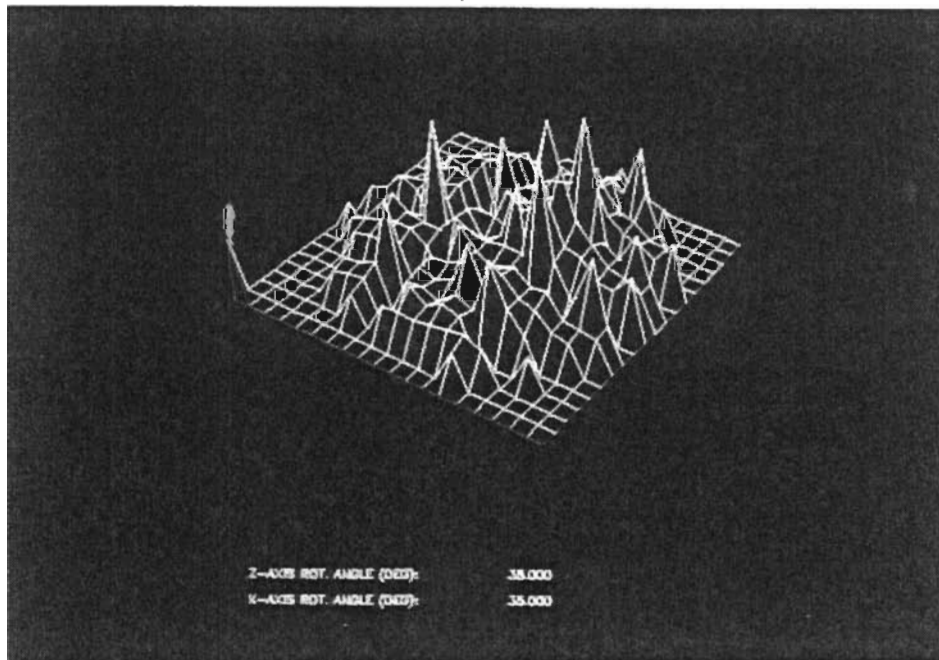


Fig 4.27. Three-dimensional surface plot for the wide-base bias 18-22.5 load range-H tire inflated to 85 psi and loaded to 8,000 pounds.



Fig 4.28. Pressure map for the wide-base bias 18-22.5 load rang-H tire inflated to 85 psi and loaded to 10,000 pounds. The pressure print is roughly 12.8 inches long and 12.1 inches wide.

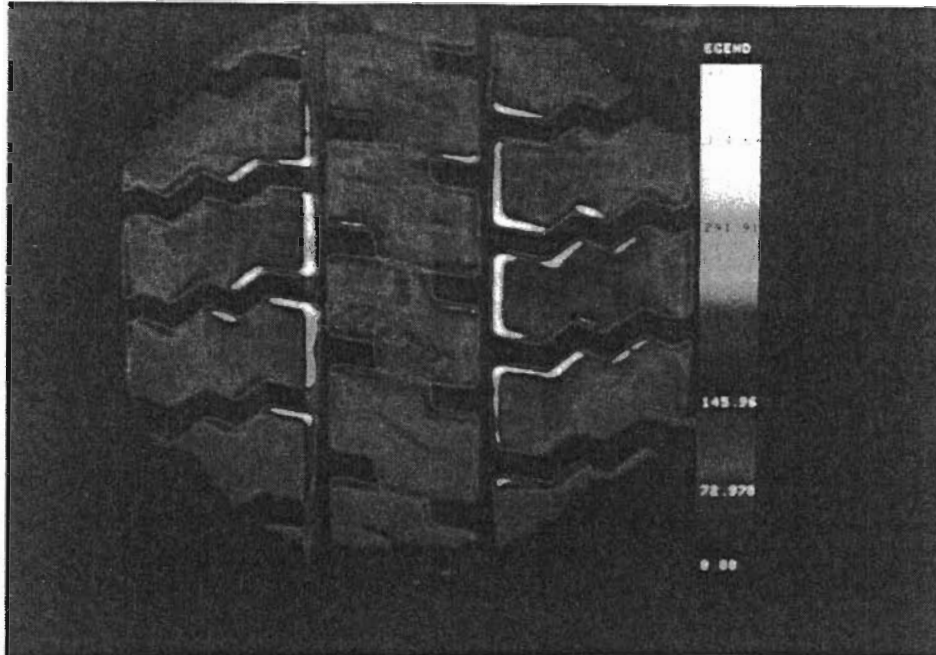


Fig 4.29. Two-dimensional spectrum graphic for the wide base bias 18-22.5 load range-H tire inflated to 85 psi and loaded to 10,000 pounds.

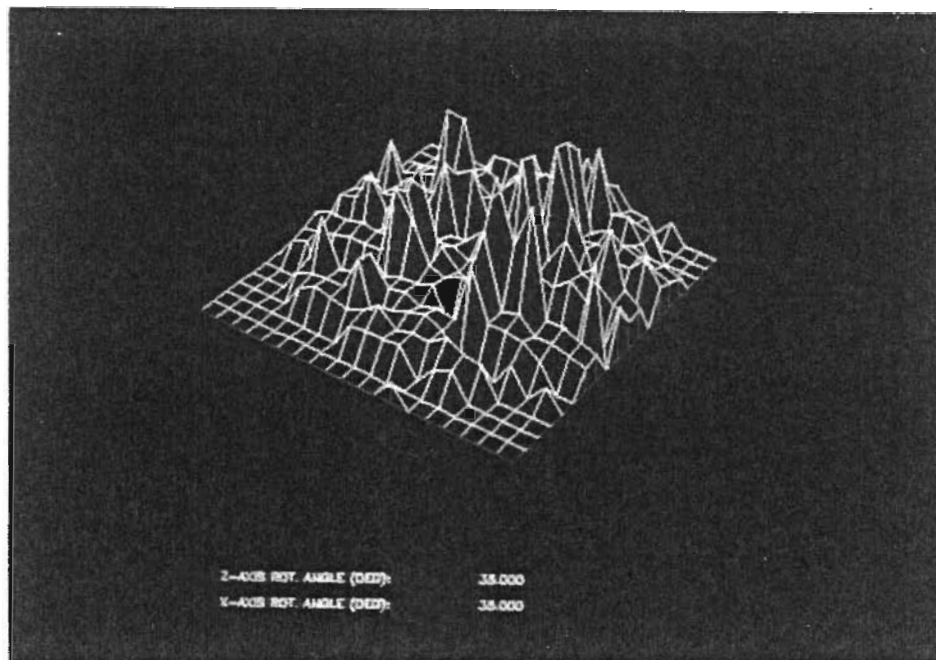


Fig 4.30. Three-dimensional surface plot for the wide-base bias 18-22.5 load range-H tire inflated to 85 psi and loaded to 10,000 pounds.



Fig 4.31. Pressure map for the wide-base bias 18-22.5 load rang-H tire inflated to 85 psi and loaded to 12,000 pounds. The pressure print is roughly 13.8 inches long and 12.4 inches wide.

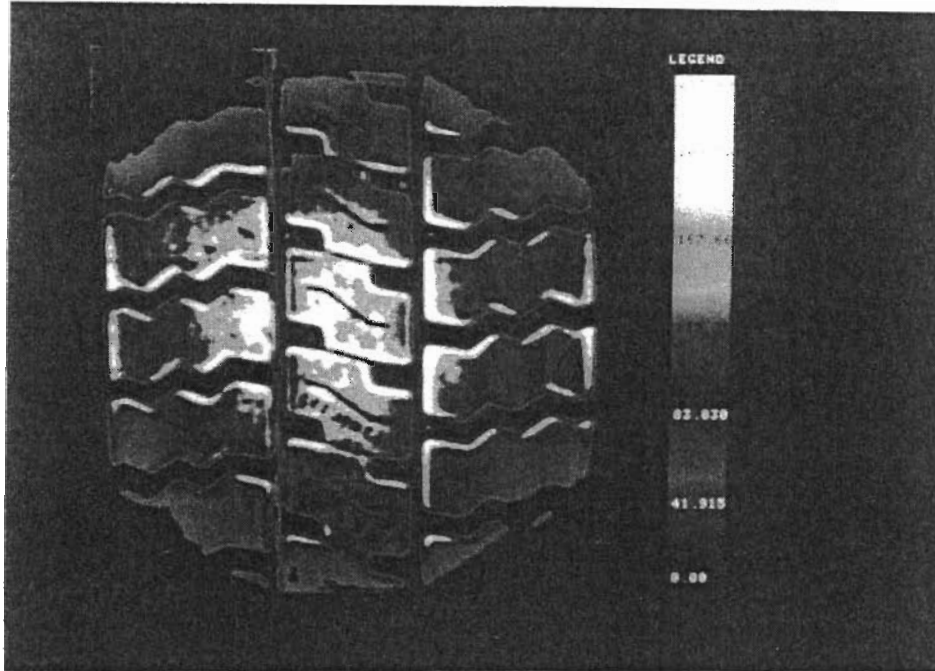


Fig 4.32. Two-dimensional spectrum graphic for the wide base bias 18-22.5 load range-H tire inflated to 85 psi and loaded to 12,000 pounds.

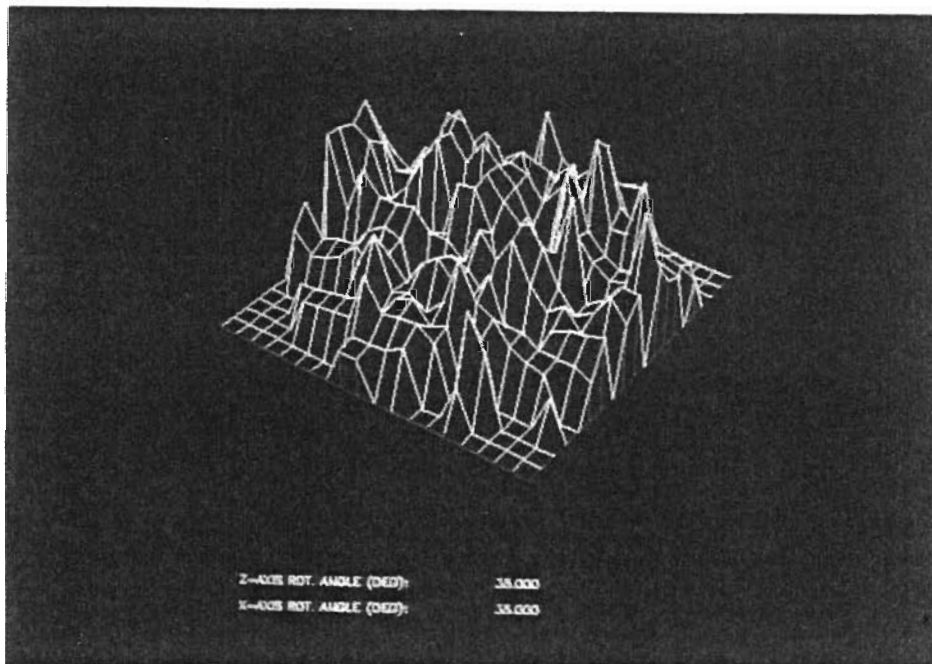


Fig 4.33. Three-dimensional surface plot for the wide-base bias 18-22.5 load range-H tire inflated to 85 psi and loaded to 12,000 pounds.

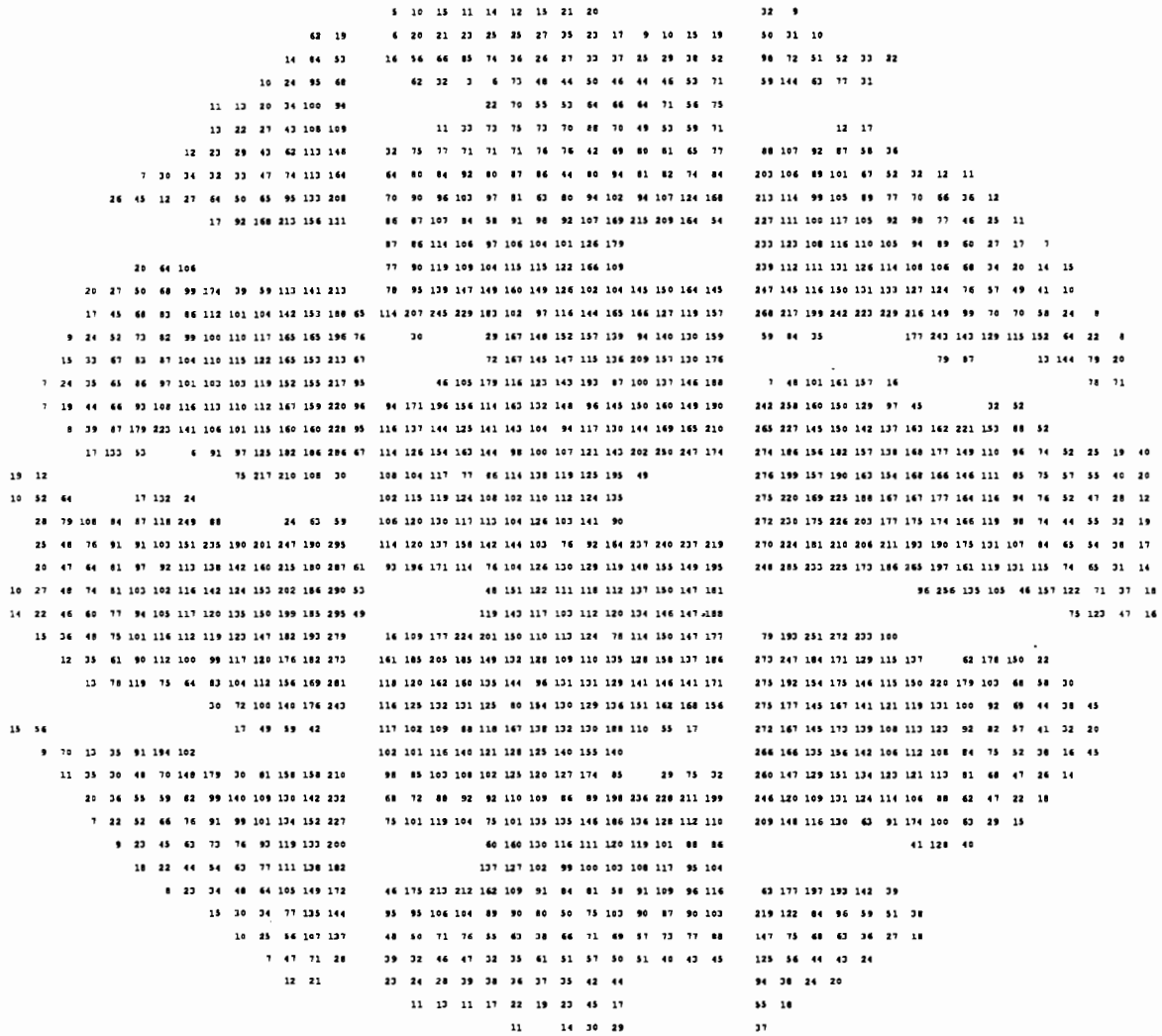


Fig 4.34. Pressure map for the wide-base bias 18-22.5 load rang-H tire inflated to 100 psi and loaded to 8,000 pounds. The pressure print is roughly 11.1 inches long and 11.4 inches wide.

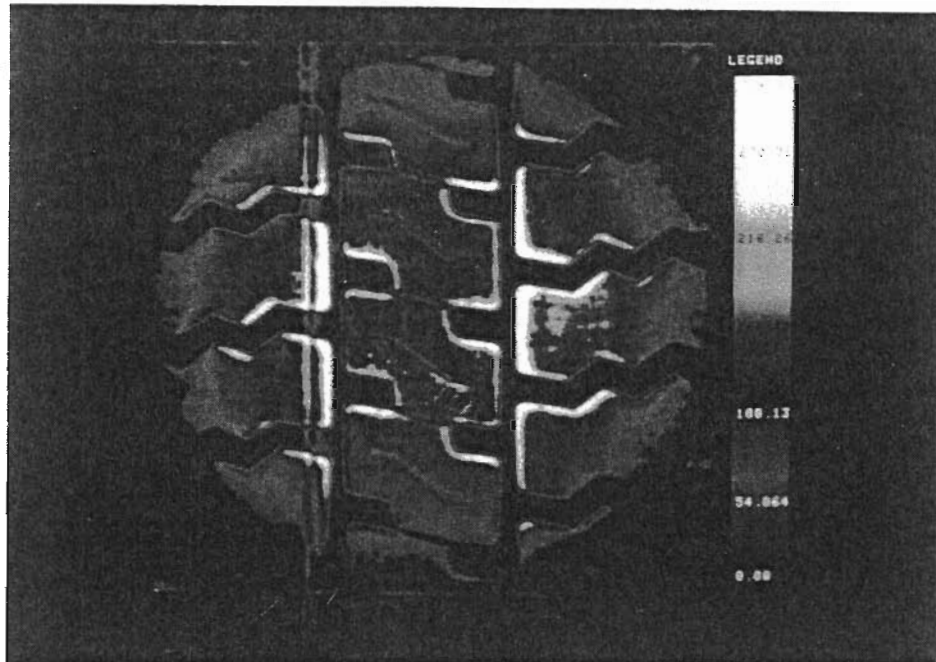


Fig 4.35. Two-dimensional spectrum graphic for the wide base bias 18-22.5 load range-H tire inflated to 100 psi and loaded to 8,000 pounds.

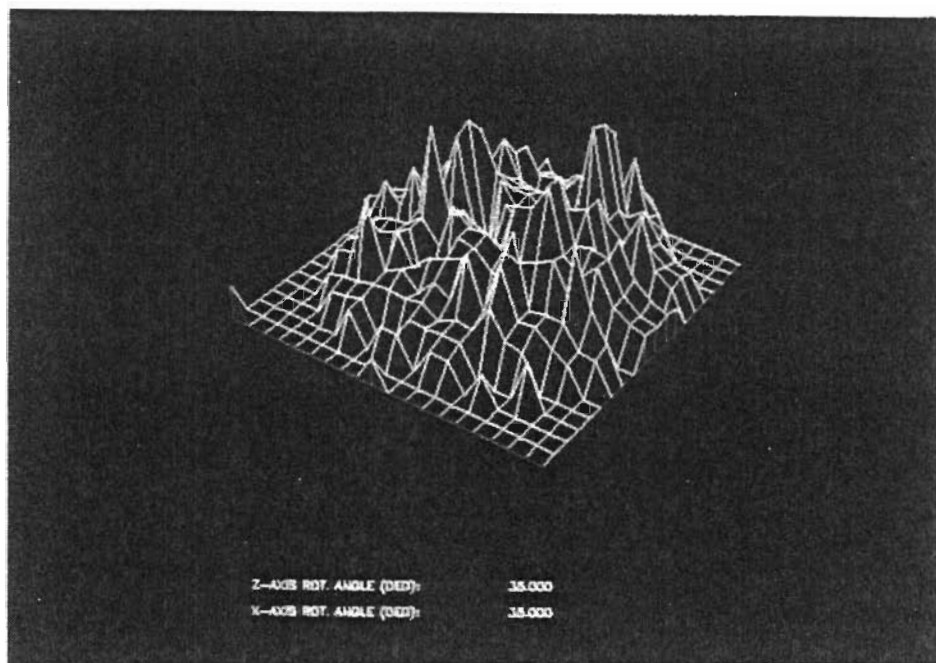


Fig 4.36. Three-dimensional surface plot for the wide-base bias 18-22.5 load range-H tire inflated to 100 psi and loaded to 8,000 pounds.

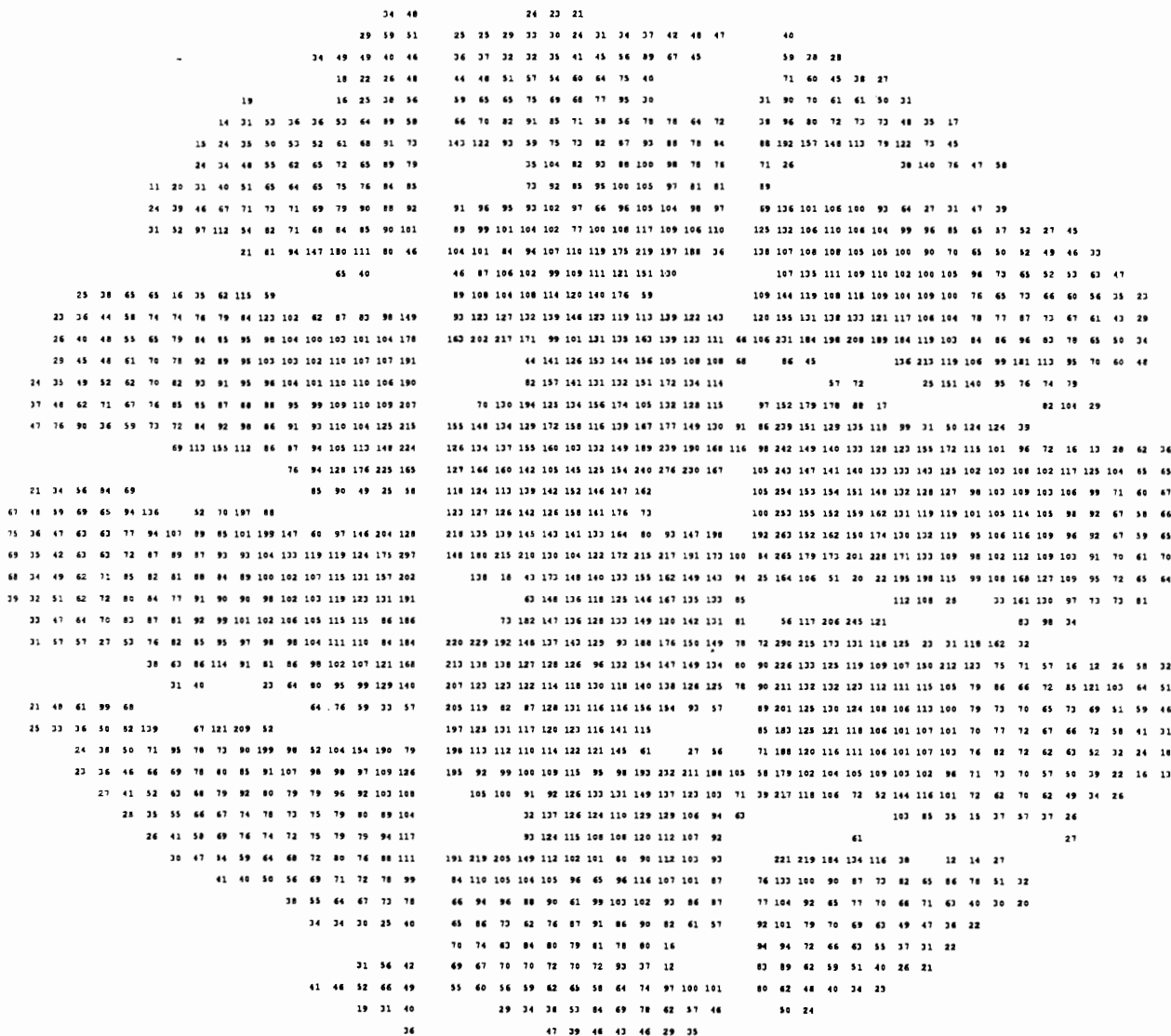


Fig 4.37. Pressure map for the wide-base bias 18-22.5 load rang-H tire inflated to 100 psi and loaded to 10,000 pounds. The pressure print is roughly 12.1 inches long and 12.1 inches wide.

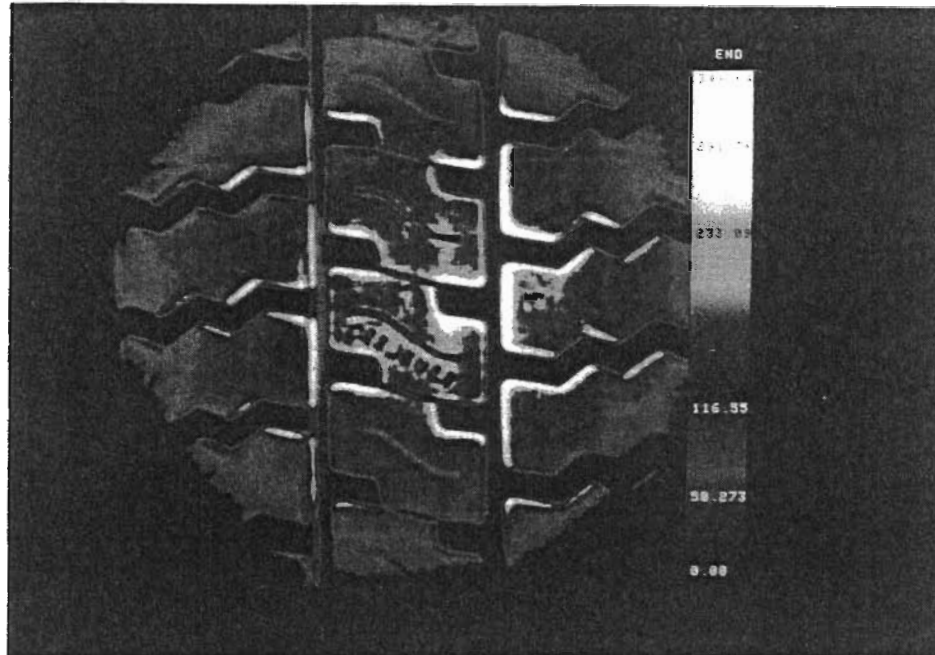


Fig 4.38. Two-dimensional spectrum graphic for the wide base bias 18-22.5 load range-H tire inflated to 100 psi and loaded to 10,000 pounds.

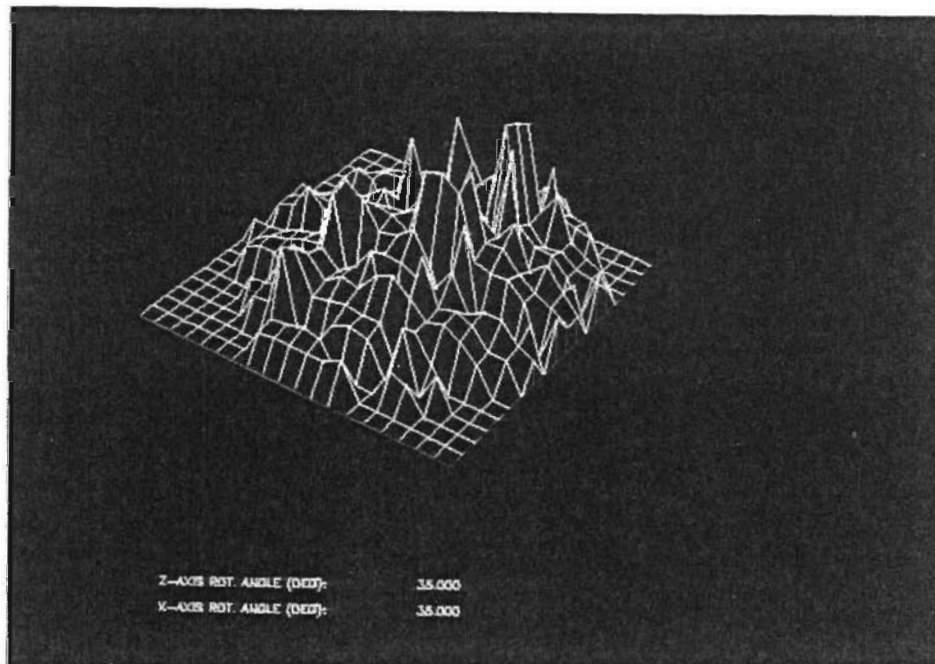


Fig 4.39. Three-dimensional surface plot for the wide-base bias 18-22.5 load range-H tire inflated to 100 psi and loaded to 10,000 pounds.

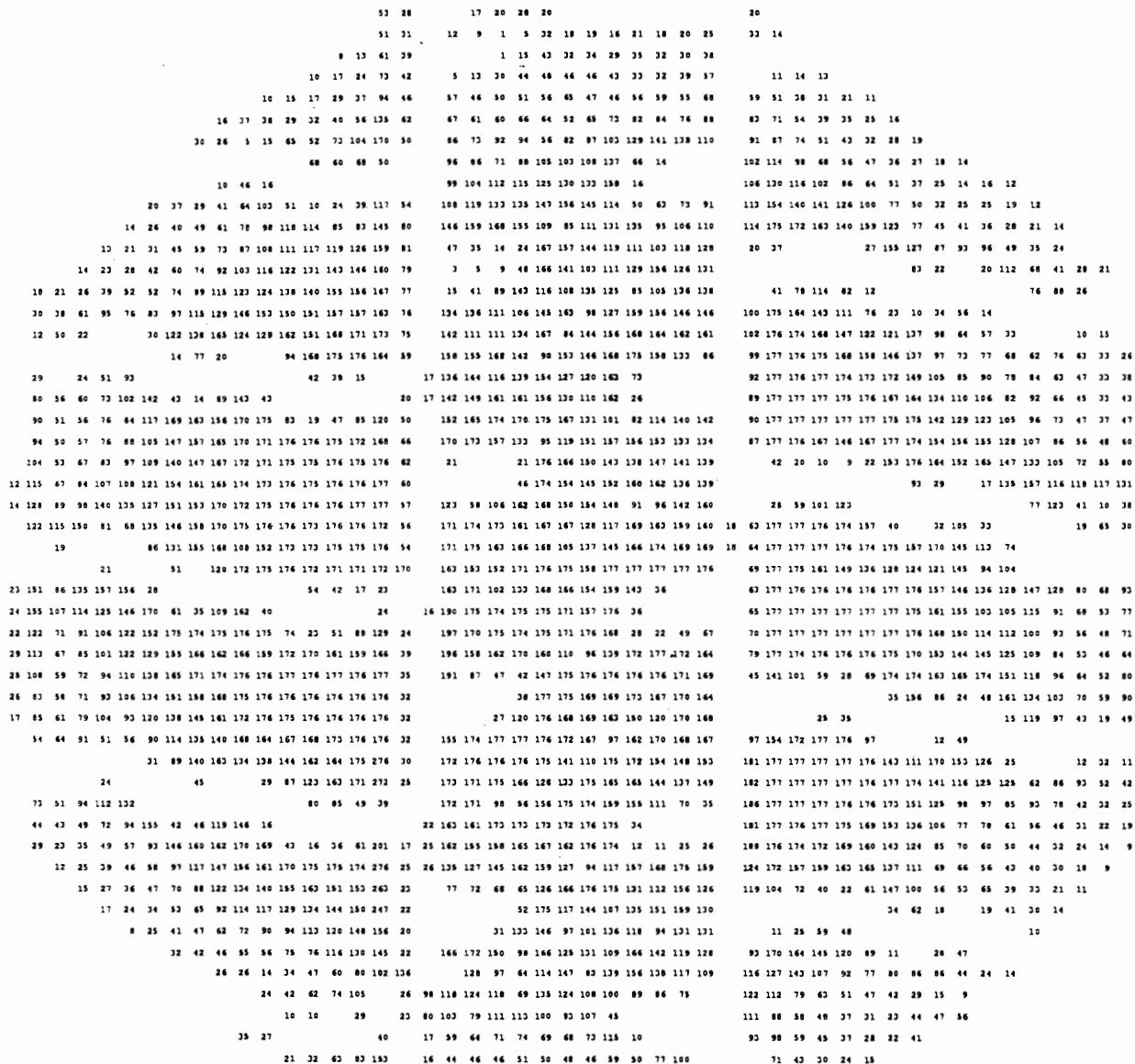


Fig 4.40. Pressure map for the wide-base bias 18-22.5 load rang-H tire inflated to 100 psi and loaded to 12,000 pounds. The pressure print is roughly 12.3 inches long and 12.4 inches wide.

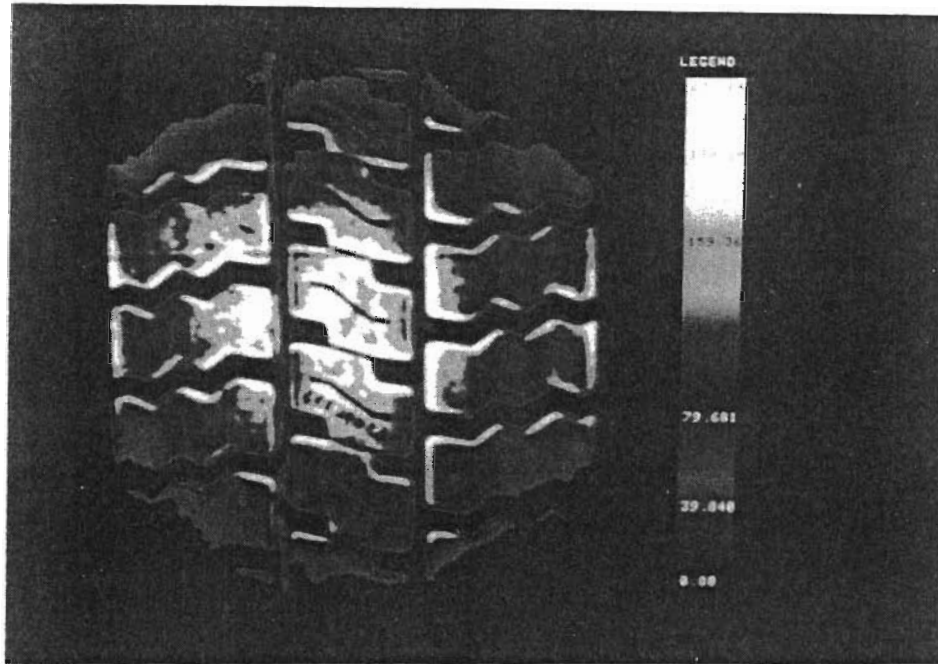


Fig 4.41. Two-dimensional spectrum graphic for the wide base bias 18-22.5 load range-H tire inflated to 100 psi and loaded to 12,000 pounds.

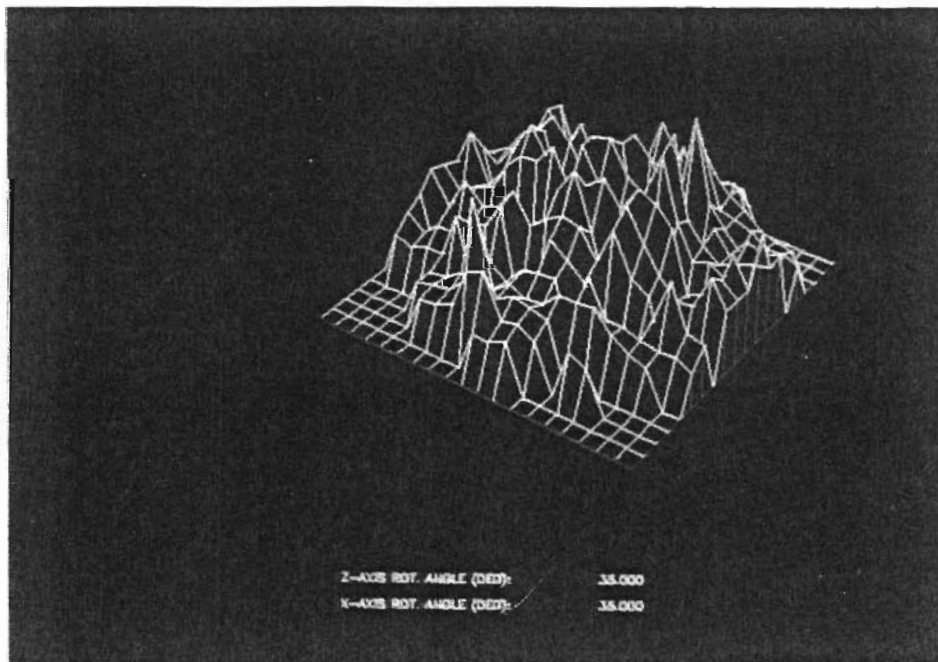


Fig 4.42. Three-dimensional surface plot for the wide-base bias 18-22.5 load range-H tire inflated to 100 psi and loaded to 12,000 pounds.

Fig 4.43. Histogram for the wide-base 18-22.5 load range-H tire, showing the change in the load distribution across the tread width at an inflation pressure of 85 psi and wheel loads of 8,000, 10,000, and 12,000 pounds.

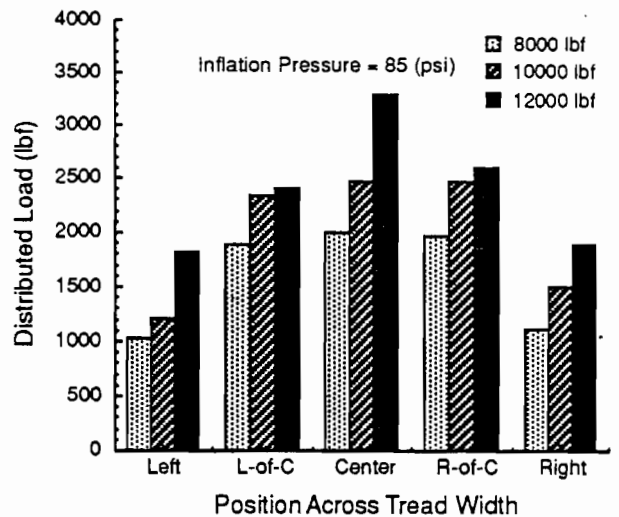


Fig 4.44. Histogram for the wide-base 18-22.5 load range-H tire, showing the change in the load distribution across the tread width at an inflation pressure of 100 psi and wheel loads of 8,000, 10,000, and 12,000 pounds.

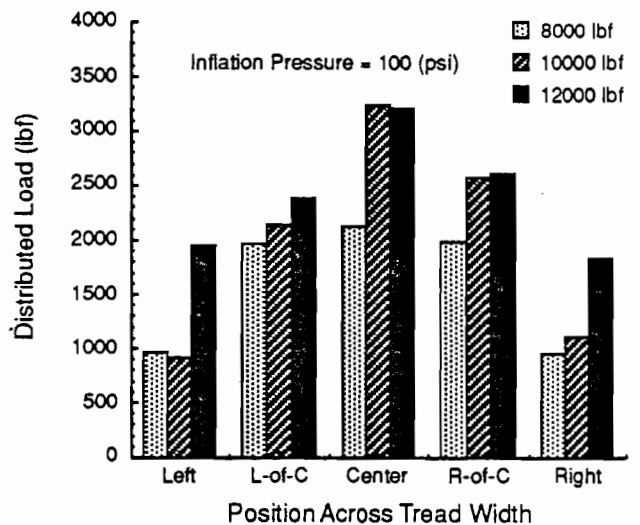
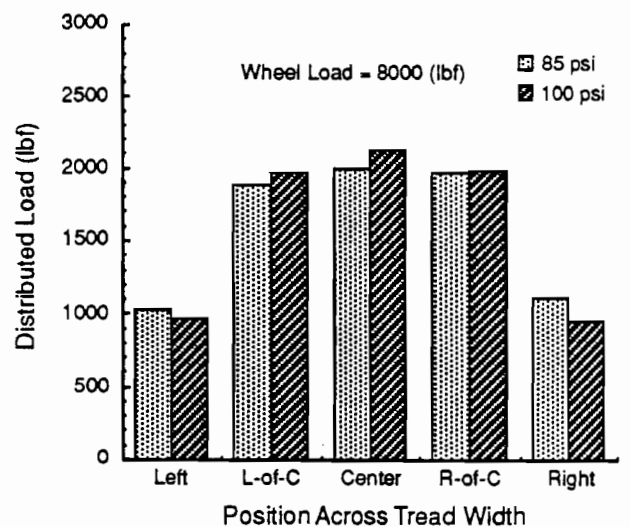


Fig 4.45. Histogram for the wide-base 18-22.5 load range-H tire, showing the change in the load distribution across the tread width at 8,000 pound wheel load and inflation pressures of 85 and 100 psi.



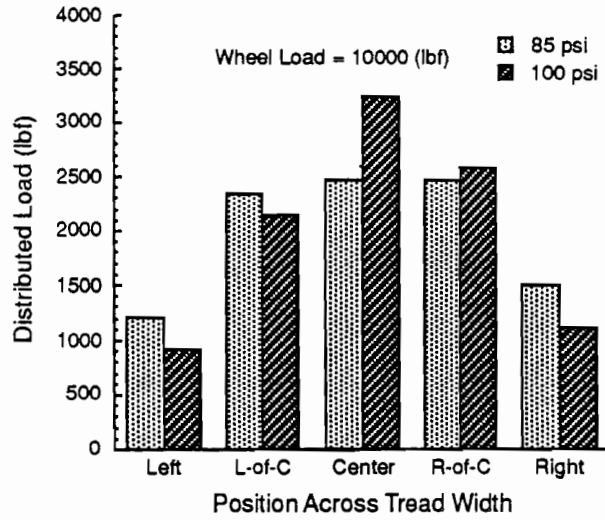


Fig 4.46. Histogram for the wide-base 18-22.5 load range-H tire, showing the change in the load distribution across the tread width at 10,000 pound wheel load and inflation pressures of 85 and 100 psi.

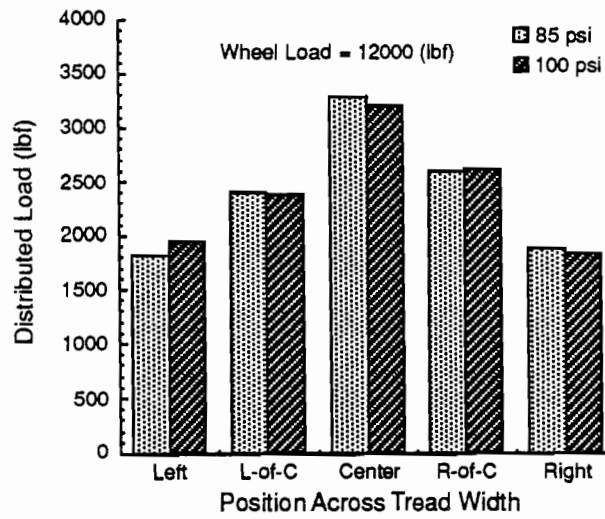


Fig 4.47. Histogram for the wide-base 18-22.5 load range-H tire, showing the change in the load distribution across the tread width at 12,000 pound wheel load and inflation pressures of 85 and 100 psi.

Fuji Prescale Film

Experimentation with the Fuji film provided an opportunity to see its advantages and disadvantages. Within a short time (approximately thirty minutes) the film allows the users to easily distinguish relative pressure magnitudes. During the experiment, the research team found that the prescale film color intensity changes with time after exposure and between boxes in different manufacturing lots. In order to compensate for the film's change with time, calibration squares were created at the same time period as the tire pressure prints were taken. To compensate for possible differences in film between boxes having different lot numbers, a set of calibration squares were produced for each box of film used during the same testing period.

The second problem with the Fuji film, as discussed in Chapter 3, was that the prescale film was not wide enough to test the 18-22.5 super single tire without overlapping the sheets. The researchers made every attempt to place the overlap so it would be within the tread groove during testing. However, even though the film was placed within the tread gap prior to loading, the overlap did not remain in the tread gap for the full duration of the testing. This caused an increased pressure reading on the super single tire prints when the overlap was loaded. The authors believe this does not invalidate the data because the error is small, is easily distinguished on the two-dimensional spectrum graphics, and, therefore, can be compensated for by the user.

The final error caused by using the Fuji film resulted from the fact that the super single tire's contact pressures may have surpassed the recommended pressure for the Fuji Super Low film in various locations on the tire print. The maximum allowable pressure for the Super Low film was approximately 285 psi. To compensate for the higher pressures the researchers produced calibration squares for pressures ranging up to 320 psi and allowed the Adage system's calibration subroutine to interpolate the higher pressures from the calibration curve. To check the accuracy an additional experiment was conducted using prescale film having a higher load range. The researchers laid two different types of Fuji film, one on top of the other, and loaded them simultaneously. The two films included the original Super Low film and a Low range pressure film. The Super Low film has an approximate measuring range of 0 to 285 psi, as stated earlier, while the Low film has a pressure range from 285 to 1,000 psi. After the prints were produced the Super Low prints were scanned and analyzed. The researchers determined that the maximum contact pressures were within a short interpolating range of the Super Low film by visually comparing the prints produced using the Low film to the Low film calibration squares.

Load Apparatus

The load apparatus was assembled many times with various pieces of equipment suitable for monitoring load

values, obtaining and maintaining a desired load, and producing contact pressure distribution prints. Many of the pieces eventually failed or were improved upon during the initial ink print testing. The equipment discussed in Chapter 3 was determined to be the most reliable, repeatable, and available equipment. Therefore, it was used to produce the pressure distribution maps presented in this report. During the testing the researchers were concerned about the amount of wheel load being lost through friction within the loading apparatus. It also became apparent that play within the load frame was causing some eccentric loading.

To insure that only a relatively low amount of wheel load was being lost through friction within the load frame, the following experiment was run. The load frame columns were greased and a load cell was placed in between the tire and steel platen during a trial loading. Readings from the load cells located at above and below the tire were within 0.6 percent of each other throughout the testing range. Therefore, a negligible loss in applied load occurred due to friction within the load frame apparatus. To insure that the load frame would continue to remain frictionless the columns were kept well greased.

It was noticed that approximately 0.125 inch of play existed in the load frame during the trial testing of the 11R24.5 tire. This play allowed the tire to wobble from side to side. The super single tire, on the other hand, exhibited very little frame play. The researchers determined that the difference in play between the tires was due to the super single tire's larger weight and size. This prohibited the horizontal movement within the load frame.

In order to remove the looseness in the load frame apparatus during the testing of the 11R24.5 tire, the various load frame parts which caused the play were shimmed into place. This action prevented most of the horizontal movement from occurring. To insure the load frame was plumb and level throughout the testing, the load frame's cross beams and load transfer arms were checked with a bubble level. Throughout the experiments the shims worked satisfactorily.

In summary, the experiments showed that, for the 11R24.5 radial tire and the 18-22.5 bias tire, increased wheel loads, at constant inflation pressures, generally resulted in more uniform contact pressures throughout the contact area. On the other hand, increased inflation pressures, at constant wheel loads, resulted in reduction of contact area and increased contact pressures in the contact patch's central region. Low inflation pressures tended to cause the wheel load to be distributed more heavily to the contact patch's central area for the radial tire and more heavily to the sidewall contact area for the bias tire. The results and conclusions are further discussed in the next chapter.

CHAPTER 5. CONCLUSIONS AND RECOMMENDATIONS

Within the last 50 years truck sizes, allowable wheel loads, truck tire sizes, and tire inflation pressures have increased. In order to establish pavements capable of sustaining this increased loading, the actual loading mechanisms and their magnitudes must first be identified. To identify the magnitudes, static testing was performed on two tires at The University of Texas at Austin. A summary of the research performed, conclusions from the results, and recommendations for future research are presented below.

SUMMARY OF RESEARCH

A load frame was reassembled to provide a static load on two tires. The first, a specially manufactured smooth tread Armstrong 11R24.5 load range-G tire, was selected so that its pressure distribution data could be used to verify contact pressure data produced by Tielking's finite element tire model. The second tire, a commercial Goodyear wide-base super single 18-22.5 load range-H tire, was selected because of increased interest in the effect these popular tires have on pavement life. The 11R24.5 radial was inflated to 90 and 105 psi and at each inflation pressure loaded to 5,000, 6,000, and 7,000 pounds. The 18-22.5 recapped tire was inflated to 85 and 100 psi and at each inflation pressure loaded to 8,000, 10,000, and 12,000 pounds.

As the tires were loaded, Fuji prescale film was used to capture the contact pressure densities. This was accomplished by converting the pressures into colors of corresponding density. An Adage 3006 graphics system using an Eikonix computer image scanner was then used to digitize the prints, producing an array of corresponding pixel intensities. This array was then converted into an array of corresponding pressure values. Once the array of pressure values was obtained, the pressure distribution data were displayed as two and three-dimensional graphics and also printed out as numerical pressure maps.

Using the Adage graphics system, various tests were performed to verify the experiment's repeatability. Results of the tests show that similar data could be reproduced 90 percent of the time with an accuracy of 85 percent.

CONCLUSIONS

From the experimentation on the smooth tread 11R24.5 radial and recapped 18-22.5 bias-ply tires the following conclusions were made.

- (1) At low wheel loads, the load was supported by the central and edge portions of the radial 11R24.5 tire.
- (2) As the wheel load was increased on the radial tire, while the inflation pressure was kept constant, the contact pressures became more uniform.

- (3) At constant wheel load, as the tire inflation pressure increased, the contact pressures in the tread's central region increased more than the pressures in the sidewall region.
- (4) Increased wheel load on the radial tire, at a constant inflation pressure, was accompanied by a lengthening in the contact patch.
- (5) Generally, as the wheel load was increased, while the inflation pressure was held constant, the contact area tended to increase. On the other hand, if the wheel load was kept constant, an increase in tire inflation pressure was accompanied by a decrease in contact area. The super single tire exhibited this characteristic only after the full tread width had established contact.
- (6) The super single 18-22.5 bias tire's sidewall regions initially established contact when loaded to 10,000 pounds. The same tire at a load below 10,000 pounds had a circular contact area. When the wheel load exceeded 10,000 pounds the contact area's shape became more oval.
- (7) At constant inflation pressure, after the bias super single's sidewall regions had established contact, additional loading was accompanied by a lengthening of the contact area.

RECOMMENDATIONS

In order to better quantify wheel loading which can be used to improve pavement design, the following recommendations suggest the direction for future research.

- (1) Test a slightly used 11R24.5 load range-G tire and compare the results to the smooth 11R24.5 tire's test results, provided in this report.
- (2) Test additional wide-base super single tires, especially radial and low profile super single tires. Both manufacturers and truck operators predict the continued increase in wide base tire popularity. The effect the wide-base tires will have on pavement life and pavement management must continue to be assessed in order to design pavements capable of sustaining the wheel and inflation pressure loads for a sufficient time period.
- (3) An additional series of tests should be performed to determine the contact pressures of a 285R/75/24.5, and 15R22.5 LR-G, as recommended by Dr. J. T. Tielking of Texas A&M.
- (4) Perform additional static testing using a simulated asphalt surface instead of the steel platen. The results could be correlated with the results of the tests performed using a steel platen. The contact pressures would be slightly higher using a rough particulate

surface as opposed to a perfectly smooth, uniform surface because the contact area would be smaller on the rough surfaces.

- (5) Develop a system capable of measuring dynamic contact stresses (normal and tangential) under a freely rolling tire. A system capable of measuring changes in pavement stresses under a freely rolling tire could provide data useful for determining the effect of cyclic loading and velocity on pavement life.

- (6) The Fuji prescale film changes with time and from box to box. Therefore, to minimize experimental error, calibration squares must be created at approximately the same time as the tire pressure prints. If the operators must use two separate boxes of film to complete the testing of one tire, then a set of calibration squares must be produced for each box of film.

REFERENCES

1. Roberts, F. L., et al, "Establishing Material Properties For Thin Asphalt Concrete Surfaces On Granular Bases," Research Report 345-1, Texas Transportation Institute, Texas A&M University, College Station, Texas, November 1985.
2. Van Vuuren, D. J., "Tyre Pressure and Its Effect On Pavement Design and Performance," *Civil Engineering In South Africa*, Vol 16, No. 8, August 1974.
3. Brown, J. L., "Proceedings Of A Symposium/Workshop On High Pressure Truck Tires," Austin, Texas, February 1987.
4. Butler, Lee, "Truck Tire Pressure And Pavement Damage," *Proceedings, Symposium/Workshop On High Pressure Truck Tires*, Austin, Texas, February 1987.
5. DeCabooter, Philip H., "Wisconsin Truck Tire Pressure Study," FHWA/WI-88/1, Wisconsin Department of Transportation, Division of Highways and Transportation Services, Madison, Wisconsin, January 1988.
6. Roberts, F. L., et al, "The Effect Of Tire Pressures On Flexible Pavements," Research Report 372-1F, Texas Transportation Institute, Texas A&M University, College Station, Texas, August 1986.
7. Planning and Statistics Bureau, Montana Department of Highways, "1984 Truck Tire Study," Helena, Montana, 1984.
8. "Tire Pressure Survey," Unpublished Data, Bureau Of Design, Division of Highways, Illinois Department of Transportation, Springfield, Illinois, 1986.
9. Thompson, Marshall R., "Analytical Methods For Considering Tire Pressure Effects In Pavement Design," *Proceedings, Symposium/Workshop On High Pressure Truck Tires*, Austin, Texas, February 1987.
10. AASHTO Road Test, Highway Research Board, "History and Description of the Project," Report 61A, 1960.
11. Sharp, Asa, "Truck Tire Pavement Interaction," *Proceedings, Symposium/Workshop On High Pressure Truck Tires*, Austin, Texas, February 1987.
12. Clark, Samuel K., Editor, *Mechanics Of Pneumatic Tires*, National Bureau Of Standards Monograph 122, November 1971.
13. Tielking, J. T., and F. L. Roberts, "Tire Contact Pressure and Its Effects On Pavement Strain," *Journal of Transportation Engineering*, Vol 113, No. 1, January 1987.
14. Sharma, J., and J. Mahoney, "Evaluation of Present Legislation And Regulations On Tire Sizes, Configurations And Load Limits," Unpublished Executive Summary Prepared by the University Of Washington for Washington Department of Transportation.
15. Lippmann, S. A., and K. L. Oblizajek, "The Distributions of Stress Between The Tread And The Road For Freely Rolling Tires," SAE 74102, Society of Automotive Engineers, Detroit, February 1974.
16. Papagianakis, A. T., and R. C. G. Haas, "Wide-Base Truck Tires: Industry Trends And State Of Knowledge Of Their Impact On Pavements," Ministry Of Transportation and Communications of Ontario, December 1986.
17. Yeager, R. W., "Tires of the Nineties and Beyond," *Elastomerics*, Vol 119, No. 2, February 1987.
18. Seitz, N., and A. W. Hussmann, "Forces and Displacement in Contact Area of Free Rolling Tires," *S. A. E. Transaction*, Vol 80, Paper No. 710626, 1971.
19. Bonse, R. P. H., and S. H. Kuhn, "Dynamic Forces Exerted by Moving Vehicles on a Road Surface," *Highway Research Board Bulletin No. 233*, 1959.
20. Ginn, J. L., and R. L. Marlowe, "Road Contact Forces of Truck Tires as Measured in the Laboratory," *SAE Transactions*, Vol 76, Paper No. 670493, 1967.
21. Zekoski, J., "Impact of Truck Tire Selection on Contact Pressers," FHWA Load Equivalence Workshop, Sponsored by the Federal Highway Administration Pavements Division, Turner-Fairbanks Highway Research Center, McLean, Virginia, September 13-15, 1988.
22. Huhtala, M., "Field Tests to Compare Tires," FHWA Load Equivalence Workshop, sponsored by the Federal Highway Administration Pavements Division, Turner-Fairbanks Highway Research Center, McLean, Virginia, September 13-15, 1988.
23. Marshek, K. M., et al., "Experimental Investigation of Truck Tire Inflation Pressure on Pavement-Tire Contact Area and Pressure Distribution," Research Report 386-1, Center for Transportation Research, The University of Texas at Austin, August 1985.
24. Haas, R. C. G., and A. T. Papagianakis, "Understanding Pavement Rutting," *Roads and Transportation Association of Canada*, Toronto, Ontario, September 28, 1986.

25. Eisenmann, J., and A. Hilmer, "Influence Of Wheel Load And Inflation Pressure On The Rutting Effects At Asphalt-Pavements-Experiments and Theoretical Investigations," Sixth International Conference on the Structural Design of Asphalt Pavements, Ann Arbor, July 1987.
26. Monismith, C. L., "Fatigue Characteristics of Asphalt Paving Mixtures and Their Use in Asphalt Pavements," Proceedings of Annual Pavement Conference, Symposium on Fatigue In Asphalt Pavements, University of New Mexico, Albuquerque, New Mexico, 1981.
27. Chen, H. H., K. M. Marshek, and C. L. Saraf, "Effects of Truck Tire Contact Pressure Distribution on the Design of Flexible Pavements: A Three-Dimensional Finite-Element Approach," Transportation Research Report 1095, Transportation Research Board, National Research Council, Washington, D. C., 1986.
28. "Fuji Prescale Film General Information," Fuji Photo Film Company, Limited, Tokyo, Japan, 1986.
29. Aalund, M., et al., "Development Of An Automated System For Analyzing Fuji Film Images With CIPD-100 Densitometer Of Tire/Pavement Interface Pressure Distribution," Mechanical Engineering Design Projects Program, The University of Texas at Austin, Spring 1988.
30. Chan, Gerard, "Computer Image Processing Technique for Analysis of the Tire Contact Pressures," M. S. Thesis, The University of Texas at Austin, December 1988.
31. Wakeland, Richard E., "Video Image Analysis of Pressure Sensitive Film," M. S. Thesis, The University of Texas at Austin, December 1985.
32. Digital Equipment Corporation, "Guide to Using DCL and Command Procedures on VAX/VMS," Maynard, Massachusetts, September 1984.
33. Research Systems Incorporated, "Users Guide to VAX IDL Interactive Data Language," Denver, Colorado, 1982.

APPENDIX A. TIRE MARKETING SURVEY

In addition to the literature concerning actual field measurements of tire types, inflation pressures, and axle loads currently running on U.S. highways, it was believed tire marketing information could also contribute to the selection of an appropriate sample of tires to evaluate in this study. The six individuals employed by the major tire manufacturers shown below were contacted by telephone. Each individual responded that he would be willing to participate in the survey to the best of his abilities, and, therefore, on September 22, 1988, the survey was mailed. A sample copy of the cover letter and the responses follow on the next pages.

Mr. Barry Petrea
Marketing Department
Department 530
Kelly Springfield Tire Company
Willowbrook Road
Cumberland, Maryland 21502
(301) 777-6475

Mr. Stephen Avery
Marketing
Michelin Tire Corporation
P. O. Box 19001
Greenville, South Carolina 29602
(803) 234-5286

Mr. James Mueller
Manager, Heavy Equipment Tires
Armstrong Tire Company
500 Sargent Avenue
New Haven, Connecticut 06536-0201
(203) 784-2231

Mr. Joseph Zekoski
Advanced Truck Tire Engineering
Department 461
Goodyear Tire Technical Center
1144 East Market Street
Akron, Ohio 44316
(216) 796-3493

Mr. Charles L. Bond
Manager, Business Research
Uniroyal Goodrich Tire Company
600 South Main Street
Akron, Ohio 44397-0001
(216) 374-3737

Mr. Thomas G. Salpietra
Product Manager
Commercial Tire Products
General Tire and Rubber Company
Akron, Ohio 44329
(216) 798-230

Overall the response was successful. Five out of six tire manufacturers surveyed responded. Their responses showed that the radial 11R24.5 load range-G, radial 11R22.5 load range-G, bias 10.00-20 load range-F, and bias 11.00-22.5 load range-F appear to be the most popular truck tires. The survey responses have been compiled and can be seen in Table A.1 on the following page. It was hoped that the data would show a definite result indicating whether the predominant truck tire was a radial or bias-ply tire design. The responses were very difficult to interpret but some useful data was obtained. Michelin makes nothing but radials; Uniroyal Goodrich does not produce radials yet, but responded that their share of the market is only two percent; Goodyear responded that 65 percent of the truck tires they sell are radials; and Armstrong replied that only 40 percent of their market are radials. The tire manufacturers didn't want to discuss how much of the total market they may possess so it was hard to judge from the responses whether more radials than bias tires are sold yearly. Although from the survey response it is not clear whether or not the radial tire is predominant in the U.S., it is apparent that many radials are marketed.

Three problems eventually arose during the survey which may have affected the results. First, a self addressed, stamped envelope was not included with the survey, as was stated in the cover letter. Three weeks after the surveys had been mailed, Michelin, Kelly Springfield, and Armstrong had not responded, and, therefore, a follow-up call was made to determine the cause of the delay. These company representatives, with the exception of Mr. Petrea, of Kelly Springfield, said the surveys had been mailed. In order to obtain the information not received, the survey was conducted over the telephone with Mr. Avery and Mr. Mueller of the Michelin and Armstrong tire companies, respectively. Mr. Petrea declined to participate because he felt that the survey requested proprietary information.

Second, questions two and three should have been more specific by asking, "What is *your* most popular radial/bias truck tire?" At the time the wording used seemed appropriate but it must have been confusing. An example of the confusion occurred when Mr. Bond of Uniroyal Goodrich responded that the company did not market radial tires but that the most popular radial tire was an 11R24.5 load range-G. Apparently he was answering for the total market, not just his sales. It is unclear if the other respondents were similarly confused because they do market radials.

The last problem was that the answer to question five, which was intended to quantify the tire types discussed in the preceding questions, was considered proprietary information by all but one tire manufacturer. As a result, it was very hard to determine which tire size is the most popular on U.S. highways from the survey responses. The survey did assist in determining which tires to include in the test sample.

TABLE A.1. TIRE SURVEY SUMMARY

<u>Manufacturer</u>	Percent Sales that are <u>Radials</u>	<u>Most Popular Truck Tires</u>			
		<u>Radial Truck Tire</u>	<u>Radial Super Single</u>	<u>Bias Truck Tire</u>	<u>Bias Super Single</u>
Armstrong	40	11R24.5-G	-	11R24.5-F	-
General	N/R	11R24.5-G	-	10.00-20	-
Goodyear	65	11R24.5-G	16.5R22.5-J	1000 R20-F	15-22.5-H
Michelin	100	275/80R-G	385/65R22.5-J	-	-
Uniroyal	0	11R24.5-G	-	11-22.5-F	-

September 22, 1988

Mr. Barry Petrea
Marketing Department
D530
Kelly Springfield Tire Company
Willowbrook Road
Cumberland, Maryland 21502

Dear Mr. Petrea,

As we discussed on the telephone, I am at the University of Texas conducting research into the effects of truck tire pressures on pavement life, with special emphasis on wide base "Super Single" truck tires. Within my report I intend to present data on the types and numbers of popular truck tires currently running on American highways. I believe you could make a valuable contribution concerning current truck tire operations which would allow me to produce a comprehensive and accurate survey. I would appreciate it if you would complete the attached, short survey and return it in the enclosed, stamped envelope within ten days. If you are able, any other information concerning this topic would also be appreciated.

Thank you in anticipation of your cooperation.

Sincerely,
Rex W. Hansen
Research Engineer

RWH/wg
Enclosure

General Tire and Rubber Company
Acron, Ohio 44329

Name and telephone

number of respondent: _____

Please give the tire type and sizes (e.g. 11R24.5 type H or 18-22.5 type G) to the following questions where appropriate. All questions relate to the total market comprising original equipment plus replacement market.

1. Of your total truck tires marketed, what percentage of sales are radials?
_____ %
2. What is the most popular radial truck tire?

3. What is the most popular bias belted truck tire?

4. What are the most popular radial and bias belted wide base "Super Single" truck tires you market?
_____ Radial
_____ Bias Belted
5. What percent of the total U.S. truck tire market do you feel your company has?
_____ %
6. Would you like a copy of our research findings?
 yes no

1190/Hansen/wg/S88

Michelin Tire Corporation
P.O. Box 19001
Greenville, South Carolina 29602

Name and telephone

number of respondent: _____

Please give the tire type and sizes (e.g. 11R24.5 type H or 18-22.5 type G) to the following questions where appropriate. All questions relate to the total market comprising original equipment plus replacement market.

1. Of your total truck tires marketed, what percentage of sales are radials?
_____ %
2. What is the most popular radial truck tire?

3. What is the most popular bias belted truck tire?

4. What are the most popular radial and bias belted wide base "Super Single" truck tires you market?
_____ Radial
_____ Bias Belted
5. What percent of the total U.S. truck tire market do you feel your company has?
_____ %
6. Would you like a copy of our research findings?
 yes no

1190/Hansen/wg/S88

Armstrong Tire Company
 500 Sargent Avenue
 New Haven, Connecticut 06536-0201

Name and telephone

number of respondent: _____

Please give the tire type and sizes (e.g. 11R24.5 type H or 18-22.5 type G) to the following questions where appropriate. All questions relate to the total market comprising original equipment plus replacement market.

1. Of your total truck tires marketed, what percentage of sales are radials?
 _____%
2. What is the most popular radial truck tire?

3. What is the most popular bias belted truck tire?

4. What are the most popular radial and bias belted wide base "Super Single" truck tires you market?
 _____ Radial
 _____ Bias Belted
5. What percent of the total U.S. truck tire market do you feel your company has?
 _____%
6. Would you like a copy of our research findings?
 yes no

1190/Hansen/wg/S88

Uniroyal Goodrich Tire Company
 600 South Main Street
 Akron, Ohio 44397-0001

Name and telephone number of respondent: C Bond

216-374-3737

Please give the tire type and sizes (eg. 11R24.5 type H or 18-22.5 type G) to the following questions where appropriate. All questions relate to the total market comprising original equipment plus replacement market.

1. Of your total truck tires marketed, what percentage of sales are radials?

0 %

2. What is the most popular radial truck tire?

11R24.5 G

3. What is the most popular bias belted truck tire?

11-22.5 F

4. What are the most popular radial and bias belted wide base "Super Single" truck tires you market?

— Radial

— Bias Belted

5. What percent of the total U. S. truck tire market do you feel your company has?

A.B.T 2% %

6. Would you like a copy of our research findings?

yes no

APPENDIX B. LOAD FRAME SCHEMATIC AND PARTS LIST

At the beginning of this project, reassembling the load frame previously constructed for Project 386 was a difficult task. The various parts had to be located or, if they could not be found, purchased or remanufactured. One of the major problems was the absence of a detailed diagram or schematic of the load frame and a parts list. For that reason a schematic and parts list are included here.

PARTS LIST

Item	No.	Description
A	2	Columns
B	1	Load Frame Cross-Head
C	2	2.25 in. x 1.0 in. dia. All-Thread Bolt
D	6	3.0 in. x 0.5 in. dia. Pin
E	2	8.0 in. x 0.5 in. dia. Hex-Head Bolt
F	2	Lock-On Collar
G	2	Column Footings
H	8	Single Bolt Assembly
I	1	Solid Axle Assembly
J*	1	Loading Cross Beam
K*	2	Load Transfer Arms
L*	4	Adaptor Guides
M	1	Sleeve With Welded Nut
N	1	20000-Pound Load Cell
O	1	Hydraulic Actuator
P	4	Countersunk Alan Head Bolt Assembly
Q	1	1.5 x 6.5 x 10 in. Steel Plate
R	1	1.5 x 10.5 x 11 in. Steel Plate
S	4	Bolt Assembly With Leveling Wedges
T	6	Support Collars
U	4	Cross Pins with 2 Cotter Pins

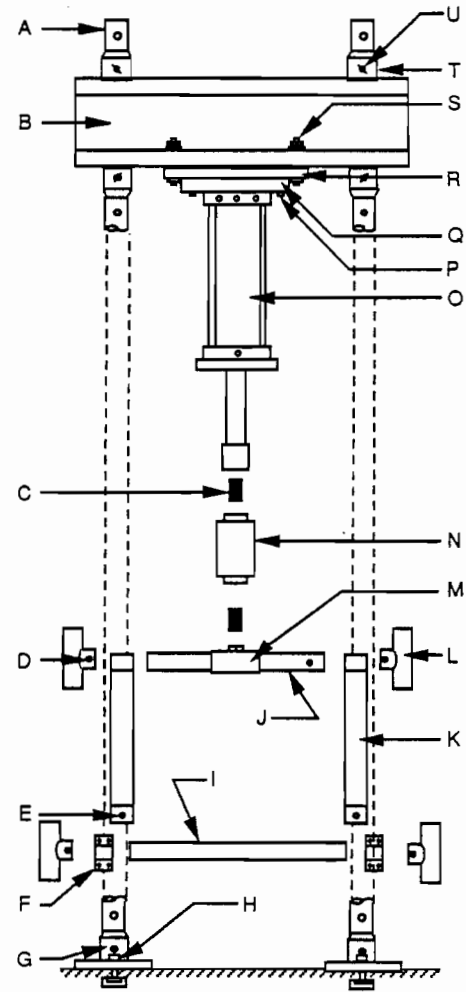


Fig B.1. Load frame schematic.

Items which have their assembly location engraved on them. For example, item L, the adaptor guides, are marked TL for top left, TR for top right and BR for bottom right.

APPENDIX C. LOAD-CELL CALIBRATION

In order to apply the desired load to the tire, two calibration curves were produced which correlated the load cell voltages as read by the HP system with the calibration load cell output (see Fig C.1). The curves were produced from the data in Table C.2. The procedure used to produce the data is presented in Chapter 3, section 1.5.

From Fig C.1, the two samples seem to come from the same population. To prove this, the residuals were computed from each sample's regression and tested for sameness using a non-paired student's t test about the mean equal to zero. From the results shown in Table C.1, it is

evident that 99.98 percent of the time the data is the same, and, therefore, it is safe to draw one regression for all the data points, such as in Fig C.2. Figure C.2 was used to calculate the multimeter readings used to monitor the applied wheel load.

TABLE C.1. CALIBRATION DATA STATISTICS

Data Set	Mean	Standard Deviation	Variances	T-Value	Probability
#1	-0.0756061	43.1886	Unequal	0.0003	0.9998
#2	-0.0796215	56.0757	Equal	0.0003	0.9998

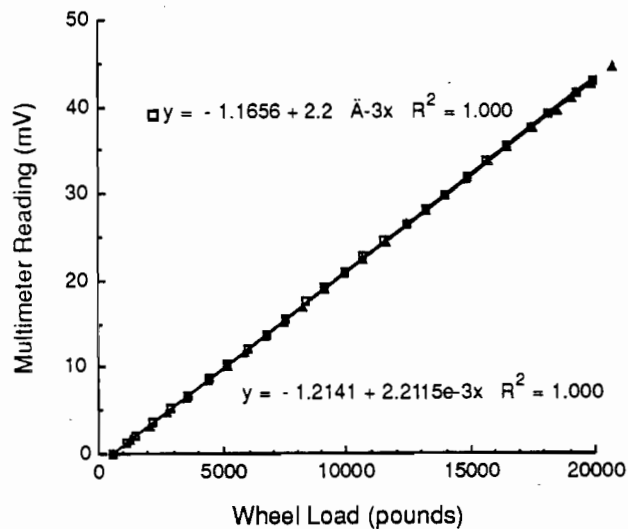


Fig C.1. Calibration curve for 60-kip load cell.

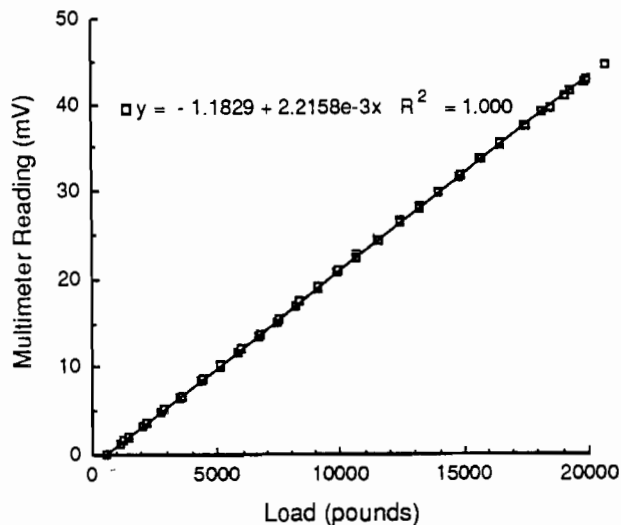


Fig C.2. Combined calibration curve for 60-kip load cell.

TABLE C.2. CALIBRATION DATA

Multimeter Reading #1 (m Volts)	Load (lb)	Multimeter Reading #1 (m Volts)	Load (lb)
0.012	592.0	0.012	592.0
1.130	1088.0	1.560	1282.0
1.950	1450.0	3.230	2020.0
3.650	2178.0	4.800	2708.0
5.150	2847.0	6.540	3491.0
6.750	3579.0	8.550	4380.0
8.680	4430.0	10.010	5136.0
10.270	5141.0	11.611	5853.0
12.150	5953.0	13.460	6660.0
13.800	6740.0	15.209	7450.0
15.480	7497.0	16.981	8210.0
17.450	8338.0	18.930	9090.0
19.180	9124.0	20.690	9905.0
20.950	9931.0	22.440	10697.0
22.700	10671.0	24.420	11568.0
24.600	11522.0	26.631	12405.0
26.500	12412.0	28.010	13165.0
28.200	13158.0	29.750	13965.0
29.850	13940.0	31.650	14820.0
31.920	14873.0	33.690	15720.0
33.680	15656.0	35.260	16470.0
35.420	16508.0	37.490	17569.0
37.500	17439.0	39.460	18500.0
39.200	18199.0	40.870	19073.0
41.500	19275.0	45.560	19850.0
42.900	19910.0	44.630	20730.0

APPENDIX D. EXPERIMENTAL PROCEDURES FOR PRODUCING PRESSURE PRINTS

To produce the digitized contact pressure prints the following procedures were performed.

1. Assemble the load frame, aligning, leveling, and plumbing the members.
2. Connect the hydraulics and HP data Acquisition system.
3. Calibrate the load cell.
4. Using the calibration data, plot the voltage versus load data to obtain a calibration curve. This curve is used to determine the voltages that correspond to the desired loads.
5. Inflate the tire to the desired maximum inflation pressure.
6. Mount the tire into the load frame.
7. Clean anticipated tire contact areas. Soil and other contaminants seem to be attracted and cling to the film; therefore, the tire and platen area need to be as clean as possible.
8. Clean the loading platen.
9. A paper target needs to be placed and taped to the platen. Use it to mark the tire groove location in order to properly place the film overlap.
10. Place the 10-mil Teflon shim stock on the platen and tape it down for a reference if multiple testing is desired. Then lay the Fuji film A and C sheets and a top sheet of Teflon shim stock onto the load platen. For expected tire footprint widths greater than 10.6 inches the film sheets must be overlapped or placed side-by-side in order to obtain a full footprint.
11. Lower the tire so that it is in contact with the surface of the Teflon shim stock.
12. Begin loading. As Fuji suggests, increase the load, eventually reaching the desired maximum load over a minimum of two minutes, as shown in Fig D.1.
13. When the maximum load is obtained, record the in-line hydraulic pressure as read by the in-line pressure gage.
14. Maintain maximum load for two minutes.
15. Unload the tires.
16. Raise the tire, then remove the top sheet of Teflon and the film. Dispose of the spent A sheet and record the following information on the C sheet: tire size, manufacturer's recommended load range, inflation pressure, load, date, time, temperature, and humidity. Also, with a pencil draw a 10-inch line and two corner points on the tire print outside the pressure print region (see Fig D.2). These are later used in the Adage analysis.
17. Select one of the three steps below.
 - a. If additional contact pressures are desired for the same inflation pressure but at different loads, go to step 18.
 - b. If additional contact pressures are desired at a different location on the tire tread, rotate the tire to a pre-cleansed area on the opposite side of the tire.
 - c. If additional contact pressures are desired for lower inflation pressures, decrease the tire's inflation pressure to the next desired testing inflation pressure.
18. Repeat steps 4 through 16 for each desired load and inflation pressure.
19. Digitize the prints, using the Adage system.

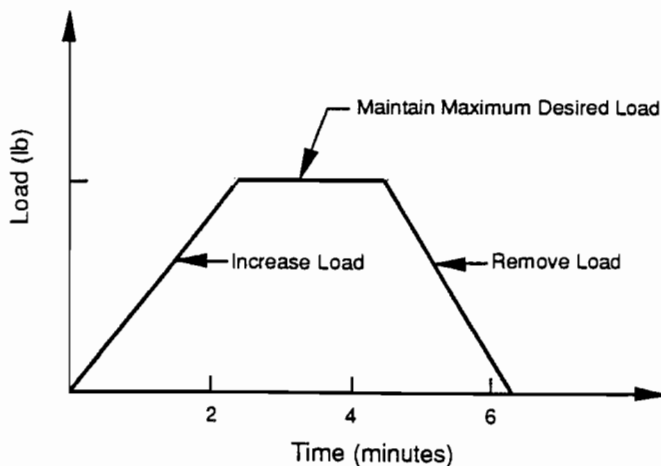


Fig D.1. The tire loading waveform.

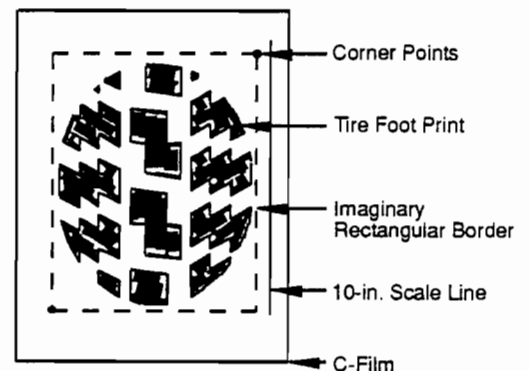


Fig D.2. Tire print preparation.

APPENDIX E. SMOOTH 11R24.5 LR-G MOVEMENT DATA

In order for Dr. J. T. Tielking, at the Texas Transportation Institute, to confirm contact pressure values produced by his finite-element tire-pavement contact model, the following sidewall deflections were measured. The smooth 11R24.5 LR-G tire deflections were measured at inflation pressures of 90 and 105 psi and at each inflation pressure the wheel was loaded to 5,000, 6,000, 7,000, and 10,000 pounds. The deflections at zero inflation pressure and zero wheel load were also measured. The sidewall deflections for the tire inflated to 105 psi are in Table E.1, the deflections for the tire inflated to 90 psi are in Table E.2, and the deflections for the tire inflated to zero psi are in Table E.3.

Five permanent reference points were selected on both sides of the tire. The reference point locations can be seen in Fig E.1. These sidewall points were aligned vertically in the middle of the tire-platen contact area. The corresponding points on the opposite side of the tire were also selected and marked. The movement values in the table were the average movement of a specific reference point with its

counterpart on the opposite side of the tire. For a vertical reference point, the vertical length of the ram-stroke was measured at a load of zero pounds. The horizontal and vertical point coordinates as well as the vertical length of the ram-stroke were measured to obtain deflection data at each load. This process was repeated for the 90-psi tire inflation pressure, as can be seen in Table E.2. Table E.3 is the deflection of the tire at zero psi and without any applied wheel load.

The total tire and axle displacement due to the load during the testing, and the average estimated value of the tire stiffness (kip/inch) are also included in Tables E.1 and E.2. Note the slight difference in the tire stiffness between the two inflation pressures.

Figures E.2 and E.3 are graphical representations of the data shown in Tables E.1, E.2, and E.3. The sidewall movement for different wheel loads and tire inflation pressures can be clearly observed. Note the pronounced vertical and horizontal movements of each point.

TABLE E.1. SIDEWALL MOVEMENTS FOR THE SMOOTH 11R24.5 LR-G RADIAL TIRE INFLATED TO 105 PSI

Points	Load (pounds)									
	0		5,000		6,000		7,000		8,000	
	<u>X*</u>	<u>Y*</u>	<u>X</u>	<u>Y</u>	<u>X</u>	<u>Y</u>	<u>X</u>	<u>Y</u>	<u>X</u>	<u>Y</u>
#1	2.0	22.60	2.3	20.30	2.3	19.90	2.4	19.60	2.4	18.60
#2	4.0	15.00	5.0	13.40	5.2	13.10	5.4	13.00	5.8	12.00
#3	4.0	11.10	5.0	9.50	5.2	9.20	5.5	8.70	5.9	8.20
#4	2.6	7.30	3.5	5.70	3.8	5.40	4.0	5.00	4.3	4.50
#5	0.0	0.00	0.0	0.00	0.0	0.00	0.0	0.00	0.0	0.00
Total Axle										
Movement	-0.00		-2.60		-3.20		-3.70		-5.20	
Average Tire Stiffness: 4,830 Pounds Per Inch										
*Movements are in centimeters.										

TABLE E.2. SIDEWALL MOVEMENTS FOR THE SMOOTH 11R24.5 LR-G RADIAL TIRE INFLATED TO 90 PSI

Points	Load (pounds)									
	0		5,000		6,000		7,000		8,000	
	<u>X*</u>	<u>Y*</u>	<u>X</u>	<u>Y</u>	<u>X</u>	<u>Y</u>	<u>X</u>	<u>Y</u>	<u>X</u>	<u>Y</u>
#1	1.9	23.00	2.3	20.40	2.3	19.70	2.3	19.40	2.4	18.10
#2	4.0	14.80	5.5	13.20	5.5	13.00	5.5	12.70	6.2	11.80
#3	4.0	11.00	5.5	9.30	5.5	8.90	5.6	8.70	6.5	7.80
#4	2.8	7.10	3.8	5.60	4.0	5.20	4.1	4.90	4.7	4.50
#5	0.0	0.00	0.0	0.00	0.0	0.00	0.0	0.00	0.0	0.00
Total Axle										
Movement	-0.00		-3.10		-3.60		-4.00		-5.80	
Average Tire Stiffness: 4,290 Pounds Per Inch										
*Movements are in centimeters.										

TABLE E.3 SIDEWALL MOVEMENTS FOR THE SMOOTH 11R24.5 LR-G RADIAL TIRE INFLATED TO ZERO PSI AND ZERO WHEEL LOAD

Points	X*	Y*
1	1.0	18.50
2	3.9	12.50
3	5.2	8.60
4	2.8	4.80
5	0.0	0.00

*Movements are in centimeters.

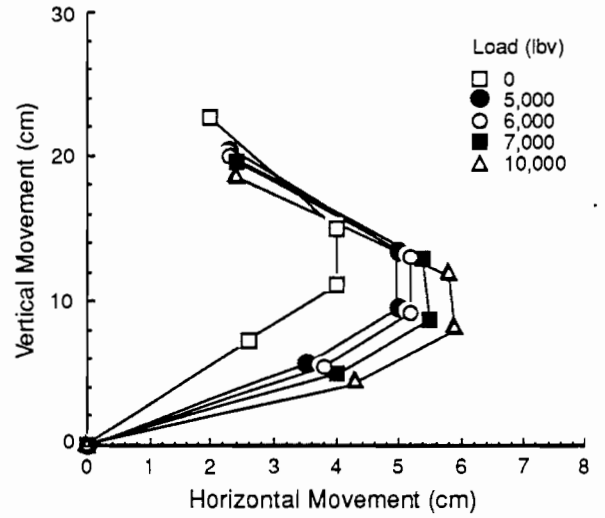


Fig E.2. Sidewall movements for the smooth 11R24.5 load range-G radial for an inflation pressure of 105 psi and wheel loads of 0, 5,000, 6,000, 7,000, and 10,000 pounds.

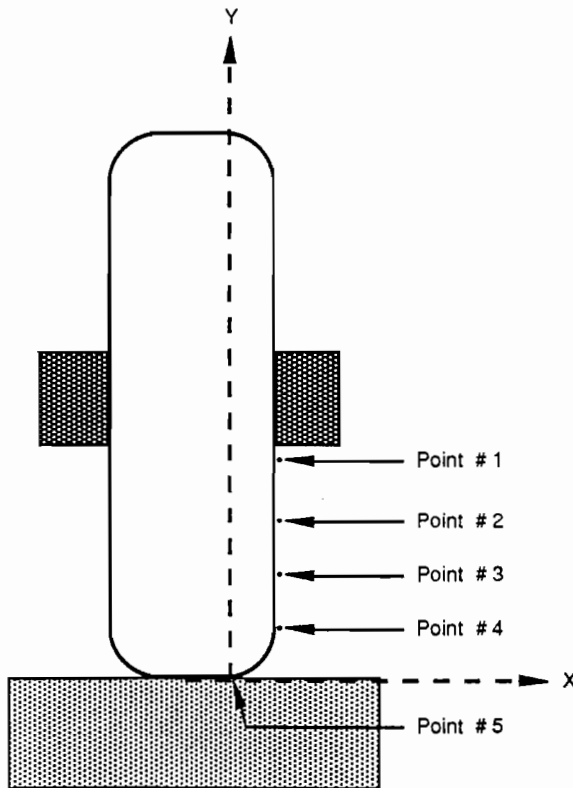


Fig E.1. Schematic of the sidewall points measured for vertical and horizontal movements.

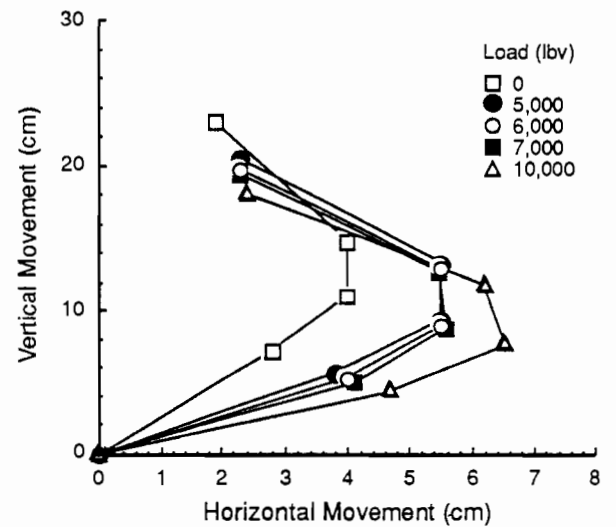


Fig E.3. Sidewall movements for the smooth 11R24.5 load range-G radial for an inflation pressure of 90 psi and wheel loads of 0, 5,000, 6,000, 7,000, and 10,000 pounds.

APPENDIX F. SMOOTH 11R24.5 LR-G TIRE PRESSURE HISTOGRAMS

In order to aid the reader in interpreting the numerical contact pressure distribution maps for the smooth treaded

11R24.5 LR-G radial tire, the frequency diagram for each contact pressure map is provided here.

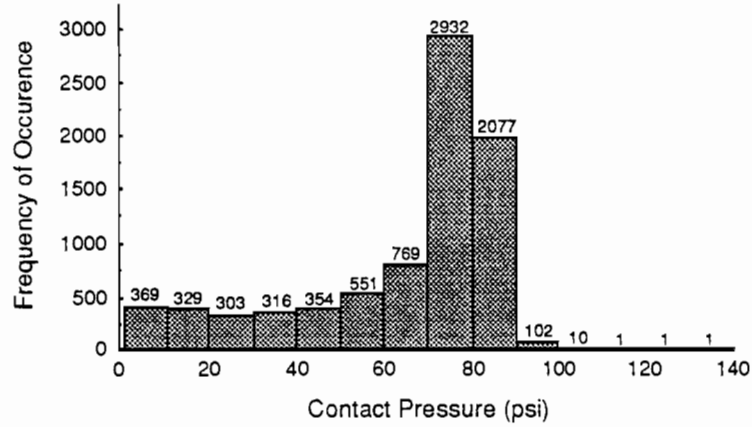


Fig F.1. Histogram for the smooth radial 11R24.5 load range-G tire inflated to 90 psi and loaded to 5,000 pounds.

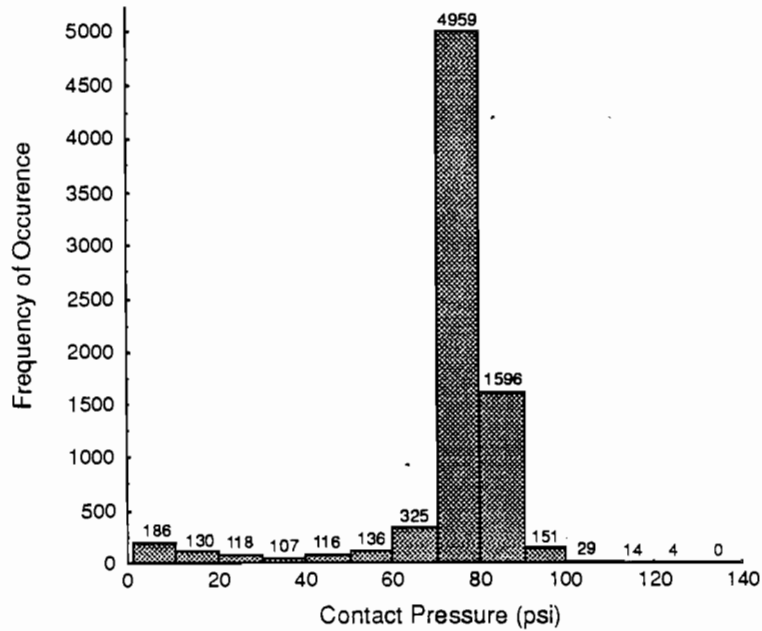


Fig F.2. Histogram for the smooth radial 11R24.5 load range-G tire inflated to 90 psi and loaded to 6,000 pounds.

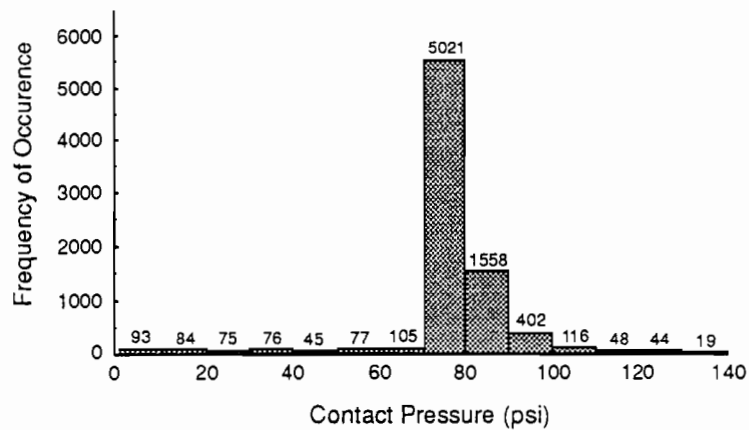


Fig F.3. Histogram for the smooth radial 11R24.5 load range-G tire inflated to 90 psi and loaded to 7,000 pounds.

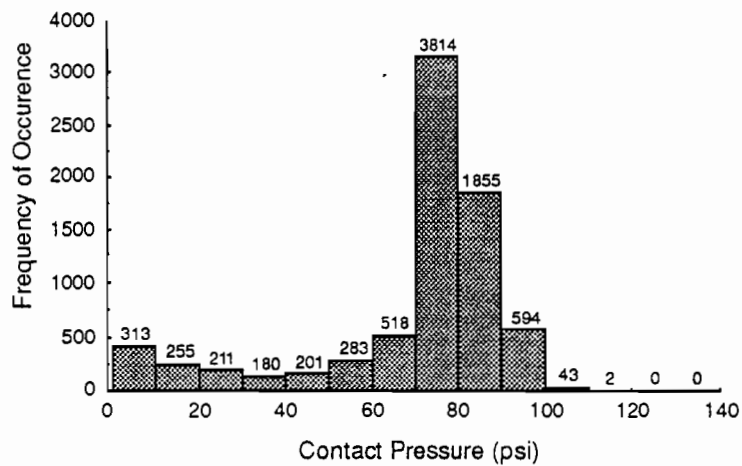


Fig F.4. Histogram for the smooth radial 11R24.5 load range-G tire inflated to 105 psi and loaded to 5,000 pounds.

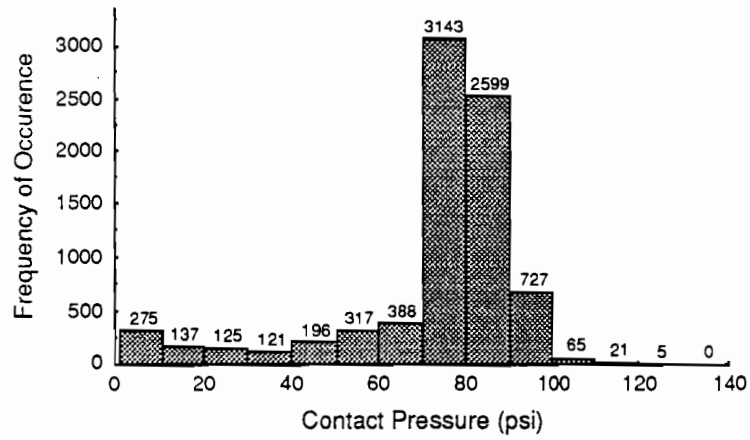


Fig F.5. Histogram for the smooth radial 11R24.5 load range-G tire inflated to 105 psi and loaded to 6,000 pounds.

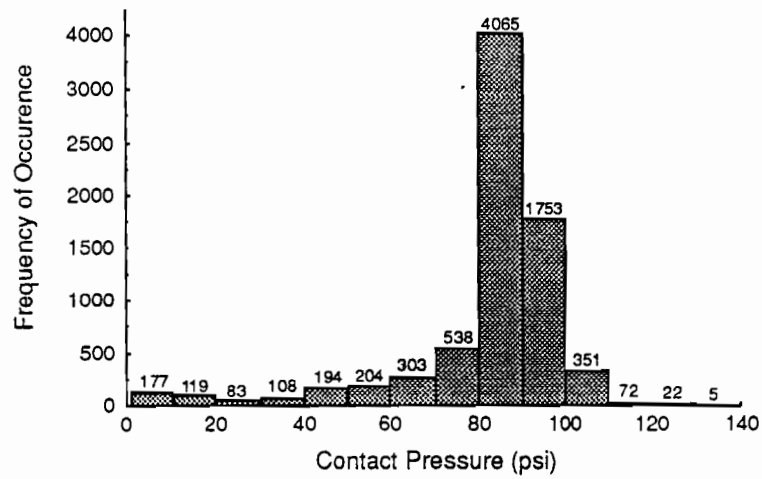


Fig F.6. Histogram for the smooth radial 11R24.5 load range-G tire inflated to 105 psi and loaded to 7,000 pounds.

APPENDIX G. WIDE-BASE 18-22.5 LR-H TIRE PRESSURE HISTOGRAMS

In order to aid the reader in interpreting the numerical contact pressure distribution maps for the bias Goodyear 18-

22.5 LR-H wide-base tire, the frequency diagram for each contact pressure map is provided here.

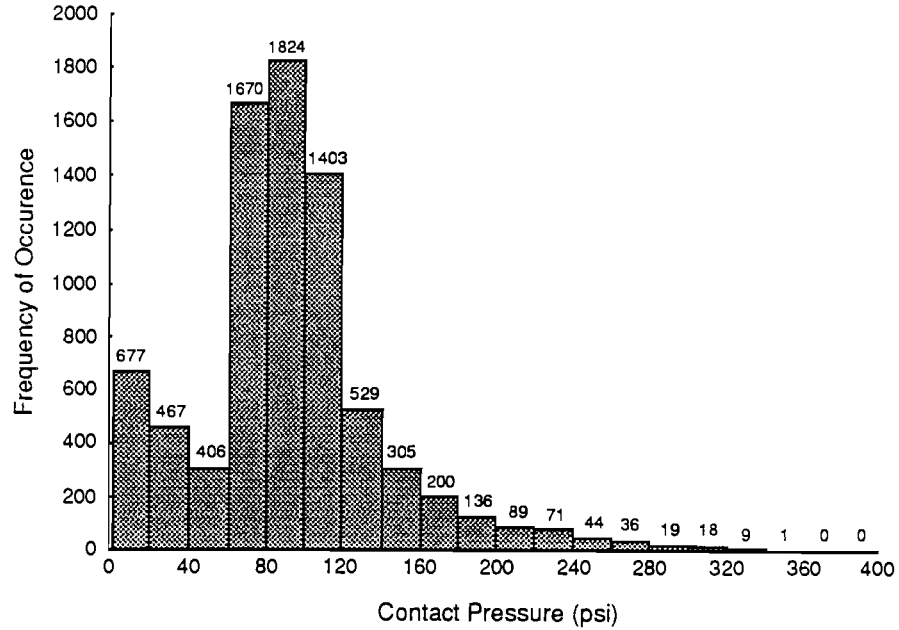


Fig G.1. Histogram for the wide-base bias 18-22.5 load range-H tire inflated to 85 psi and loaded to 8,000 pounds.

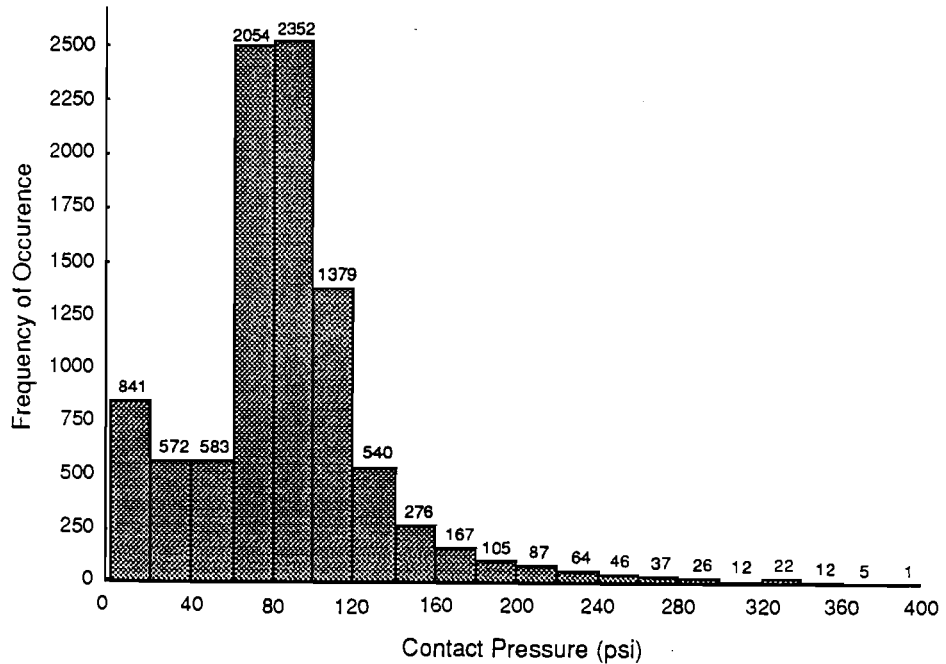


Fig G.2. Histogram for the wide-base bias 18-22.5 load range-H tire inflated to 85 psi and loaded to 10,000 pounds.

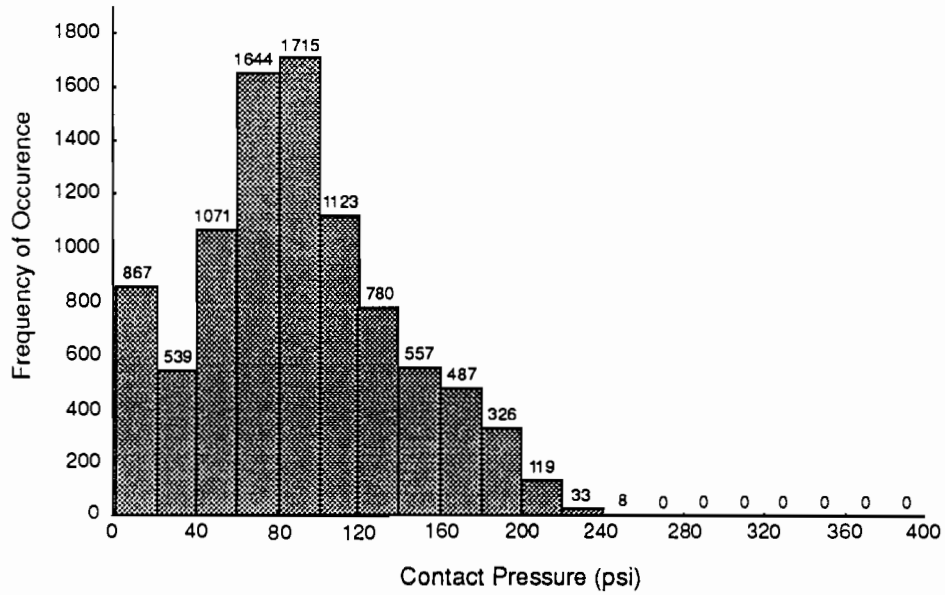


Fig G.3. Histogram for the wide-base bias 18-22.5 load range-H tire inflated to 85 psi and loaded to 12000 pounds.

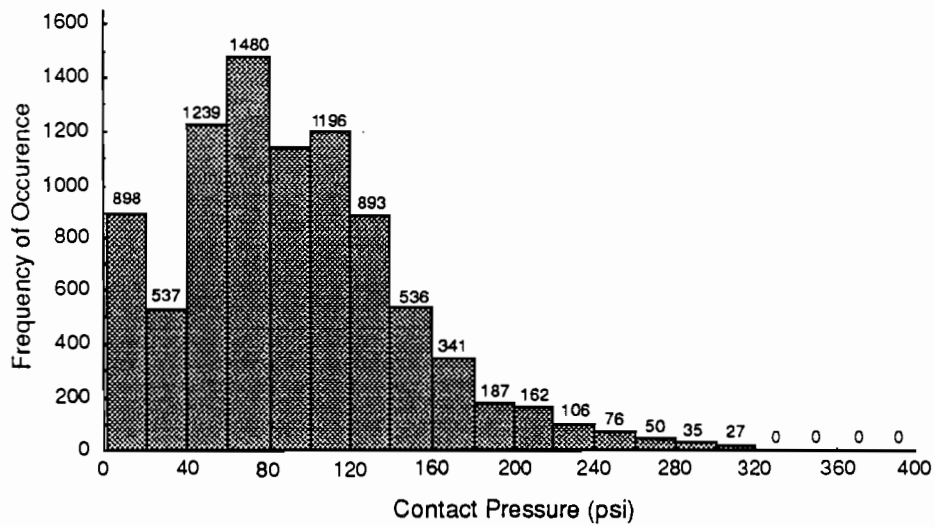


Fig G.4. Histogram for the wide-base bias 18-22.5 load range-H tire inflated to 100 psi and loaded to 8,000 pounds.

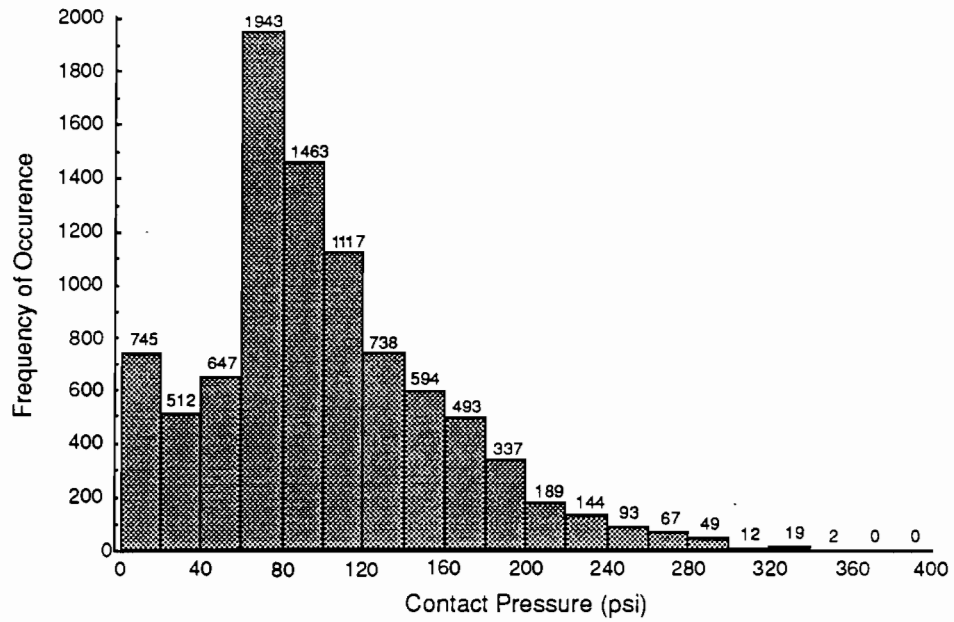


Fig G.5. Histogram for the wide-base bias 18-22.5 load range-H tire inflated to 100 psi and loaded to 10,000 pounds.

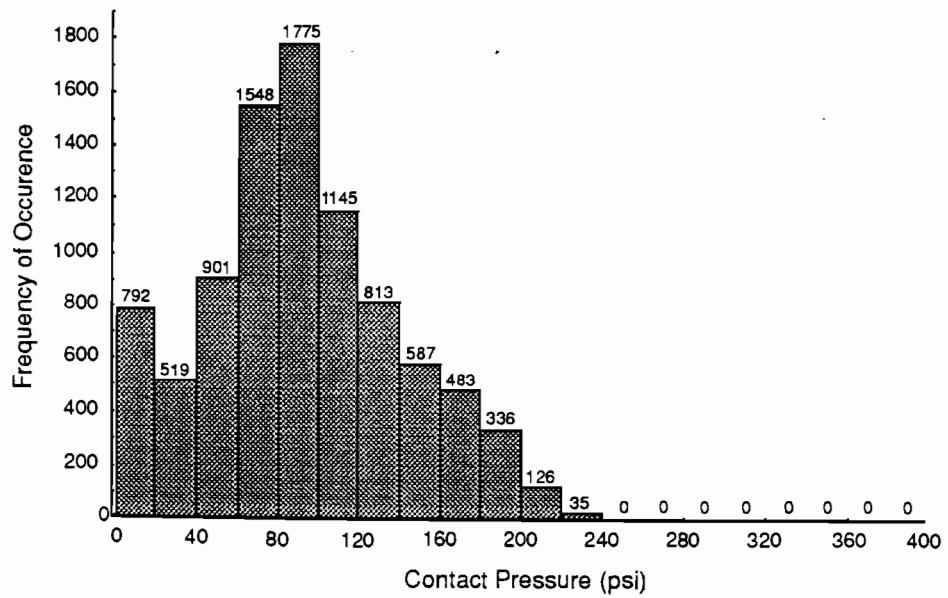


Fig G.6. Histogram for the wide-base bias 18-22.5 load range-H tire inflated to 100 psi and loaded to 12,000 pounds.

APPENDIX H. ADAGE PRINT ANALYSIS PROCEDURE

The procedure for analyzing the tire-print using the Adage system consists of five steps. The first step is to set up the scanner, the second to execute the program, the third to create a filter, the fourth to construct a calibration curve, and the fifth to perform the tire-print analysis. The procedures for each step are given below.

At each session, the lighting and scanner settings were not altered once the filter was created. Both a filter and a calibration curve were recreated at the beginning of each print analyzing session. The print analysis program was user friendly and with practice a print could be fully scanned, digitized, saved, and printed in approximately thirty minutes.

SCANNER SETUP

The Adage system is available for use by many students; therefore, the scanning hardware settings generally change from session to session. This is the standard setup used throughout the testing:

1. Install the Sigma lens on the lens housing.
2. Set the scanner height so that the largest print of the group to be analyzed can be fully scanned. This can be determined by pushing the scanner head in and looking through the lens at the largest image. The scanner height should be adjusted so that the image fits in the frame. For this project the lens height was set at 64 and 65 cm for the 11R24.5 LR-G tire-prints and 65 to 81 cm for the 18-22.5 LR-H tire-prints.
3. Set the lens aperture to 4.
4. Focus the lens by pushing the scanner head in and looking through the lens.
5. Move the overhead table lights so that they are approximately horizontal to the table top and the elevation arms to approximately 40 degrees from the plane of the table top (see Fig H.1).
6. Turn on the four overhead table lights by turning on the white and black switches.
7. Turn the room lights on and execute the scanning program.

EXECUTING THE PRINT ANALYSIS SCANNER PROGRAM

To execute the print analysis program, first log in at the Adage/VAX terminal by clicking the mouse and creating a new VT200 window. Then enter the proper user name and password. At the time of this writing the user name was **MEFZ660**.

Prior to executing the scanner program it is suggested the scanner documentation be read and available disk space be checked. A copy of the scanner documentation is available in the AGL but can also be printed out by typing

PRINT SYSSDOC:SCANNER.DOC. The document may also be displayed by typing **TYPE SYSSDOC:SCANNER.DOC**.

The user should remember that many subroutines are run and temporary files created during the execution of the analysis program. To scan, digitize, and obtain a data file, about 15,000 blocks (1 block = 512 bytes) of disk space are required. If color images on the AGL Adage monitor are desired for viewing the pressure distribution, about 5,000 additional blocks per image are required. This can create a problem with the limited disk space available in the AGL. The researchers found that it was possible to overcome the lack of sufficient disk space by (1) continually monitoring the available disk space, (2) deleting unnecessary files, and (3) obtaining temporary disk space from the AGL. Helpful commands which may aid the user to determine the amount of available disk space are **SHOW QUOTA** and **DIR/SIZE** at the system (\$) prompt.

Prior to executing the tire-print analysis program, ensure that the plotting pen is operating. To do so, turn the Digi-Pad power supply on. It is the black box located on the floor. On a separate VT200 window enter **@SYSSSYSTEM:IDL ADAGE [RET]** at the system (\$) prompt. The IDL system (IDL>) prompt will then appear in the VT200 window. First enter **TVINIT,0 [Ret]** at the IDL system prompt, followed by **TTVCRS,1 [Ret]** at the next IDL system prompt. To test whether or not the digitizing pen and table are working, enter **TVRDC,X,Y,1 [Ret]** at the IDL system prompt. The cursor should appear on the Adage monitor. As the digitizing pen is moved over the digitizing pad, the cursor should simultaneously move on the Adage screen. Click the digitizing pen and enter **TVCRS,1[Ret]** to get back to software control of the pen plotter.

The tire-print analysis system is executed by typing **@BATMAN** at the system (\$) prompt. The program

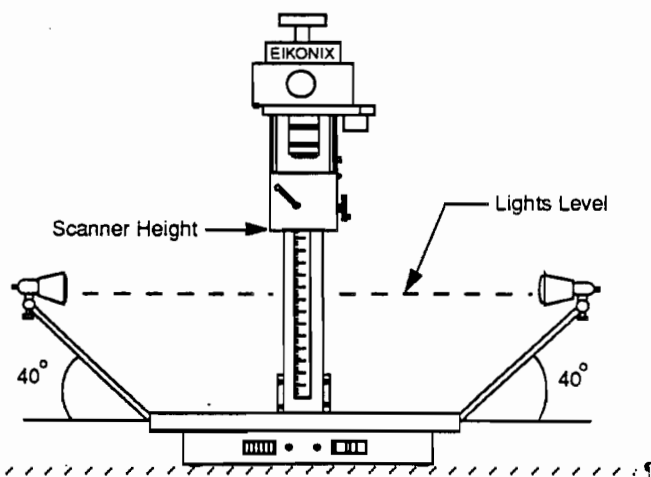


Fig H.1. Scanner setup.

responds with a main program menu displaying options to (1) create a filter, (2) calibrate a roll of film, (3) execute the actual tire-print analysis subroutine, or (4) look at the present calibration curve. The third option should be selected only after a filter and a calibration curve have been created.

FILTER CREATION PROCEDURE

The filter was created at the start of each print reading session. The filter was used to compensate for uneven lighting and any possible changes in the lighting which existed during the construction of the new calibration curve.

In order to create a filter, follow this procedure.

1. Select the menu option (1) to create a filter.
2. Study the instructions displayed on the monitor in order to set up the scanner control panel for calibration and actual scanning. For calibrating the scanner the exposure should be 100 and the range should be 0 to 4095. For scanning the smooth 11R24.5 LR-G tire, the exposure was set at 60 and the range at 60 to 2600, as shown in Fig H.2.
3. Hit the return key to execute the scanner program.
4. When the scanner control panel appears on the monitor, use the mouse and keyboard to select the appropriate scanner settings for the calibration routine. Select a 1024 X 1024 Image Size with the mouse. Since only the greyscale color mode is used, the One Mode box may be selected as shown in Fig H.2. Selecting the

One Mode box will avoid the red, green, and blue calibrations, thus shortening the scanner calibration time.

5. Make sure that the white table top surface is clean and free from marks.
6. Select **Calibrate** with the mouse. When calibrating the scanner, the exposure must be equal to 100. After the calibration is complete the user may change the exposure and range before scanning.
7. Select **Scan** with the mouse.

While the scanner is operating, make sure that the lighting is uniform. This is done by viewing the plot line on the scanner control panel. The line should be approximately horizontal. If it is not horizontal, adjust the overhead lights such that the plot becomes horizontal.

If this is the user's first attempt at scanning a particular type of tire-print, a new set of tire-prints, or at a previously unused lens height, it is suggested that, instead of scanning the table top to obtain a filter, first scan a tire-print and the calibration squares to determine if the exposure and range settings are correct.

- a. Place the calibration image on the table.
- b. Select **Scan** with the mouse.
- c. Allow part of the calibration squares to be scanned. Then select **pause** with the mouse.
- d. At this point the user may select different exposure and range settings and then resume scanning. This enables the user to see the

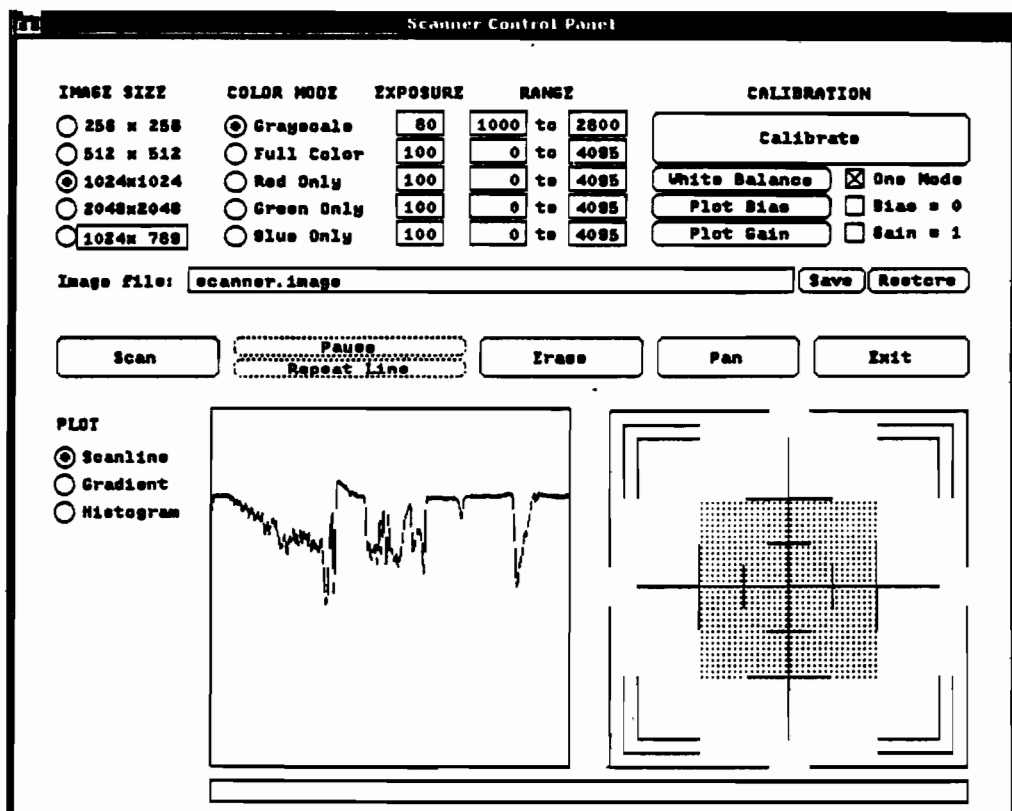


Fig H.2. Scanner control panel setup.

effect of various exposure and range settings in order to optimize the image resolution. If the users desire, they may also select the **Repeat Line** and **Pause** options with the mouse simultaneously. This allows the user to see the effect of different exposure and range settings on the plot while the same line is being scanned. If saturation occurs, reduce the exposure setting and continue scanning. (Saturation occurs when the image appears washed out or, in other words, the whites are so bright that the image is less clear.) A good way to obtain the best exposure and range setting is to select an exposure setting during scanning. If the data plot is thin, a larger contrast is desired, and, if the data plot exceeds the boundaries, a smaller contrast must be used. To change the contrast, select pause with the mouse. Then type in the new desired range values and unselect pause. The plot will shift after the scanner calibrates itself. The user should attempt to fill as much of the plot window with data as possible.

- e. Perform this for all the calibration squares to determine the best range.
 - f. When the best exposure and range settings have been determined, remove the print from the table and rescan the table top at the desired settings to create a new filter.
8. To speed up the scanning process, the user may reselect the settings already chosen underneath the **Plot** option, which is generally set at **Scanline** during the tire-print analysis. This disables the plotter located on the scanner control panel by eliminating the required calculations and thus allows the scanning speed to increase.
 9. When a suitable image is obtained, note the scanner range and exposure settings and **Exit** the scanner program. When the program is exited the filter is automatically calculated and saved. The program then displays the filter average value on the monitor and returns to the main program menu. A good average filter intensity is near or above 150.

CALIBRATION CURVE CONSTRUCTION PROCEDURE

Constructing the calibration curve consists of two steps. First, the calibration square images must be constructed using Fuji prescale film, and second, the images must be scanned and stored in a data file. In order to reduce experimental error, calibration squares were produced at the same time as the tire-prints for each film type used. In the analytical process a suitable calibration curve was produced at the beginning of each print analysis session. The two procedures are presented in more detail below.

Creating the Calibration Image

The calibration square images were prepared in a procedure similar to the construction of the actual tire contact pressure prints but on a smaller scale. Small squares of Fuji A and C film were cut out and loaded to predetermined loads, in the same manner as the the actual tire contact pressure prints, using a universal compression testing machine. The more calibration squares produced, the more accurate the Adage calibration curve will be. For further details of the loading procedure, consult Appendix D and Fuji (Ref 28).

Due to the Fuji film's tendency to change color intensity with time, calibration squares were created at the same time as the tire-prints. One set of calibration squares was sufficient for testing the 11R24.5 tire; however, during the testing of the 18-22.5 super single tire both Super Low and Low Fuji prescale films were used. Therefore, two sets of calibration squares had to be produced, a set for each of the Super Low and Low Fuji films.

Calibration squares were prepared using a one-inch-square piece of rubber similar to tire rubber. An attempt to use tire rubber was made, but the tire's cord construction made the calibration square prints nonuniform in color intensity. The calibration squares were loaded to known loads. The load for each square was divided by the area of the stained color density to produce corresponding pressure values. These squares were then taped on a white piece of paper, as shown in Fig H.3.

The squares were oriented such that lighter squares were adjacent to darker squares in order to provide a sharp contrast between pixel intensities during the digitizing process. If the calibration squares turned out to be more rectangular in shape than square, then each calibration square was digitized such that the longer side of the calibration square was parallel to the horizontal axis of the Adage screen. It is important that each calibration square be oriented properly because the pixel intensity of each square is calculated from the average of a 60 x 30 rectangular pixel array (0.72 x 0.36 inch on the Adage monitor). This array is extracted from each calibration squares center (with the 60-pixel dimension parallel to the Adage monitor's horizontal axis).

Scanning the Calibration Image

1. Select **menu** option (2) to construct a calibration curve.
2. Hit the **Return** key [Ret] to execute the scanner program.
3. **Calibrate** the scanner as before.
4. **Scan** the calibration square image. The image must first be framed by pushing the scanner head in, enabling the user to look through the lens. Center the image in the frame but do not alter the lamp angles, lens height, or aperture setting.
5. **Exit** the scanner program.

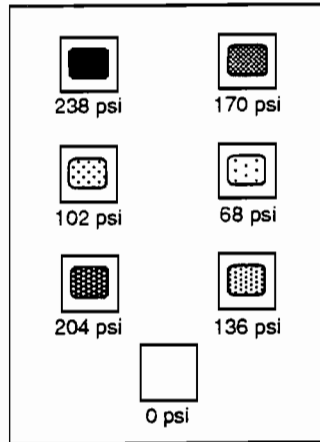


Fig H.3. Fuji film calibration image.

6. Follow the program instructions to obtain the pressure versus pixel intensity data required to construct the calibration curve. **Enter the number of calibration squares** but do not include the 0 psi square [Ret]. Starting with the calibration square having the lowest pressure, enter the pressure value using the VAX keyboard [Ret].
 7. Use the digitizer-pen/pad to move the Adage screen cursor to the center of the corresponding calibration square and click on the digitizer pen to read in its pixel intensity value. Be sure to click on the center of the calibration square because a 60 x 30-pixel intensity value is averaged and if the corner is selected the 60 x 30 image will overlap onto the white paper. This has caused many zeros to be averaged into the resultant pixel intensity.
 8. Repeat the procedure by typing in the pressure value and printing and clicking with the digitizer-pen/pad until all the calibration squares have been digitized. Entering 999 [Ret] exits the calibration square data collection subroutine.
 9. The user may select either a quadratic or a cubic curve fit for the pressure versus pixel intensity data. Select each curve fit in turn to view a display of the resulting calibration curve on the Adage monitor. When the curve is plotted the image also displays the pixel intensity value (INTN), the actual pressure input value (ACT), and the curve calibrated pressure value (CURVE) for each calibration square. This assists the user in selecting the best fit curve. Once a selection is made, the program returns to the main program menu.
- ### TIRE PRINT ANALYSIS PROCEDURE
1. Select option (3) to execute the tire-print analysis subroutine from the main program menu.
 2. A new menu appears on the VAX monitor with the following options:
 - a. Digitize and analyze a tire-print.
 - b. Display pressure contour plot on the Adage.
 - c. Display a 3D map on the Adage monitor.
 - d. Display a 2D contour map on the Adage monitor.
 - e. Print the pressure distribution.
 - f. Return to the main program menu.
 - g. Exit the program.
 3. Select option (1). Digitize and analyze a tire-print [Ret].
 4. Hit **Return** again to execute the scanner program.
 5. **Calibrate** the scanner as before (remember the exposure must be 100 for scanner calibration).
 6. Place the tire-print on the light table. Orient it so that it is centered and the tread is parallel to the vertical frame lines as seen through the viewer. As in the calibration procedure, move the tire-print into position but do not alter the lamp angles, lens height, or aperture setting. Taping the print corners and sides down with masking tape helps reduce shadows on the print caused by a curled print.
 7. Adjust the scanner range and exposure settings to the settings previously used to create the filter and calibration curve.
 8. **Scan** the tire-print.
 9. **Exit** the scanner program.
 10. Follow the program instructions to read in the end point screen coordinates of the 10-inch line. Use the digitizer-pen/pad to move the Adage screen cursor to each end point location. Click the digitizer pen on the digitizer pad to read the 10-inch line's end point coordinates. The program displays a 10-inch line on the Adage monitor which is used to calculate the area of the tire-print to determine an equivalent wheel load from the pressure distribution.
 11. If the 10-inch line is acceptable, enter (1) [Ret] at the program prompt. If the line is unacceptable, enter any other number to redefine the 10-inch line.
 12. The user now selects a rectangular image around the tire-print to reduce calculations and speed up calculation time. Enter (1) [Ret] if the coordinates are known; otherwise enter in any other value.
 - a. If (1) was entered, a rectangular border is drawn around the tire-print image. Go to step 13.
 - b. If (1) was not entered, the user must use the digitizer pen to locate the coordinates. Use the digitizer-pen/pad to move the Adage cursor to the point just outside the bottom left corner of the tire-print image and another just above the tire-print's top right corner, clicking at both points. Based on the selected corner points, the program displays the coordinates on the VAX monitor and a rectangular border encloses the tire-print image on the Adage monitor. This enclosed image is extracted

from the Adage's 1024 x 1024 displayed image, improving computation speed and accuracy.

13. If the rectangular border is acceptable, enter (1) [Ret] at the program prompt. If the border is unacceptable, enter any other number to redefine the border. If (1) is entered, the image defined by the border is extracted and converted from an array of pixel intensities into an array of pressure values.
14. Record the area value as prompted on the VAX monitor. This is the pixel area as displayed on the Adage monitor. This value is later used in a separate analysis program.
15. A subroutine then calculates a wheel load from the pressure distribution data. The calculated load is then displayed. Enter the actual load applied to the tire when prompted by the program. The percentage difference between the actual and calculated load is computed and displayed.
16. Enter (1) [Ret] to command the program to adjust the data so that the actual and calculated wheel loads are equal. Entering (1) also computes and displays calculated loads for five sections of the tire. The tire is separated into five sections left (L), left of center (LC), center (C), right of center (RC), and right (R). The minimum and maximum pressure values for the entire tire-print are also displayed. The pressure values are then adjusted so that the calculated load equals the actual load. The adjusted data are then smoothed and stored in a file called SMOOTH.DAT, which is used by subroutines to view the pressure distribution on the Adage.
17. Program control returns to the print analysis subroutine menu. Select one of the options to view the tire pressure distribution.
18. After viewing the pressure map print-out and spectrum graphic, the user may opt to remove the "noise" from the print. The program NOW.PRO, when executed, prompts the user for a desired minimum value, then replaces all values less than the input minimum with a zero. NOW.PRO is executed in another VT200 window which is opened by clicking on the mouse and selecting "create a new VT200 window." When the window is opened the program is executed by typing @NOW.PRO [Ret] at the system prompt (\$). After entering the **desired minimum value** [Ret] and **area value** [Ret] recorded in step 14, the gross contact area and calculated load are displayed on the VAX monitor. The new calculated load enables the user to see the consequences of his sweeping of the lower pressure values. The user is then prompted for the actual wheel load. The pressure values are then adjusted once more so that the calculated load equals the actual applied load. Also, to assist the user to determine the consequences of sweeping, the maximum and minimum contact pressures are displayed. The adjusted data are then stored in a new version of SMOOTH.DAT. The swept tire pressure data may then be viewed by returning to the original window which displays the print analysis subroutine menu and selecting one of the options to view the data.
19. Exit the program or select the option to digitize another print. Remember to **RENAME** file SMOOTH.DAT before terminating the session for future use.

APPENDIX I. NUMERICAL PRESSURE MAP PROCEDURE

The numerical contact pressure distribution maps were produced by downloading the pressure data from the AGL VAX computer to a Macintosh II personal computer. The programs for converting the pressure data from IDL format into ASCII formatted files reside in the AGL VAX computer under account number MEFZ660. The procedures for converting the IDL data file and printing the contact pressure maps are detailed below. A listing of the programs can be found in Chan (Ref 30).

File Conversion Procedure

1. Log on to the AGL VAX terminal.
2. Run tire-print analysis program to obtain a SMOOTH.DAT file.
3. Convert the data file for the graphics display and print out by typing `@Run IBMDATAPREP [Ret]`, at the system prompt. When the program has finished converting the data, a message will appear on the VAX monitor stating that two files, IBM2D3D.DAT and IBMPRESS.DAT, have been created and are ready for transfer.
4. Go to the IBM or Macintosh terminal that is to receive the files.
5. Use the file transfer program, Kermit, or any other suitable file transfer program to transfer copies of IBM2D3D.DAT and IBMPRESS.DAT.

Contact Pressure Map Print Out

A 50 x 50 element sample contact pressure map of the tire-print can be obtained by printing the data file **IBMPRESS.DAT**. For a clearer presentation of the data, **IBMPRESS.DAT** should be printed using a Macintosh wide base printer. Figures 4.2 and 4.25 were printed on a Macintosh Laserwriter. To produce the pressure figures, the following procedure was used.

1. Execute Microsoft Word.
2. Select all the data.
3. Change font to Times and font size to 9 point
4. Using the ruler to adjust the paper width to 14 inches and select the center justified option.
5. Select page setup underneath the file menu, and change (1) the paper height to 20 inches and (2) all the margins to 0.5 inch.
6. Select paragraph underneath the format menu and change the line spacing to a value between 13 and 17.
7. Print the data using a 50 to 55 percent reduction, as desired, to obtain a contact pressure map.